IONIZATION METHODS APPLIED TO NEUTRON DOSIMETRY

JACQUELINE A. SPENCER B.Sc.

THESIS PRESENTED FOR THE DEGREE OF DOCTOR OF PHILOSOPHY OF THE UNIVERSITY OF EDINBURGH, FEBRUARY 1982

D E C L A R A T I O N

I hereby declare that this thesis contains the results of my own work, and that it has been composed by myself.

Jacqueline A. Spencer February 1982

ABSTRACT

A parallel-plate ionization chamber with variable plate separation, variable gas and gas pressure facilities and detachable wall materials has been constructed for use in a (d(15MeV) +Be) cyclotron produced neutron field.

Charge per unit plate separation (q_{sat}/d) measurements as a function of plate separation have been made with tissue-equivalent plastic/tissue equivalent gas (TE/TE), TE/Air, C/CO_2, C/Air and C/TE chambers in the range 0.1-18mm. It was shown that measurement errors occur with C/CO_2 and C/TE chambers in an air atmosphere as a result of the porosity of the graphite wall. All chamber combinations gave (q_{sat}/d) distributions as a function of d, in agreement with existing kerma, stopping power and range data.

A theoretical analysis of the relative charged particle distribution in C/CO_2, C/Air and C/TE chambers due to the individual wall and gas particles has been made and the calculated results have been compared with the (q_{sat}/d) against d measurements. The predominant particles considered in each case are as follows -

C/CO_2 - ^{12}C, ^{9}Be, ^{16}O, ^{13}C recoils and α particles

C/Air - ^{12}C, ^{9}Be, ^{16}O, ^{13}C, ^{14}N, ^{14}C, ^{11}B recoils, α particles and protons

C/TE - ^{12}C, ^{9}Be, ^{16}O, ^{13}C, ^{14}N recoils, α particles and protons

In the cases of C/CO_2 and C/Air chambers, close agreement has been obtained between the theory and experiment; in the case of C/TE

chamber, agreement is poor, due primarily to the high proton contribution from TE gas.

A method has been described for deriving the $\overline{W}$ values in any gas for recoils from any conducting solid, based on a Bragg-Gray Approximation. Experiments to substantiate this derivation were carried out using TE plastic and carbon chambers filled with TE gas, air, CO_2, CH_4 and argon. For protons issuing from the TE plastic wall, the present measurements support the $\overline{W}$ values as recommended by ICRU 31 for CO_2, air and argon; new values of $\overline{W}$ are suggested for TE gas and CH_4. For recoil particles issuing from the carbon wall, the present measurements for TE gas, CO_2 and CH_4 agree with the measurements of other authors, to within the limits of experimental error; new values of $\overline{W}$ are suggested for air and argon.

It has been established that a photon calibration in 300kv x-rays compared with direct dimension measurement in the determination of the mass of gas, m, in the cavity, gives good agreement for the C/Air and TE/TE chambers. Therefore, having obtained a reliable value of m for TE/TE chamber, the absorbed dose in the neutron beam was measured, and consequently the absorbed dose in tissue was derived. The TE/TE chamber gave the same absorbed dose value, to within 1%, as a thimble type polythene/air chamber, which is used in routine dosimetry.

ACKNOWLEDGEMENTS

My thanks go to my supervisor Professor J.R. Greening for his advice and guidance throughout this project and for allowing me to study in his department; thanks also go to the Faculty of Medicine for providing financial assistance through a Crichton Scholarship.

I would also like to thank Mr Jeremy Williams for his invaluable advice and encouragement in experimental and theoretical aspects of this thesis, and the staff of the M.R.C. Cyclotron Unit in Edinburgh, especially Mr Tim Saxton for allowing me the use of the Cyclotron Research Facilities.

On the mechanical side, I would like to thank Mr Louis Mackie for allowing me the use of his workshop facilities and Mr Gerald Kelly for his advice and supervision. For the vacuum work, mechanical and electrical advice, my thanks go to Mr William Rankin and Mr Robert Goodall of the M.R.C. Cyclotron Unit.

Credit for the typing and presentation of this thesis must go to Mrs Carole Allan; thanks must also go to Mrs June Whittet for her advice and assistance during my stay at the Cyclotron Unit.
Mr Ronald Robertson receives my thanks for his time and effort in producing the photographs for this thesis.

My special thanks go to the above people but a general 'thank you' must go to all the staff of the M.R.C. Cyclotron Unit and the Medical Physics Department of the Western General Hospital in Edinburgh for their advice, encouragement and sense of humour, resulting in a very enjoyable three years of study.

PREFACE

Fast neutrons have been used since 1938 for the treatment of malignant disease in humans. Stone and his colleagues (1940, 1942, 1948) abandoned their programme of therapy in 1948 because of discouragingly poor results, especially distressing late effects. Stone's failure was due to lack of knowledge regarding the influence of the fractionation scheme on the Relative Biological Effectiveness (RBE) of the neutrons, resulting in an under-estimation of the doses applied (Sheline et al 1971).

An important hypothesis which has emerged since then, is that of the Oxygen Enhancement Ratio (OER), (Churchill-Davidson et al 1957, Gray et al 1953). Anoxic cells in a tumour are not killed as readily by x-rays and γ-rays as are well-oxygenated healthy cells. A practical method of reducing this differential effect would be to use radiations of a quality which cause cell injury irrespective of the amount of oxygen present, i.e. high Linear Energy Transfer (LET) radiations. Therefore, the use of fast neutrons with more rational schemes of fractionation makes neutron therapy a definite and desirable possibility.

In 1967, a clinical trial of fast neutrons began at Hammersmith Hospital, London, using patients with very poor prognoses. Before analysis had been completed, the results of fast neutron therapy (Catterall et al 1974, 1975, 1977) were sufficiently encouraging for the Medical Research Council to approve the establishment of a new facility at the Western General Hospital, Edinburgh specifically for fast neutron therapy. This thesis arises from the Neutron Dosimetry Programme associated with the Edinburgh Neutron Trial.

CONTENTS

CHAPTER 1

INTRODUCTION

Efficient neutron therapy can only be achieved by accurate neutron dosimetry. Since neutrons dissipate their energy in tissue through different nuclear reactions with the various constituents of the material, the energy deposition is characterised by a complex spectrum of secondary charged particles. The type of interaction processes depend strongly upon the energy of the neutrons, hence a knowledge of the neutron energy spectrum is required. The fast neutron beam from the M.R.C. cyclotron at Edinburgh results from the bombardment of a beryllium target with 15 MeV deuterons, producing deuteron stripping and the $^{9}Be(d,n)^{10}B$ reaction, among others. The resulting neutron spectrum extends from 0 to 18 MeV, the mean energy of the spectrum being 6.5 MeV (Bonnett, 1979) (Fig. 1.1).

Auxier et al (1969) have listed 33 possible mechanisms whereby neutrons in the range 0 to 20 MeV deposit their energy in tissue. At an average neutron energy of 6.5 MeV, approximately 85 per cent of the absorbed dose in tissue is due to recoil protons resulting from elastic scattering of the fast neutrons with hydrogen (Bewley, 1963). The remaining 15 per cent is due to heavy recoil nuclei, such as carbon, oxygen and nitrogen and the products of nuclear reactions with these elements, e.g. α particles from the $^{16}O(n,\alpha)^{13}C$, $^{12}C(n,\alpha)^{9}Be$ and $^{12}C(n,n')3\alpha$ reactions. Although only approximately 15 per cent of the absorbed dose in tissue is due to reactions other than with hydrogen, the biological effect of this fraction might be greater than its contribution to the absorbed dose suggests, since the particles responsible can have LET values much higher than those of recoil protons.

The objective of dose-determinations carried out for the application of neutrons in radiotherapy is to obtain a precise description of the energy deposition in irradiated material, in order to obtain an unambiguous correspondence with observed responses of biological systems.

The tissue-equivalent ionization chamber is a convenient and reasonably accurate method of measuring the total absorbed dose of radiation. The introduction of this radiation sensitive device into a medium necessitates the consideration of cavity-chamber theory; in the case of x and γ - radiation, the Bragg-Gray Theory is normally employed. The Bragg-Gray relation which relates the absorbed dose D in the material of the wall of the ionization chamber to the charge collected, Q, is:

$$D = \frac{\overline{W}}{e} \left(S_{m,g}\right) \frac{Q}{m}$$

where $\overline{W}$ is the average energy to create an ion pair, e is the electronic charge, $S_{m,g}$ is the mass stopping power ratio of wall to cavity material and m is the mass of the gas in the cavity. This theory rests on the basic requirement that the dimensions of the cavity should be a very small fraction of the range of the charged particles which cross it. For x and γ-ray dosimetry at energies used in therapy this condition presents no problems as the electrons produced in cavity gases, such as air and CO_2, have ranges of the order of metres. However, neutron dosimetry becomes more complicated in that the secondary particles produced by neutrons include a variety of charged particles of vastly differing ranges.

For example, in air at atmospheric pressure, the maximum range of protons at a neutron energy of 6.5MeV is likely to be about 40cm because of the predominance of elastic scattering, while the maximum ranges of α particles and heavy nuclei, such as ^{12}C and ^{16}O, are about 2cm and 3mm respectively. Generally for a given neutron energy, the maximum range of the recoil protons is about 20 times that of the α particles and 200 times that of the heavy recoils of carbon and oxygen (ICRU 26). On the other hand, recoil protons produced by neutrons of a given energy have ranges of less than a tenth of the ranges of secondary electrons produced by photons of the same energy. Therefore, the size of cavity which satisfies the Bragg-Gray Theory for neutrons can be easily achieved for recoil protons, but is inconveniently small for the heavier secondary recoils.

However, the Fano Theorem (Burlin, 1968), which is a modification of the Bragg-Gray Theory, recognises that the charged particle flux will remain undisturbed when the atomic composition of the gas is the same as the wall material, so that the size limitation can be relaxed. In practice, it is only rarely that the gas and wall material can be chosen with identical atomic composition. Generally the effective atomic numbers of wall and gas are matched by adjusting the proportions of mixtures of materials with different atomic numbers; it is particularly important that the hydrogen content be the same because of the preponderant influence of interactions with hydrogen. Therefore, most ionization chambers employed in practical neutron dosimetry are more or less homogeneous, so that a stopping power ratio of unity between wall and gas is expected, in the absence of any phase effect (Watt et al 1977). The different composition

between Shonka tissue-equivalent plastic (Smathers et al 1977) and tissue-equivalent gas is expected to introduce corrections of only a few percent (Dennis 1979). The subject of stopping power ratios for inhomogeneous chambers in neutron dosimetry is poorly documented.

A saturation value of collected charge is required in the Bragg-Gray Theory. As a result of neutron irradiation, initial recombination takes place along the tracks of the recoil particles, as opposed to general recombination as in the case of electrons resulting from x-irradiation. In experimental studies by Scott and Greening (1963), different extrapolation approaches in the near saturation region must be applied according to the predominance of the respective recombination processes.

The ratio of $\overline{W}$ values for neutrons compared to photons or electrons presents another source of uncertainty in the Bragg-Gray Theory because of the variety of ions produced. It is recommended that $\overline{W}_C/\overline{W}_N$ (ratio of $\overline{W}$ for a calibration using photons to $\overline{W}$ for neutrons) for tissue-equivalent gas be taken to be 0.95 (ICRU 26). Recent $\overline{W}$ measurements in tissue-equivalent gas for protons and other heavy recoil nuclei have been combined with neutron energy transfer data to derive $\overline{W}_N$ as a function of neutron energy (Goodman and Coyne 1980). A single average value of $\overline{W}_N = 31.9 \pm 0.9$eV over the energy range 0.1 - 20MeV is recommended.

All materials irradiated by neutrons are also exposed to gamma rays, as, even in the unlikely event of the neutron beam being free of gamma rays, inelastic collisions within the irradiated material will give rise to gamma rays. The method normally used for the measurement of the neutron and gamma ray dose components in a mixed n-γ field

involves comparison of the response of a hydrogenous ionization chamber with that of a non-hydrogenous one. A knowledge of the neutron and gamma ray sensitivities of the two chambers then allows the solution of two simultaneous linear equations to obtain separately the neutron and gamma ray absorbed doses (ICRU 26). In practice, the major source of error is the inability to determine an accurate value of the neutron sensitivity of the gamma ray detector.

This project is an attempt to investigate the energy deposition of neutrons in the gas cavity of an extrapolation chamber, bearing in mind the uncertainties described above. The extrapolation chamber is parallel-plate with demountable wall materials made of both hydrogenous and non-hydrogenous substances, i.e. tissue-equivalent Shonka plastic and graphite, thus presenting the situation of having both neutron sensitive and neutron insensitive devices. A gas flow facility allows the introduction of tissue-equivalent gas, CO_2 and dry air at atmospheric pressure for a homogeneous or inhomogeneous chamber as required. An adjustable plate separation gives a wide range of cavity sizes. When the reduction of plate separation becomes physically inadvisable, a variable gas pressure facility for pressures less than atmospheric gives the equivalent of reduced plate separation.

With these variables, it should be possible to obtain the fraction of ionization from "wall" particles, "gas" particles, "heavy" ions, protons and electrons, by measuring the increment of ionization per increment of chamber volume.

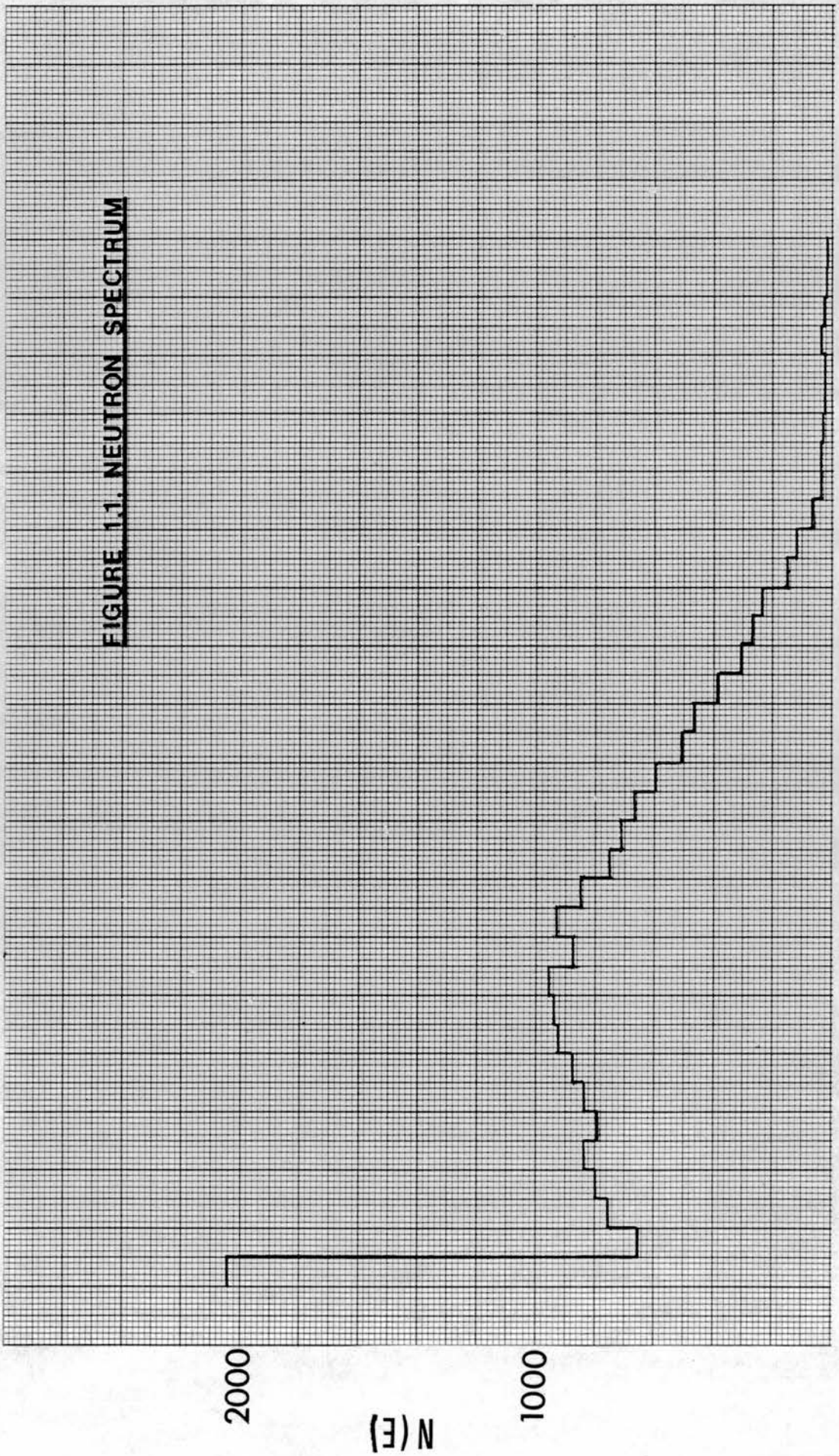

FIGURE 1.1. NEUTRON SPECTRUM

CHAPTER 2

THE DESIGN AND CONSTRUCTION OF THE PARALLEL-PLATE IONIZATION CHAMBER

A schematic diagram of the extrapolation chamber chosen to carry out the objectives described in the previous chapter is shown in Figure 2.1. This is a parallel-plate chamber with relatively large diameter of collecting electrode (3.3cm) to give well-defined geometry and good sensitivity. For large plate separations, however, the electric field may be irregular at the edges of the collecting volume due to space charge effects, the electric field strength being considerably higher at the plates than at the centre of the gap (Boag, 1963).

Two sets of collecting electrodes, high tension electrodes and guard rings of 2mm thickness were constructed of A-150 Shonka tissue-equivalent plastic and graphite. These electrodes were made exchangeable by the construction of specially machined screws of the same materials which hold each set in position.

The plate separation was made adjustable by threading a large support made of perspex for the H.T. electrode onto a smaller support made of P.T.F.E. which accommodates the centre electrode and guard ring. P.T.F.E. was chosen as a base for the collecting electrode because it is not hydrogenous, therefore contributing minimal charge through protons produced by neutron interactions to the collected charge. The outer support although made of perspex, a hydrogenous material, is not so important as far as the hydrogen content is concerned, because any protons should be intercepted by the guard ring before reaching the collecting electrode. Perspex was chosen for ease of machining and rigidity.

A gas flow facility was required for cavity gases at atmospheric and below atmospheric pressures. It would have been very difficult to simultaneously seal off the gas cavity of the chamber and also provide a variable plate separation. Also a pressure differential between the cavity pressure and atmospheric pressure may have distorted both H.T. electrodes, and would probably have resulted in the shattering of the graphite H.T. electrode. For this reason, gas entry and exit apertures were constructed for flow through the chamber of gases such as CO_2 at atmospheric pressure. For pressures below atmospheric, a vacuum tight tank of mild steel with external manometer has been constructed as shown in Figure 2.2. Stainless steel windows of 0.5mm thickness were placed at both end plates. Figure 2.3 shows the relatively large diameter valve (1) which enables the system to be pumped down to low pressures e.g. 10^{-3} Pa ($\sim 10^{-5}$ Torr). The actual pressure range required in this experiment is from 5×10^3 to 10^5 Pa ($\sim$40-760 Torr) but the fact that the apparatus can sustain lower pressures indicates that the leak rate will be minimal. A needle valve (2) enables the desired gas to be introduced in correct quantities, the final required pressure being displayed on a 0 - 1000mm mercury manometer.

To allow the plate separation to be varied remotely while the chamber is contained in the tank, teeth were cut in the outer support of the chamber and a motor was fitted to a rotating support holding a piece of threaded brass (Figure 2.4) which rotates the outer support. A continuous H.T. connection and a counting system in the form of an on-off switch were also required for non-manual and non visual manoeuvring. Electrical connections (3) to the chamber were made through the back of the tank (Figure 2.3).

The collected charge is displayed on a Keithley Digital Electrometer, Model 616, as integrated charge. Connection was made from the electrometer to the chamber via triax cable, the outer screen of which carries the H.T. voltage, the inner screen connecting the guard ring to earth potential and the central conductor connecting the centre electrode to the electrometer input. The fact that the plate separation is variable required the precaution of an 'electrometer protection circuit' (Appendix 1) as designed by Bottrill and Jeffries (1979) in the event of the H.T. electrode touching the collecting electrode.

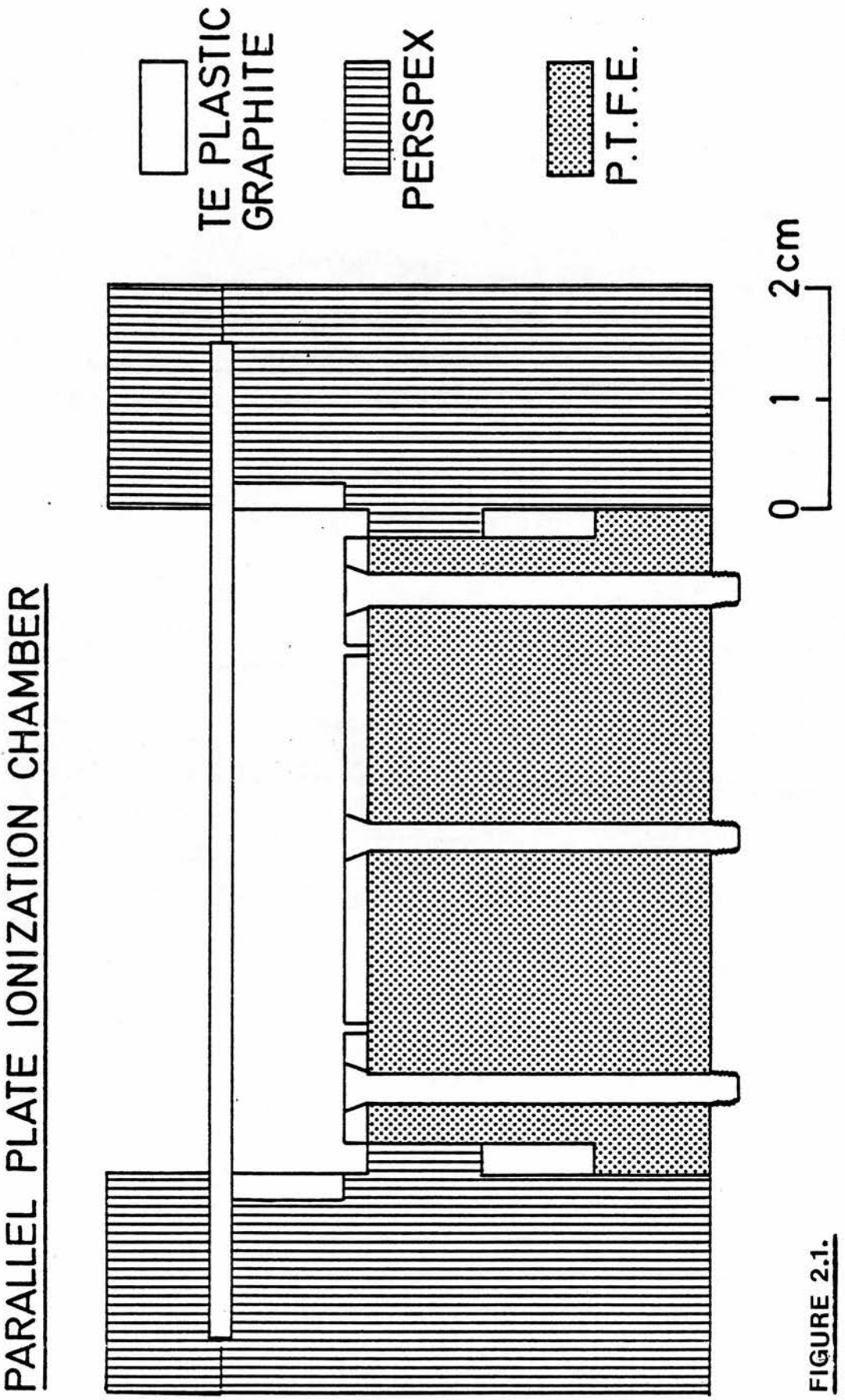
PARALLEL PLATE IONIZATION CHAMBER
TE PLASTIC GRAPHITE
PERSPEX
P.T.F.E.
0
1
2cm

FIGURE 2.1.

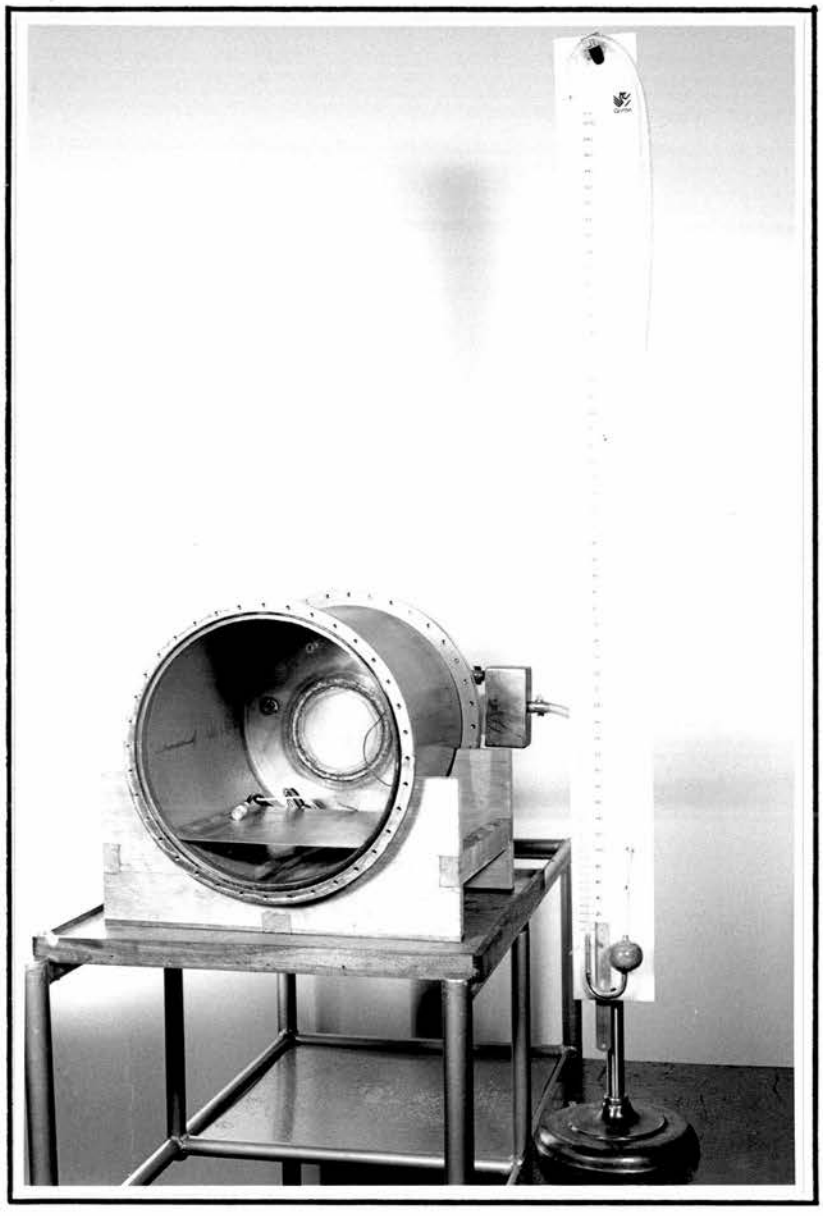

FIGURE 2.2.

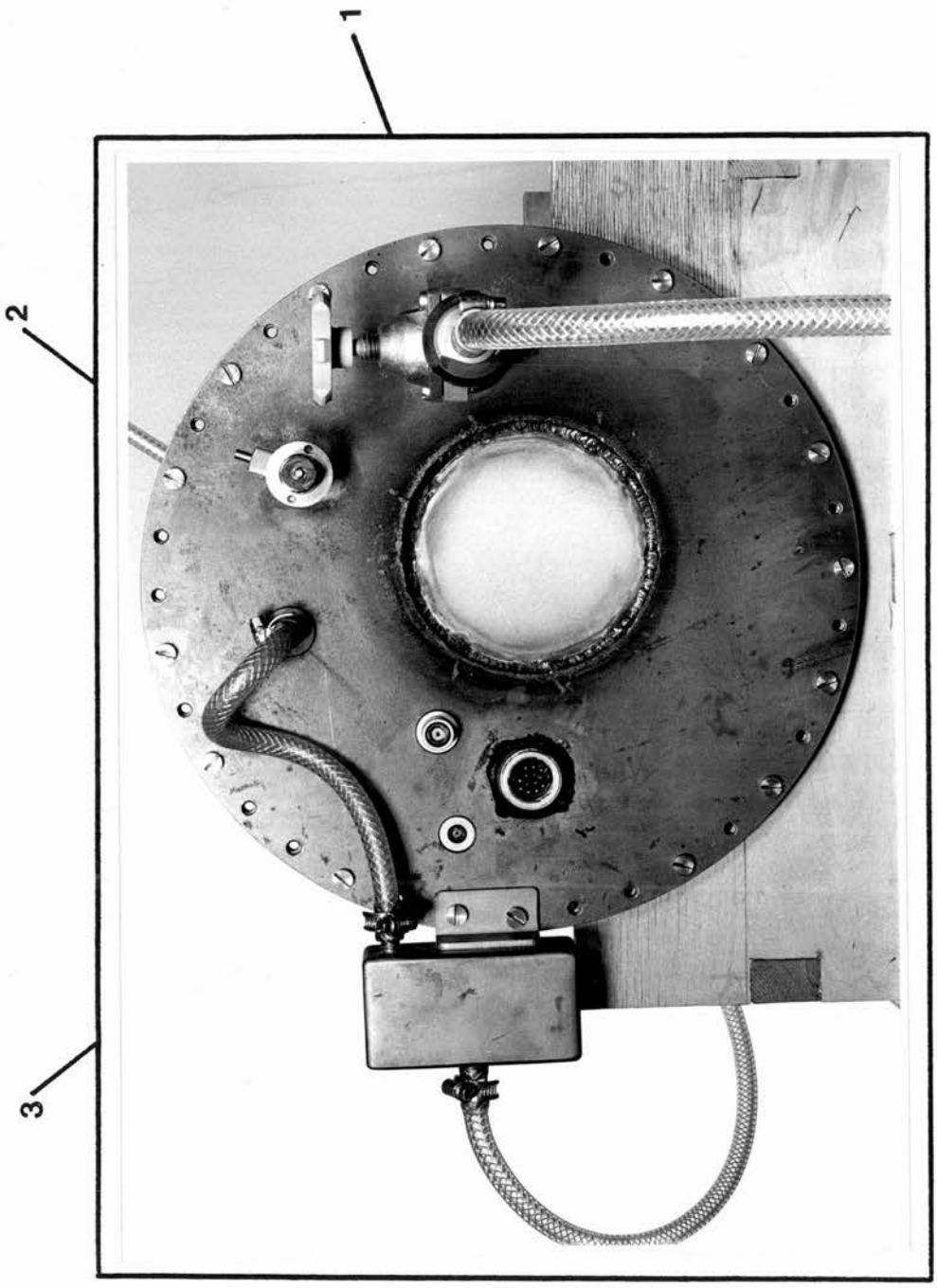

FIGURE 2.3.

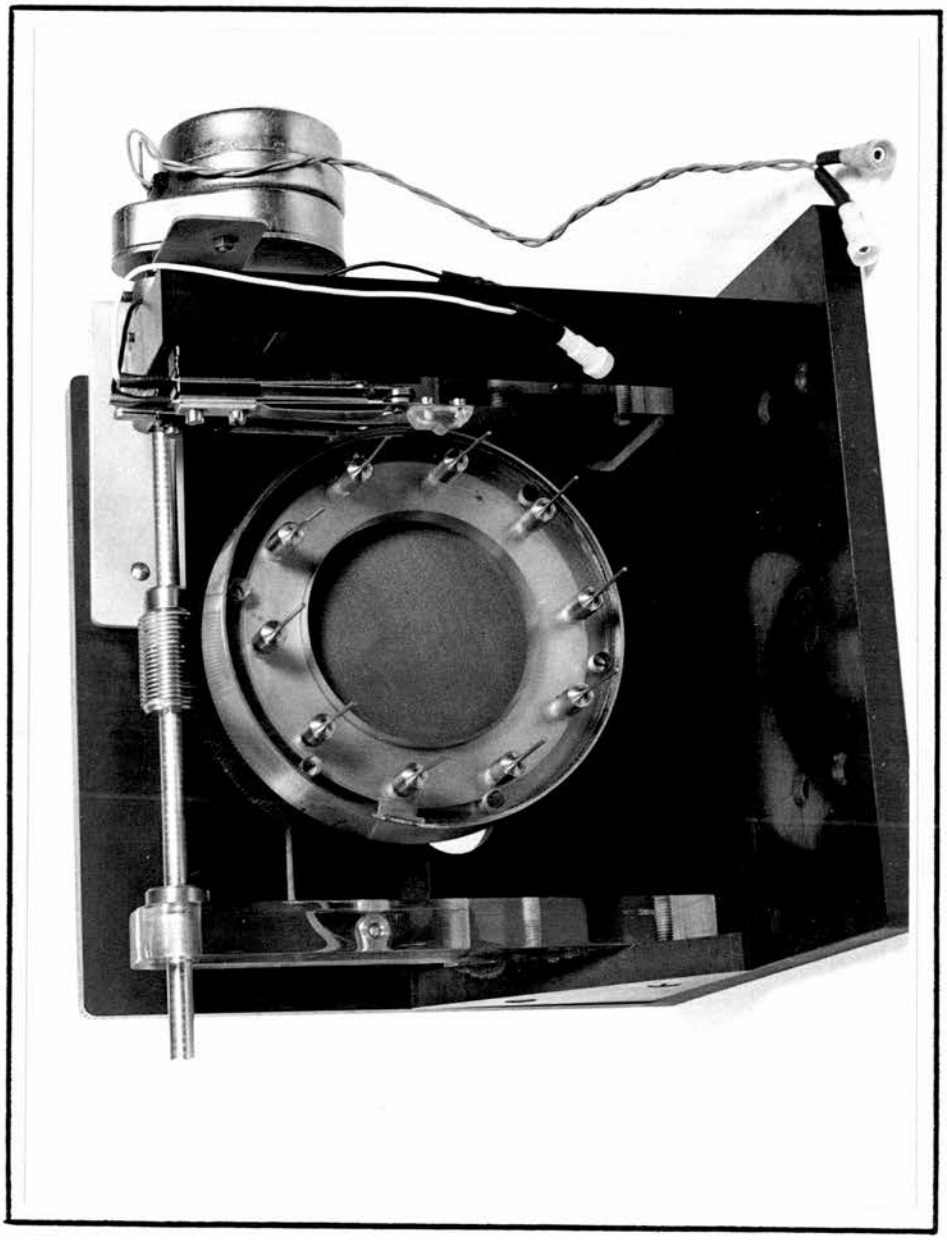

FIGURE 2.4.

CHAPTER 3

PROBLEMS OF THE IONIZATION CHAMBER

To test if the ionization chamber functioned properly, the saturation characteristics of the tissue-equivalent (TE)/air and graphite (C)/air configurations when exposed to 250 kv X-rays, were measured.

According to Greening (1964), the predominant recombination process expected for X-rays is general or volume recombination which follows the relationship:-

$$\frac{1}{q} = \frac{1}{q_{sat}} + \frac{\text{constant}}{V^2} \qquad (3.1)$$

where q is the measured charge, q_{sat} is the saturation charge and V is the polarizing voltage.

Thereafter, a measurement of charge per unit volume was expected to be constant for an X-ray source.

Charge measurements were made using a Keithley Digital electrometer, with dose comparisons obtained using a second graphite ionization thimble type chamber. The X-ray source was a Siemens 250 kv X-ray set (2.7mm Cu H.V.L.).

3.1 Saturation Measurements

The first saturation measurements of the basic chamber, both in the TE/air and C/air configurations, did not follow the linear relationship

of equation (3.1). Instead $1/V^2$ varied as $1/q^n$, where $n > 1$. The following modifications were therefore made:-

3.1.1 Screening

The non-linear relationship would have been present if there was radiation induced leakage from the PTFE and perspex supports, (Fowler, 1956),(Fowler et al., 1955, 1954). To combat this effect, these supports were coated with a conducting layer of DAG (Graphite diluted in alcohol), which effectively screened all external surfaces. A continuous earthed connection was required at the back of the chamber to allow the variation of plate separation.

3.1.2 Air Gaps

The additional contribution to the collected charge at high voltages, may have originated at the rear of the collecting screw, where a section of unscreened cable was exposed to the surrounding air. A new collecting system was implemented, which involved a specially fabricated nut (Fig. 3.1). A BNC connector was housed in a brass nut, which in turn was housed in a 'Tufnol' support, all gaps being filled with silicon rubber solution.

3.1.3 Insulating Tissue-Equivalent Guard Ring

Certain problems may have arisen from the use of a TE plastic guard ring. Due to the small gap between the high voltage electrode and the guard ring, there could be a small current flowing across the surface of the insulator to the guard. TE plastic can have a high surface resistance of up to 1MΩ according to ICRU 26.

A high resistance at the contact between the retaining screw and the plate, and a high resistance at the point at which the screw is connected to the inner screen might have caused a potential difference between the guard ring and earth due to this leakage current.

This would in turn create a potential difference between the collecting electrode and guard ring, thereby causing irregular field patterns and inaccurate charge collection (Boag, 1964).

To eliminate the problem entirely, the poorly conducting TE guard ring was discarded and the conducting graphite guard ring used in all chamber configurations.

3.1.4 Polarity Effect

After the above modifications were made, the chamber exhibited an unexpected polarity effect. Most ionization chambers exhibit a polarity effect to a greater or lesser degree, with many possible causes, e.g. contact, thermal or electrolytic emf's in the measuring circuit, the different mobilities of +ve and -ve ions, space charge distortion of electric field in the gas etc. (Boag, 1966). The resulting saturation curves for positive and negative polarizing voltages normally have the same value of slope, one being displaced from the other by a constant amount. This, however, was not the case for either the TE/air or C/air chambers. For negative polarizing voltages, the saturation curves followed the linear relationship of equation (3.1), but for positive polarizing voltages, $1/V$ varied as $1/q^M$, where $M > 1$.

This could have been because of a difference in property of the collecting electrode and guard ring, e.g. their surfaces non-planar, or a difference in their potential. To test if this was the case, large collecting electrodes of both TE plastic and graphite with the same outer diameter as the guard rings were used in the chamber without a guard ring present. The resulting saturation curves did not follow the linear relationship of equation (3.1), (and were not expected to do so for a variety of reasons, for example, air gaps, no guard ring to intercept any leakage current and badly defined electric fields because of the resulting shape of the collecting volume) but were similar for both positive and negative polarizing voltages.

If there was a difference in potential between the collecting electrode and the guard ring, this could have been due to a contact potential between graphite and brass and TE plastic and brass, resulting in the situation described in section (3.1.3). A potential was applied to the guard ring, which was varied such that at both positive and negative low polarizing voltages, the collected charge readings were similar. This occured at 0.084 $\pm$ 0.005V for the graphite chamber and 0.100 $\pm$ 0.005V for the TE chamber.

The resulting saturation curves now followed the linear relationship of equation (3.1) for both positive and negative polarities and all plate separations.

3.2 Charge Per Unit Volume Measurements

The charge per unit volume was measured by varying the plate separation (d) and calculating the saturation charge per unit plate separation (q_{sat}/d) which should be constant for an X-ray source. As shown in Table 3.1, q_{sat}/d was not constant for either the TE/air or C/air chambers.

3.2.1 Large Insulating Gap between Centre Electrode and Guard Ring

The additional charge at small d was thought to originate from the relatively large gap of 1mm between the collecting electrode and guard ring. For a 1mm plate separation the collecting volume is supposed to be $0.855 cms^3$. This additional volume is $0.021 cms^3$ which would have contributed a maximum of 2.46% to the collecting volume. There would also have been field distortion at the edges of the collecting volume.

A PTFE ring was constructed such that it would fill the gap between the collector and guard ring. This ring was used in two forms, first as an insulator between collector and guard ring, and secondly with a conducting layer of DAG on the upper surface to minimise the insulating gap (Fig. 3.2). In both cases, measurement of q_{sat}/d as a function of d, indicated that there was still field distortion.

Therefore, a new guard ring of smaller inner diameter had to be constructed to minimise the additional volume: the estimated gap width is now 0.2mm. New saturation curves with no potential applied

to the guard ring now followed the relationship of equation (3.1), indicating that the polarity effect was not due to a difference in potential between collector and guard ring but due to the insulating gap being too large (Love et al. 1935). The applied potential would have counteracted this effect.

3.2.2 Plate Separation Inaccuracy

An accurate method of measurement of plate separation must be used to ensure accurate q_{sat}/d measurements. Originally d was determined by placing a spacer of thickness 5mm between the collector and H.T. electrode, and each subsequent revolution increasing or reducing d by 1mm. This method assumed the thread pitch to be exactly 1mm. Another method was to set the exact distance from the inside face of the H.T. electrode to the centre electrode, using a depth micrometer. This method again assumed that the thread pitch was exactly 1mm and that all faces were exactly parallel and planar.

The most accurate method was to take measurements from an independent origin. By placing the chamber on a stationary solid object (e.g. the bed of a milling machine) and measuring the horizontal movement with a dial test indicator, d could be set to the desired value, and subsequent errors in thread pitch could be measured. Table 3.2 shows that with an accurate d = 10mm setting, the subsequent error in thread pitch can be as much as 6% at d = 1mm.

Using this method of determination of d, the saturation charge per unit volume was constant for both C/air and TE/air chambers when

exposed to 250kv X-rays (Table 3.3). The corresponding saturation characteristics for both TE/air and C/air chambers are shown in Figures 3.3 and 3.4 for plate separations of 10.0, 8.03, 6.05, 4.06, 2.06 and 1.06mm.

TABLE 3.1

	TE/air Chamber	C/air Chamber
d. mms.	q_{sat}/d (10^{-8}Cmm^{-1})	q_{sat}/d (10^{-8}Cmm^{-1})
10	0.588	0.565
8	0.584	0.566
6	0.591	0.572
4	0.605	0.576
3	0.616	0.580
2	0.636	0.590

The results for TE/air and C/air are not comparable.

TABLE 3.2

No. of clockwise revolutions	Plate Separation assuming 1mm thread pitch (mm)	Actual plate separation (mm ± 0.005 mm)
0	10.0	10.000
1	9.0	9.018
2	8.0	8.029
3	7.0	7.033
4	6.0	6.048
5	5.0	5.055
6	4.0	4.055
7	3.0	3.055
8	2.0	2.055
9	1.0	1.055

TABLE 3.3

	TE/Air Chamber		C/Air Chamber	
d(mms) ± 0.005mm	$(q_{sat}/d)_1$ $(10^{-8}Cmm^{-1})$	$(q_{sat}/d)_2$ $(10^{-8}Cmm^{-1})$	$(q_{sat}/d)_1$ $(10^{-8}Cmm^{-1})$	$(q_{sat}/d)_2$ $(10^{-8}Cmm^{-1})$
10.0	0.614	0.612	0.612	0.610
8.029	0.615	0.610	0.612	0.610
6.048	0.611	0.612	0.611	0.610
4.055	0.613	0.611	0.613	0.613
2.055	0.611	0.610	0.618	0.617
1.055	0.613	0.613	0.612	0.613

$(q_{sat}/d)_1$ uses the value of q_{sat} obtained from a saturation curve.

$(q_{sat}/d)_2$ measures one value of collected charge q at one particular polarizing voltage. q is corrected for saturation to obtain q_{sat}.

The results for TE/Air and C/Air chambers are not comparable.

REAR CONNECTOR OF IONIZATION CHAMBER

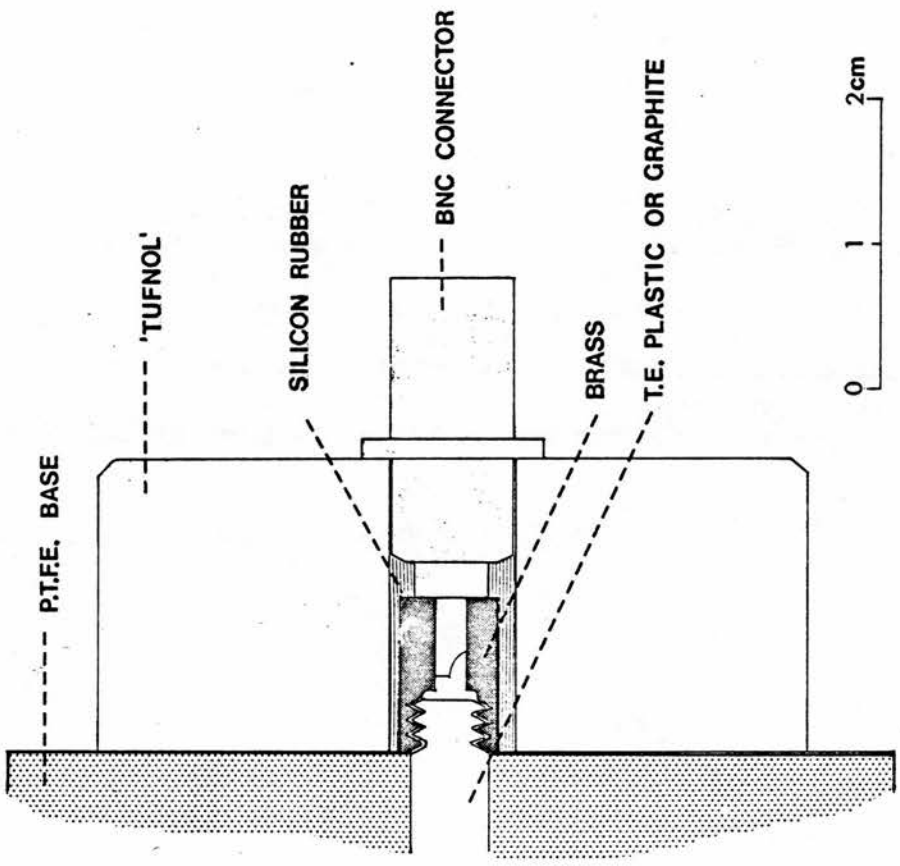

FIGURE 3.1.

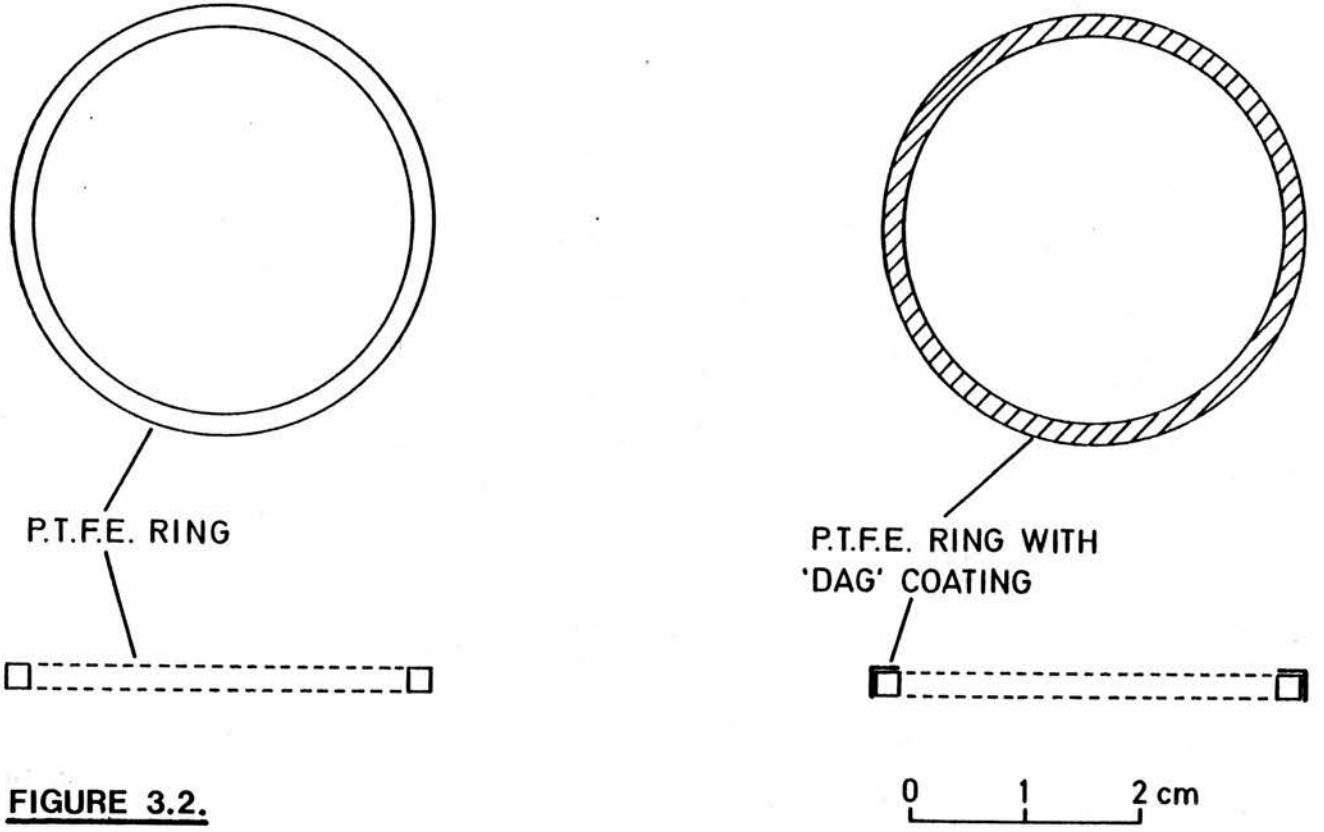

FIGURE 3.2.

FIGURE 3.3 SATURATION CHARACTERISTICS OF T.E. PLASTIC/ AIR CHAMBER EXPOSED TO 250KV X-RAYS

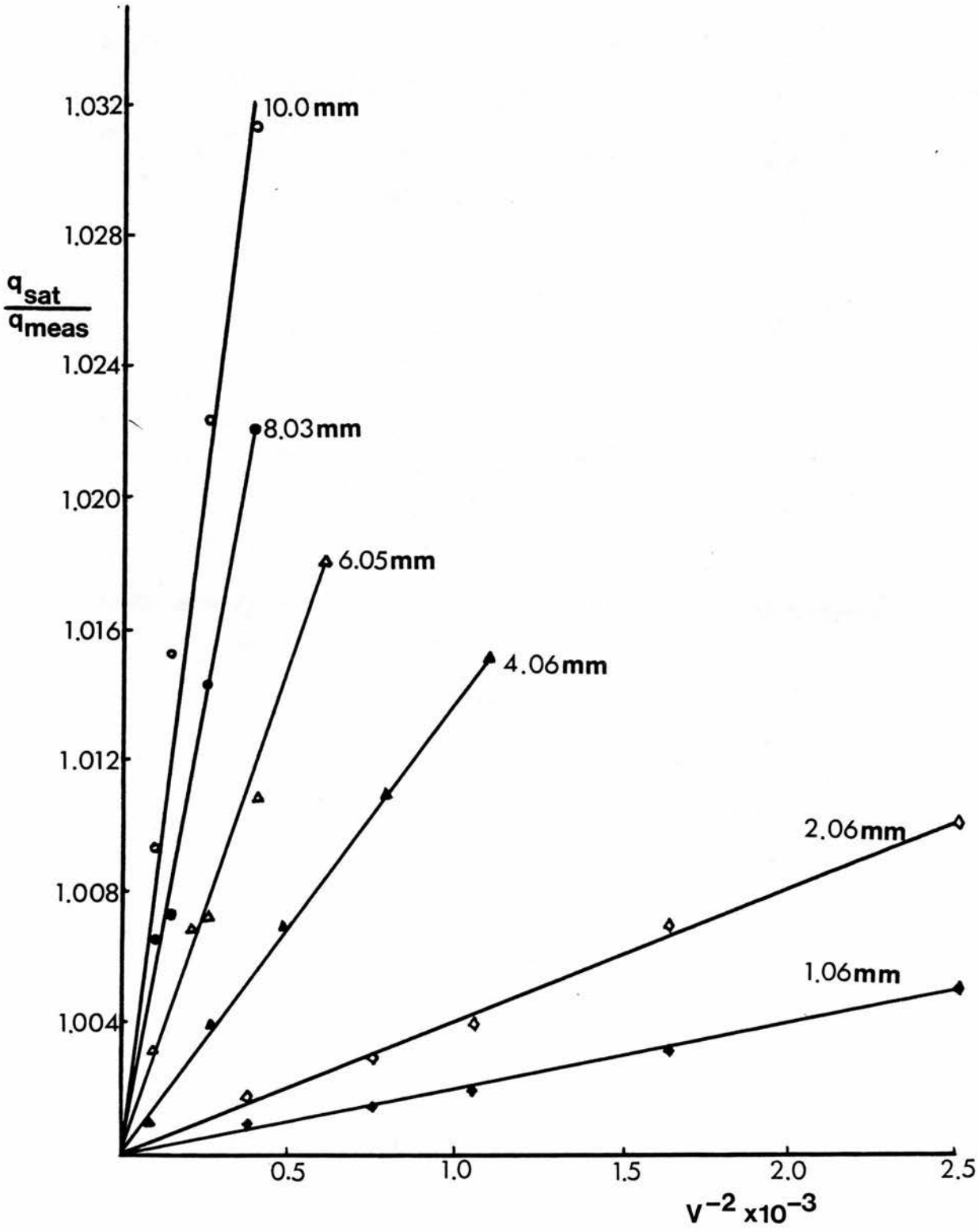

FIGURE 3.3.

FIGURE 3.4 SATURATION CHARACTERISTICS OF GRAPHITE/AIR CHAMBER EXPOSED TO 250KV X-RAYS

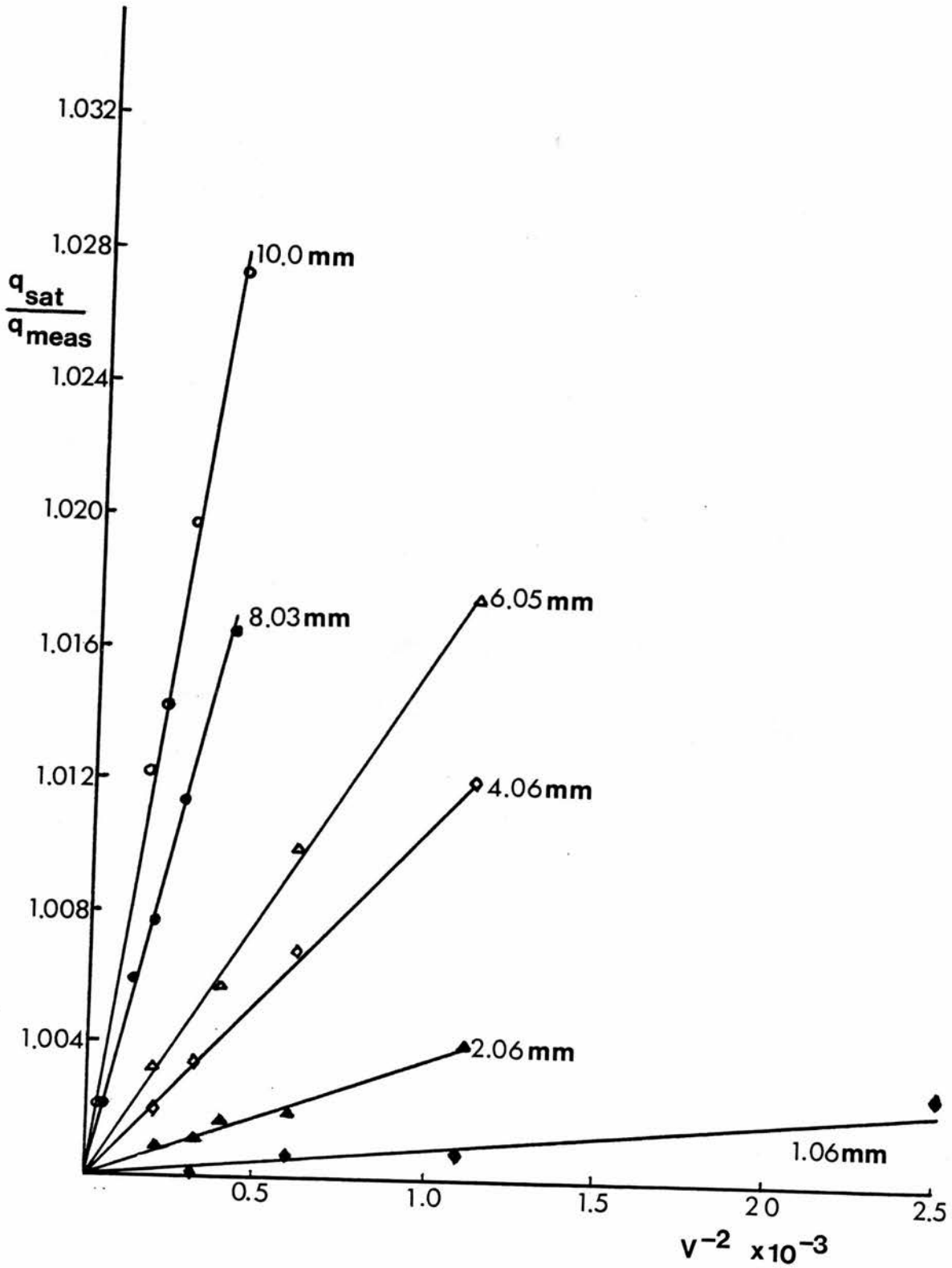

FIGURE 3.4.

CHAPTER 4

IONIZATION MEASUREMENTS AT ATMOSPHERIC PRESSURE

4.1 Experimental Arrangement

The design of the Fixed Horizontal Beam (FHB) of the MRC Cyclotron is shown in Fig. 4.1, the physical aspects of which have been described by Williams et al. (1979). The front surface of the ionization chamber was placed at a distance of 125cm FSD (Fig. 4.2), which, for experimental purposes, means that the distance from the end of the collimator to the front surface of the ionization chamber is 33cm. This distance was maintained when the ionization chamber was contained in the pressure tank, or corrections made accordingly. The 11 x 11cm and 12 x 10cm collimators were used throughout to give uniform dose distribution over the collecting area of the chamber.

The calibration of the FHB was checked at regular intervals using a conducting polythene/air thimble type chamber, which is calibrated against an A-150 tissue-equivalent chamber which was used as a calibration standard. A set of readings from the polythene/air chamber was also obtained before neutron irradiation of the extrapolation chamber, thereby relating all subsequent charge measurements.

4.1.1 Saturation Characteristics

The type of recombination expected for neutron irradiation is initial recombination. The procedure for the determination of saturation charge in the presence of initial recombination is based on the Jaffé theory of Columnar Ionization (Zanstra, 1935). Most of the ionization

is secondary, as the primary particle leaves along its tracks clusters of secondary ions. If these clusters are close enough together, they become cylindrical in shape, hence columnar. The ion density at distance r from the axis is proportional to e^{-b^2/r^2} where b is the initial radius of column.

The fraction of ions which escapes recombination is:-

$$\frac{N}{No} = \frac{1}{1+\frac{\alpha No}{8\pi D} f(x)} = \frac{\text{measured charge}}{\text{saturation charge}} \qquad (4.1)$$

where α = recombination coefficient

No = number of ion pairs per cm of path length

D = diffusion coefficient

$f(x) = e^{x} \frac{i\pi}{2} H_o^{(1)} (ix)$, H_o is a Hankel function (Zanstra, 1935)

$$x = \left(\frac{bk}{2D} X \sin \phi\right)^2 \qquad (4.2)$$

where k = average mobility

X = $\frac{\text{polarizing voltage}}{\text{plate separation}}$

$\sin\phi$ = average angular distribution

Re-arranging equation 4.1 -

$$\frac{1}{q_{meas}} = \frac{1}{q_{sat}} + \frac{g\, f(x)}{q_{sat}} \qquad (4.3)$$

For each value of x, f(x) can be obtained from Zanstra's tables. For $x > 10$, Zanstra approximates f(x) to $(\pi/2x)^{\frac{1}{2}}$; it is normally assumed

that this approximation holds and that f(x) is therefore proportional to V^{-1}.

From equation 4.3 -

$$\frac{1}{q_{meas}} = \frac{1}{q_{sat}} + \frac{\text{constant}}{V} \qquad (4.4)$$

4.1.1.1 TE Plastic Chamber Saturation Curves

As shown in Figures 4.3 and 4.4, the normalized relationship of q_{sat}/q_{meas} against 1/V provides an adequate extrapolation procedure for the TE plastic chamber with both air and TE gas filling at all plate separations. A linear regression calculation has been performed on all the measured charge values in order to obtain the most accurate values of saturation charge. The values of saturation charge at all plate separations for both TE/Air and TE/TE chambers are shown in Table 4.1. Using this saturation method of determination, the amount of ionization per increment of plate separation is constant in the range 1 - 10mm, within an experimental error of $\pm$ 1%.

4.1.1.2 Graphite Chamber Saturation Curves

Pearson et al. (1979) have pointed out that a problem may arise with the use of gases other than air in a graphite ionization chamber due to the porosity of graphite. At high flow rates, the porosity of graphite should not present any problems as the flow rate of, for example, CO_2, would be greater than the rate of diffusion of air back into the chamber. If the gas flow rate was not sufficiently high, the cavity gas would be impure and an

ionization error would arise. To avoid the issue entirely, the ionization chamber could be placed in the vacuum tight tank filled with the required gas.

To find out if the porosity of graphite would affect ionization measurements, and to obtain the saturation characteristics of the graphite chamber with pure cavity gases, saturation measurements were made both in air atmosphere and cavity gas atmosphere.

4.1.1.2.1. Graphite/Air Saturation Curves

As shown in Fig. 4.5 the normalized relationship of q_{sat}/q_{meas} against 1/V again provides an adequate extrapolation procedure for the graphite/air chamber at all plate separations. The values of saturation charge are shown in Table 4.2, and show a constant q_{sat}/d for plate separations in the range 1 - 5mm, to within an experimental error of $\pm$ 0.5%. There is a slight increase in q_{sat}/d in the range 6 - 8mm, which may be incorporated in a constancy from 1 - 8mm to within an experimental error of $\pm$ 1%. There is then a definite increase in q_{sat}/d for plate separations of 9 and 10mm.

4.1.1.2.2 Saturation Curves for both Graphite/TE gas in Air Atmosphere and Graphite/TE gas in TE gas Atmosphere

As shown in Figures 4.6 and 4.7, both sets of curves follow the relationship of equation (4.4) as an extrapolation procedure at all plate separations. The values of saturation charge for both cases are shown in Table 4.3. At all plate separations, the values

of q_{sat}/d for the chamber in an air atmosphere are less than q_{sat}/d values in a TE gas atmosphere, the largest difference being a 2.9% difference at 8mm.

This would indicate that there is, in fact, air contamination of the TE cavity gas when the chamber is in an air atmosphere. This is further confirmed by comparing Tables 4.2 and 4.3(ii), where the q_{sat}/d values in Table 4.3(ii) correspond to a pure TE cavity gas. The neutron sensitivity of the graphite/air chamber is lower than that of the graphite/TE gas chamber, so air contamination of the TE gas would result in lower q_{sat}/d values.

Regarding Table 4.3(ii), graphite/TE gas chamber in TE gas atmosphere, q_{sat}/d is constant in the range 1 - 6mm to within an experimental error of $\pm$ 1%, then there is a steady increase in q_{sat}/d for plate separations in the range 6 - 10mm.

4.1.1.2.3 Saturation Curves for Both Graphite/CO_2 in Air Atmosphere and Graphite/CO_2 in CO_2 Atmosphere.

The Jaffé approximation of q_{sat}/q_{meas} as a function of 1/V does not provide the required extrapolation procedure as shown in Figures 4.8 and 4.9. Therefore, a modification of the Jaffé theory, involving the Jaffé function f(x), must be used as follows.

From equation (4.2), the product bk/2D sin ϕ (= Z) is a constant value for a particular gas at a particular pressure. The value of Z which corresponds to a linear relationship of q_{sat}/q_{meas} and f(x), equation 4.3, can be determined by adopting a trial and error numerical procedure.

Values of Z are fed into a Fortran computer programme to obtain a series of q_{sat}/q_{meas} against f(x) for 3 plate separations, 10, 5 and 1mm. A further Fortran programme performed a linear regression on this series of graphs. A single value of Z corresponds to the best agreement between q_{sat}/q_{meas} by experiment and q_{sat}/q_{meas} after linear regression for the 3 plate separations. This value of Z was, therefore, used in the Jaffé theory for all plate separations.

For a Graphite/CO_2 chamber, both in an air atmosphere and in a CO_2 atmosphere, a value of Z = 0.006 $\pm$ 0.0005 produces a linear relationship between q_{sat}/q_{meas} and f(x) for all plate separations as shown in Figures 4.10 and 4.11.

If the scattering distribution is assumed to be isotropic, then the average angular distribution is 45° and sin ϕ = 0.707, giving a value of bk/2D = 0.008 for CO_2 at atmospheric pressure.

The values of q_{sat}/d for the Graphite/CO_2 chamber both in air atmosphere and CO_2 atmosphere are shown in Table 4.4. Again, at all plate separations, the values of q_{sat}/d for the chamber in an air atmosphere are less than q_{sat}/d values in a CO_2 atmosphere, the largest difference being 2.9% at 8mm. This would again indicate that there is air contamination of CO_2 in the gas cavity, since, from Tables 4.2 and 4.4(ii), it is shown that the neutron sensitivity of the graphite/air is lower than that of the graphite/CO_2 chamber.

Regarding Table 4.4(ii), Graphite/CO_2 chamber in CO_2 atmosphere, there is a sharp decrease in q_{sat}/d in the range 1 - 6mm, thereafter q_{sat}/d is constant in range 7 - 10mm to within an experimental error of $\pm$ 1%.

4.2 Measurement of q_{sat}/d at Fixed Polarizing Voltages

q_{sat}/d for each plate separation was also measured by varying the plate separation while keeping a fixed polarizing voltage on the H.T. electrode, then correcting each q_{meas} for saturation effects. This was done to minimize any errors resulting from the saturation curves, for example:

4.2.1 The saturation curves making up a set of curves for each chamber combination may not all have been obtained on the same day, therefore, introducing an additional error between q_{sat}/d for each plate separation. This error is therefore a function of the second reference ionization chamber and is not likely to be greater than $\pm 1\%$.

4.2.2 The F.S.D. setting of the chamber may not be consistent from day to day. This error is probably within $\pm$ 2mm at a required F.S.D. of 125cm, so would contribute $\pm$ 0.3% to the overall error.

4.2.3 There may also be a 'soakage' error associated with saturation curve measurement. After each measurement q_{meas}, there may be a residual charge left in the graphite or TE plastic plates of the ionization chamber, which may add or subtract to the next reading of q_{meas}, depending on the magnitude of the polarizing voltage.

The same combinations of chamber wall and gas materials were investigated and the results are shown in Tables 4.1 - 4.4. Comparing these results, there appears to be very good agreement between q_{sat}/d measured by a saturation curve and q_{sat}/d obtained at a fixed voltage, to within an experimental error of $\pm$ 1.5%, indicating that the error between saturation curves is minimal and that there is no apparent indication of any 'soakage' problem.

4.3 (q_{sat}/d) in the Range d = 10 → 18mm

It has been established that the ionization chambers are functioning correctly, and that the method of extrapolation to (q_{sat}/d) is adequate. In order to obtain maximum data from all chambers, q_{sat}/d was measured in the range d = 10 → 18mm for each chamber combination.

The results for the TE/Air and the TE/TE chambers overlap with values of q_{sat}/d in the range 1 → 10mm i.e. measurement of q_{sat}/d results in values of $0.285 \times 10^{-8} Cmm^{-1}$ and $0.355 \times 10^{-8} Cmm^{-1}$ for TE/Air and TE/TE chambers respectively, at all plate separations.

Values of q_{sat}/d for C/Air, C/CO_2 and C/TE in the range 10 → 18mm are shown in Table 4.5 and again there is an overlap between the 1 → 10mm and 10 → 18mm results. q_{sat}/d values for C/CO_2 and C/TE chambers were obtained in a CO_2 and TE environment respectively.

TABLE 4.1

Plate separation d (mm)	TE/Air :- q_{sat}/d (10^{-8}Cmm^{-1})		TE/TE :- q_{sat}/d (10^{-8}Cmm^{-1})	
	(a)	(b) V = -300V	(a)	(b) V = -300V
1.055	0.288	0.288	0.355	0.358
2.055	0.288	0.288	0.356	0.354
3.055	0.288	0.287	0.358	0.355
4.055	0.287	0.287	0.354	0.354
5.055	0.285	0.284	0.352	0.355
6.048	0.285	0.283	0.352	0.353
7.033	0.282	0.283	0.353	0.354
8.029	0.286	0.282	0.352	0.352
9.018	0.287	0.283	0.356	0.353
10.000	0.287	0.284	0.359	0.356

(a) q_{sat}/d obtained from saturation curve measurements.

(b) q_{sat}/d obtained from fixed voltage measurements.

TABLE 4.2

Plate separation d (mm)	C/Air :- q_{sat}/d (10^{-8} Cmm^{-1})	
	(a)	(b) V = -300V
1.055	0.0604	0.0606
2.055	0.0609	0.0606
3.055	0.0605	0.0603
4.055	0.0607	0.0605
5.055	0.0607	0.0608
6.048	0.0614	0.0611
7.033	0.0615	0.0613
8.029	0.0615	0.0612
9.018	0.0622	0.0616
10.000	0.0630	0.0623

(a) and (b) as Table 4.1

TABLE 4.3

(i) C/TE gas in air atmosphere			(ii) C/TE gas in TE gas atmosphere		
Plate separation d (mm)	q_{sat}/d (10^{-8}Cmm^{-1})		Plate separation d (mm)	q_{sat}/d (10^{-8}Cmm^{-1})	
	(a)	(b) V=-300V		(a)	(b) V=-300V
1.055	0.0808	0.0811	1.055	0.0813	0.0817
2.055	0.0794	0.0795	2.062	0.0812	0.0815
3.055	0.0798	0.0795	3.169	0.0823	0.0824
4.055	0.0792	0.0796	4.263	0.0821	0.0817
5.055	0.0805	0.0813	5.356	0.0811	0.0814
6.048	0.0802	0.0828	6.446	0.0825	0.0822
7.033	0.0813	0.0839	7.539	0.0835	0.0830
8.029	0.0830	0.0860	8.635	0.0855	0.0841
9.018	0.0860	0.0870	9.720	0.0866	0.0853
10.000	0.0874	0.0883	10.811	0.0879	0.0867

(a) and (b) as Table 4.1

TABLE 4.4

(i) C/CO_2 in air atmosphere			(ii) C/CO_2 in CO_2 atmosphere		
Plate separation d (mm)	q_{sat}/d (10^{-8}Cmm^{-1})		Plate separation d (mm)	q_{sat}/d (10^{-8}Cmm^{-1})	
	(a)	(b) V=-300V		(a)	(b) V=-300V
1.055	0.0808	0.0898	1.055	0.0899	0.0901
2.055	0.0853	0.0841	1.962	0.0859	0.0897
3.055	0.0813	0.0806	2.969	0.0834	0.0867
4.055	0.0801	0.0795	3.963	0.0814	0.0844
5.055	0.0770	0.0769	4.956	0.0792	0.0834
6.048	0.0775	0.0775	5.946	0.0779	0.0818
7.033	0.0763	0.0756	6.939	0.0785	0.0789
8.029	0.0756	0.0731	7.935	0.0778	0.0791
9.018	0.0772	0.0737	8.920	0.0775	0.0781
10.000	0.0776	0.0741	9.911	0.0781	0.0788

(a) and (b) as Table 4.1

TABLE 4.5

Plate Separation d (mm)	C/Air	C/CO_2	C/TE
	q_{sat}/d (10^{-8} Cmm^{-1})		
10.0	0.0629	0.0780	0.0870
11.0	0.0632	0.0775	0.0883
12.0	0.0637	0.0780	0.0901
13.0	0.0640	0.0775	0.0920
14.0	0.0641	0.0780	0.0933
15.0	0.0647	0.0786	0.0950
16.0	0.0649	0.0780	0.0961
17.0	0.0650	0.0780	0.0970
18.0	0.0653	0.0777	0.0997

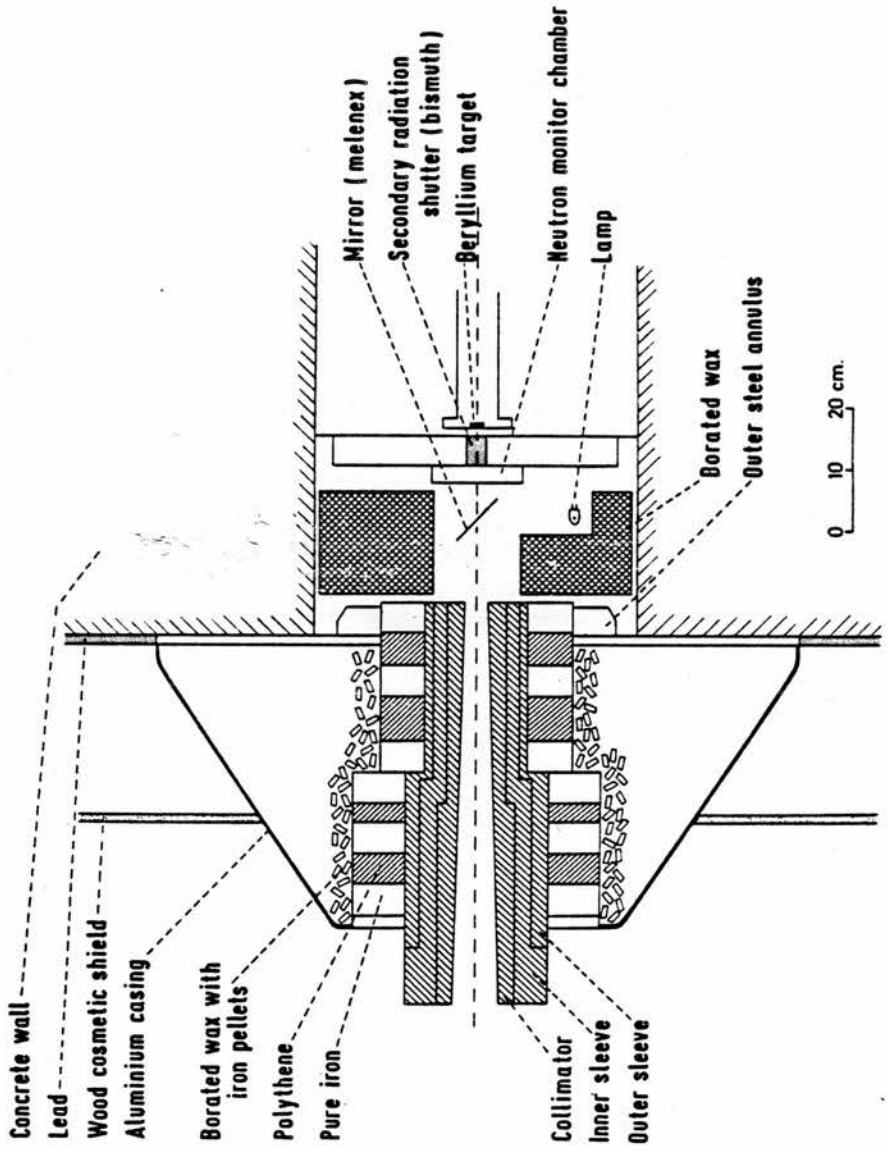

FIGURE 4.1.; FIXED HORIZONTAL BEAM

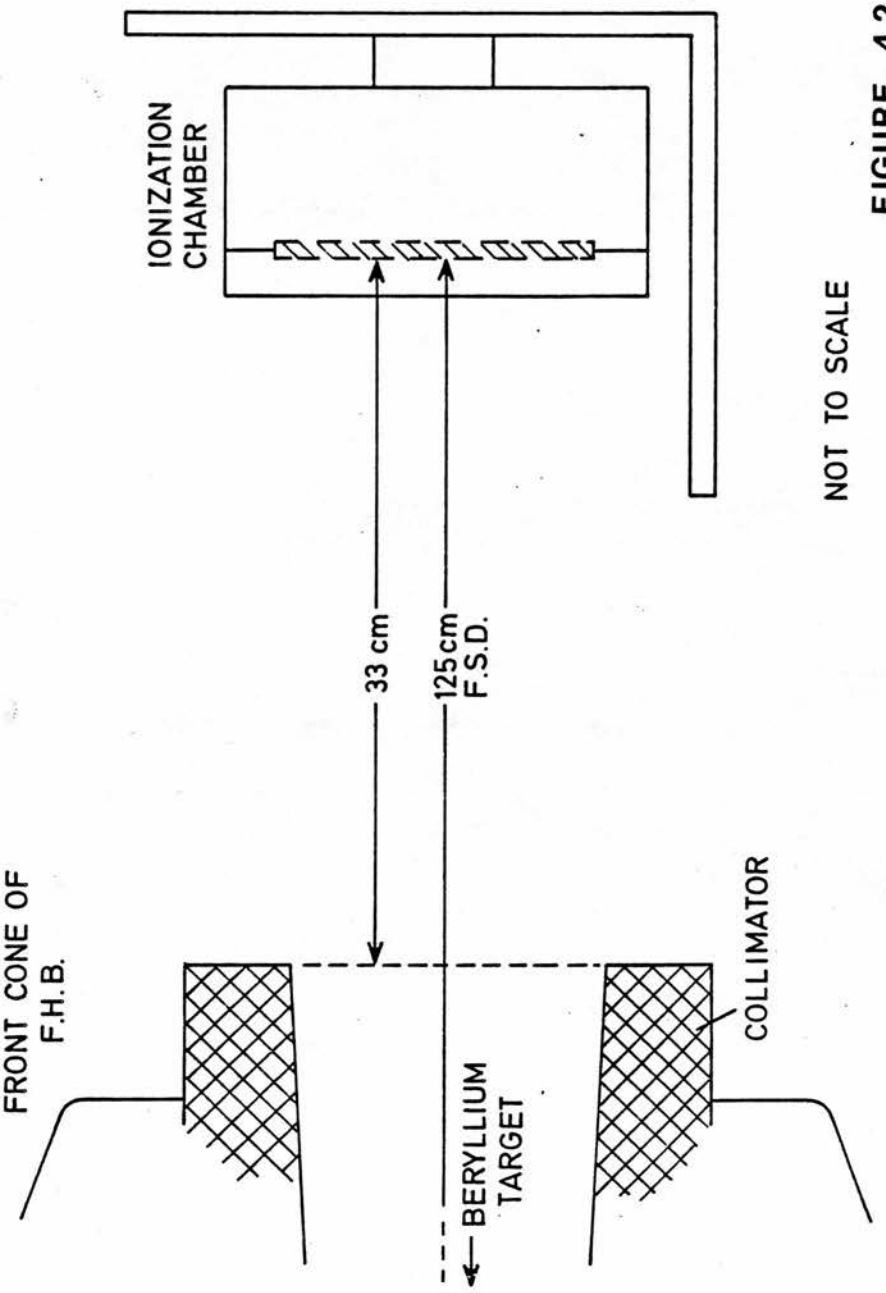
IONIZATION CHAMBER
33 cm
125cm F.S.D.
FRONT CONE OF F.H.B.
BERYLLIUM TARGET
COLLIMATOR
NOT TO SCALE

FIGURE 4.2.

FIGURE 4.3 SATURATION CHARACTERISTICS OF T.E. PLASTIC/ AIR CHAMBER EXPOSED TO d(15MeV) + Be NEUTRONS

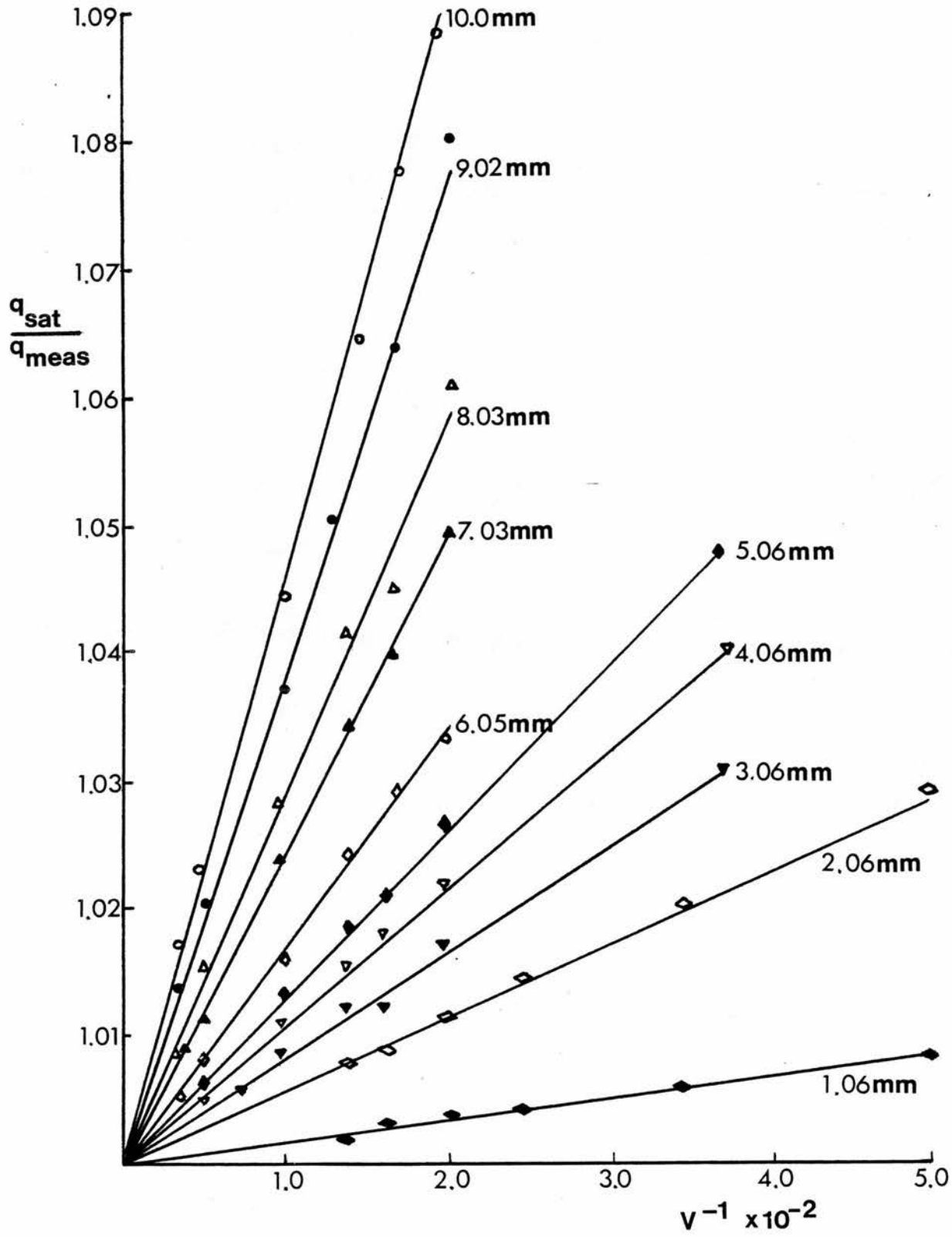

FIGURE 4.3.

FIGURE 4.4 SATURATION CHARACTERISTICS OF T.E. PLASTIC/ T.E. GAS CHAMBER EXPOSED TO d(15MeV) + Be NEUTRONS

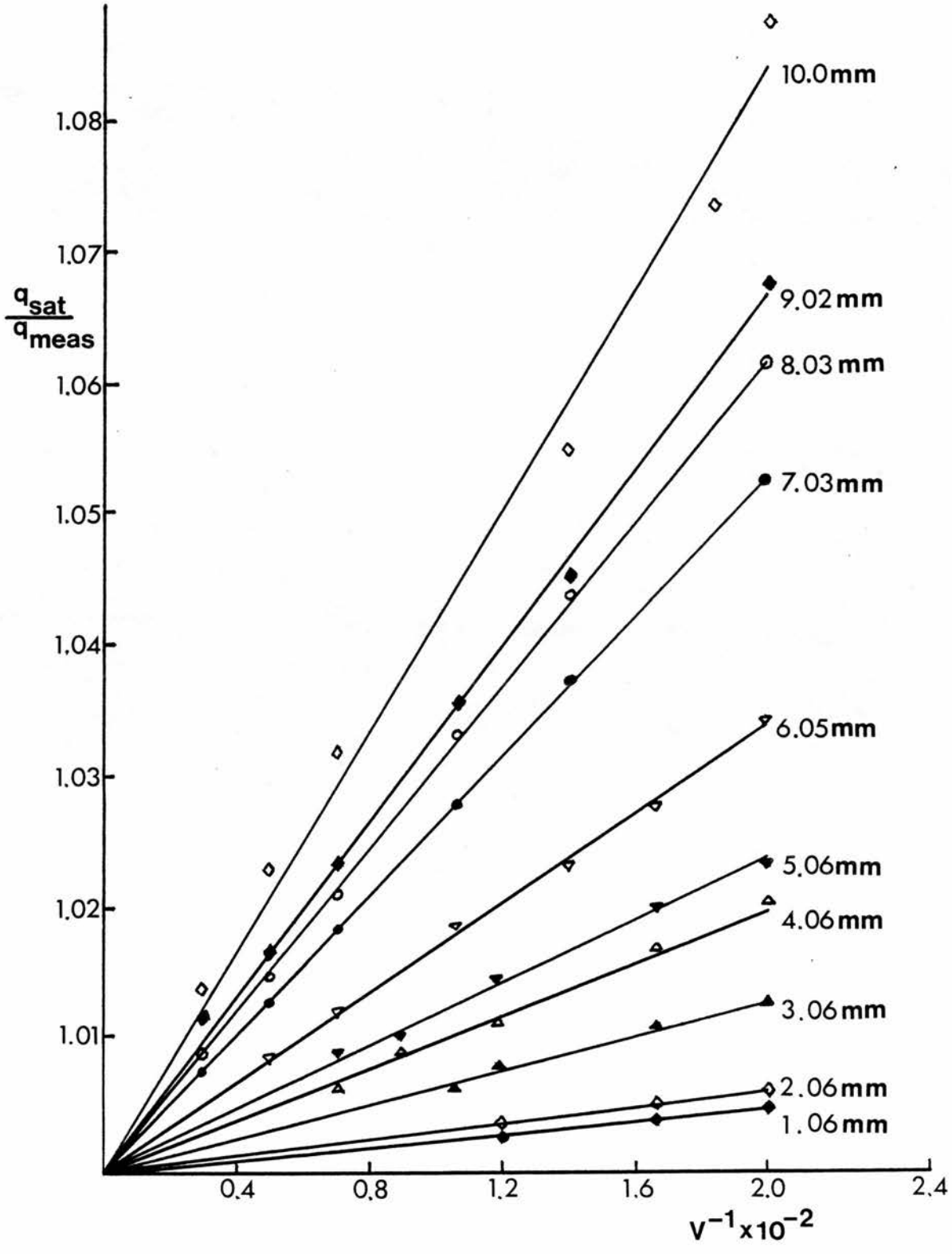

FIGURE 4.4.

FIGURE 4.5 SATURATION CHARACTERISTICS OF GRAPHITE / AIR CHAMBER EXPOSED TO d(15MeV) + Be NEUTRONS

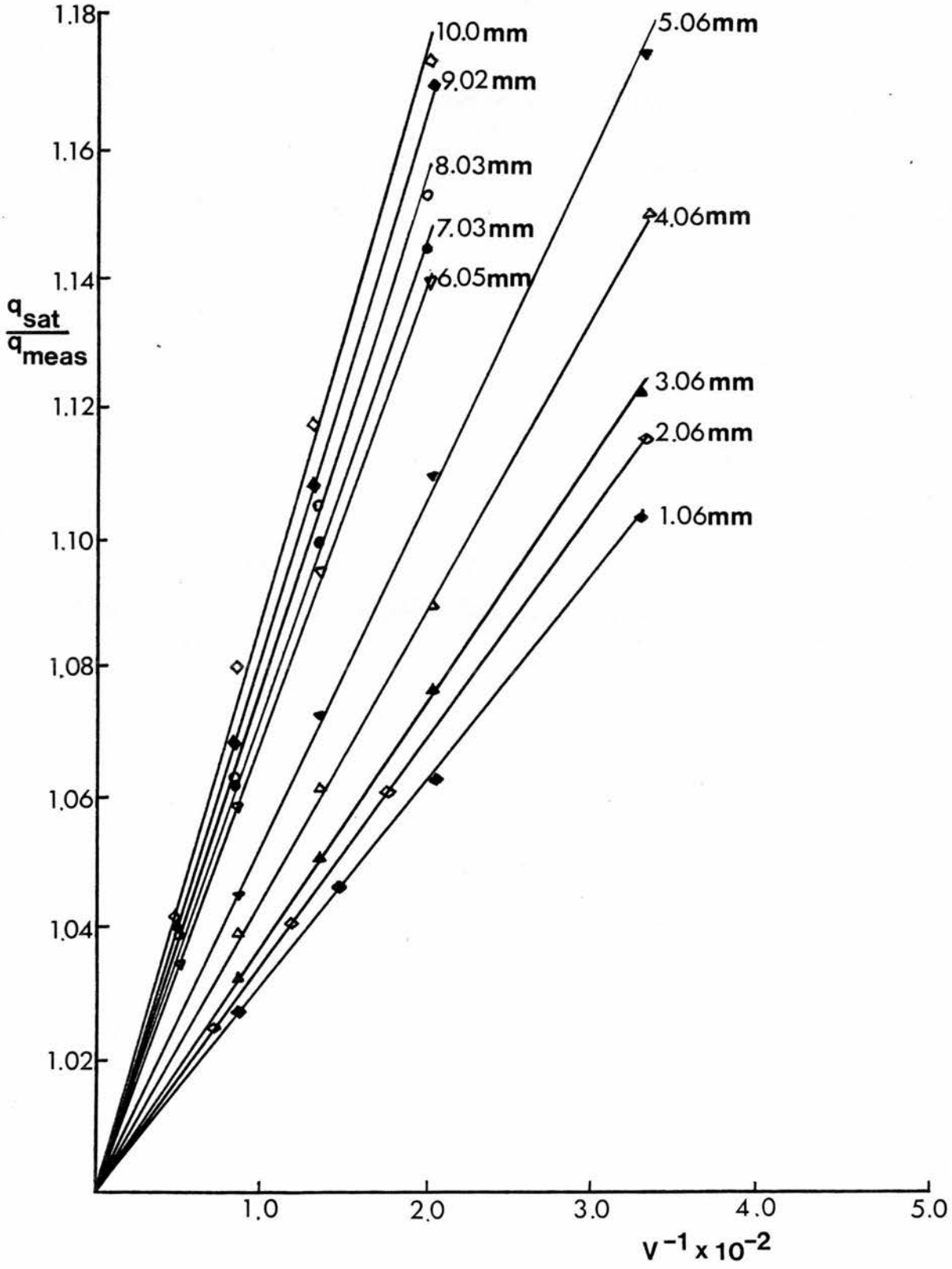

FIGURE 4.5.

FIGURE 4.6 SATURATION CHARACTERISTICS OF GRAPHITE/ T.E. GAS CHAMBER IN AIR ATMOSPHERE EXPOSED TO d(15MeV) + Be NEUTRONS

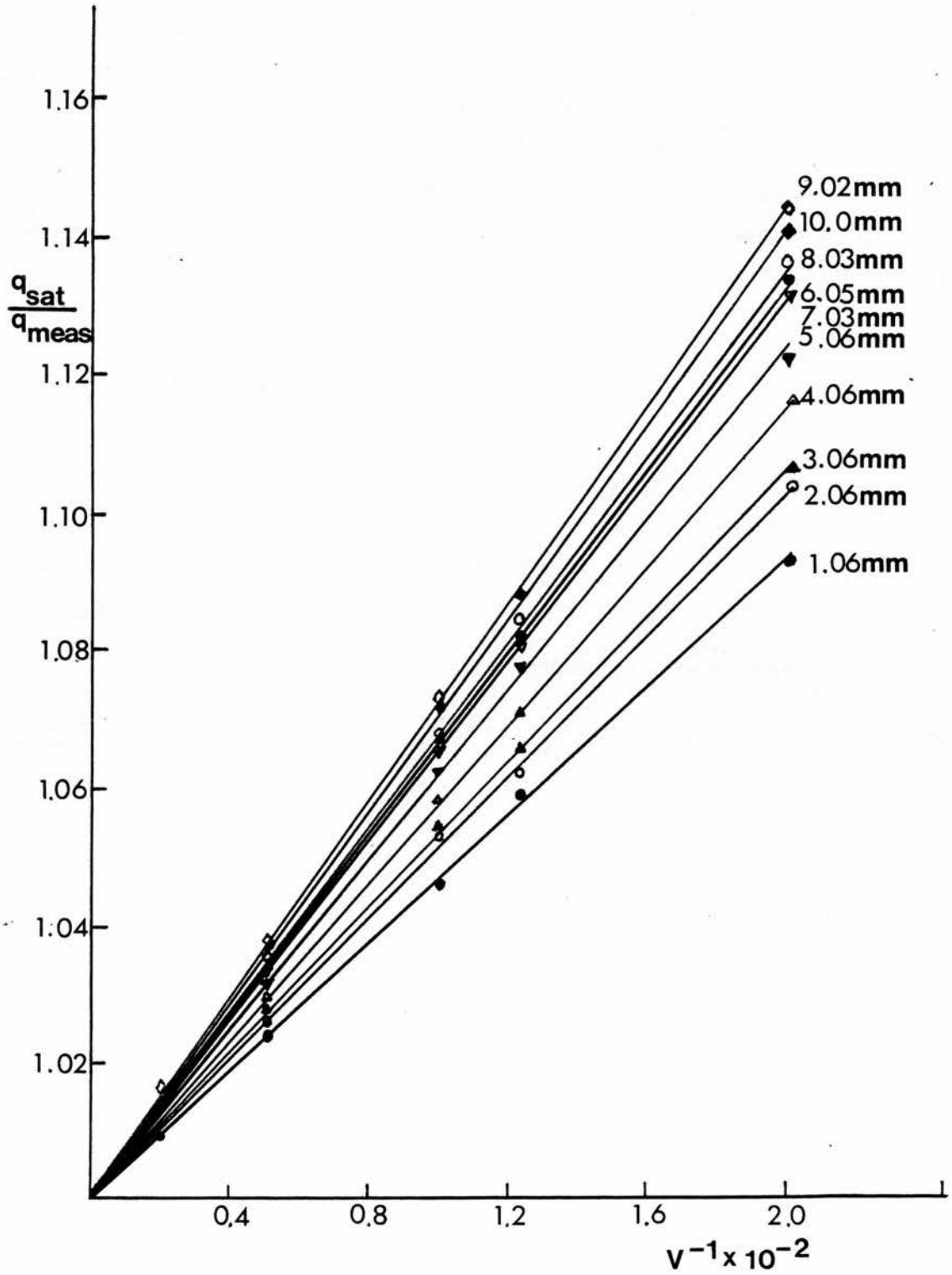

FIGURE 4.6.

FIGURE 4.7 SATURATION CHARACTERISTICS OF GRAPHITE/ T.E. GAS CHAMBER IN T.E. GAS ATMOSPHERE, EXPOSED TO d(15MeV) + Be NEUTRONS

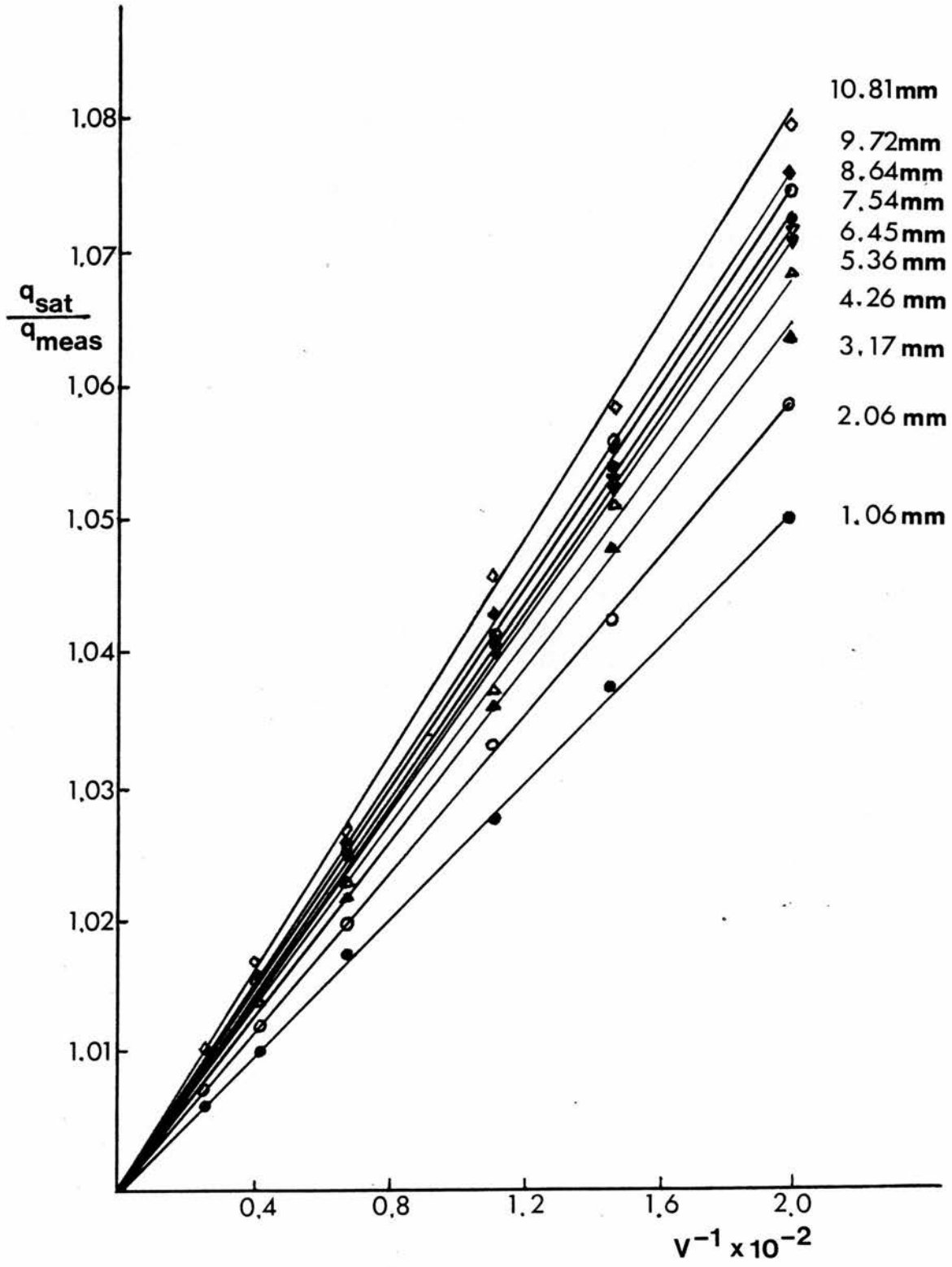

FIGURE 4.7.

FIGURE 4.8 SATURATION CHARACTERISTICS OF GRAPHITE/CO_2 CHAMBER IN AIR ATMOSPHERE, EXPOSED TO d(15MeV) + Be NEUTRONS

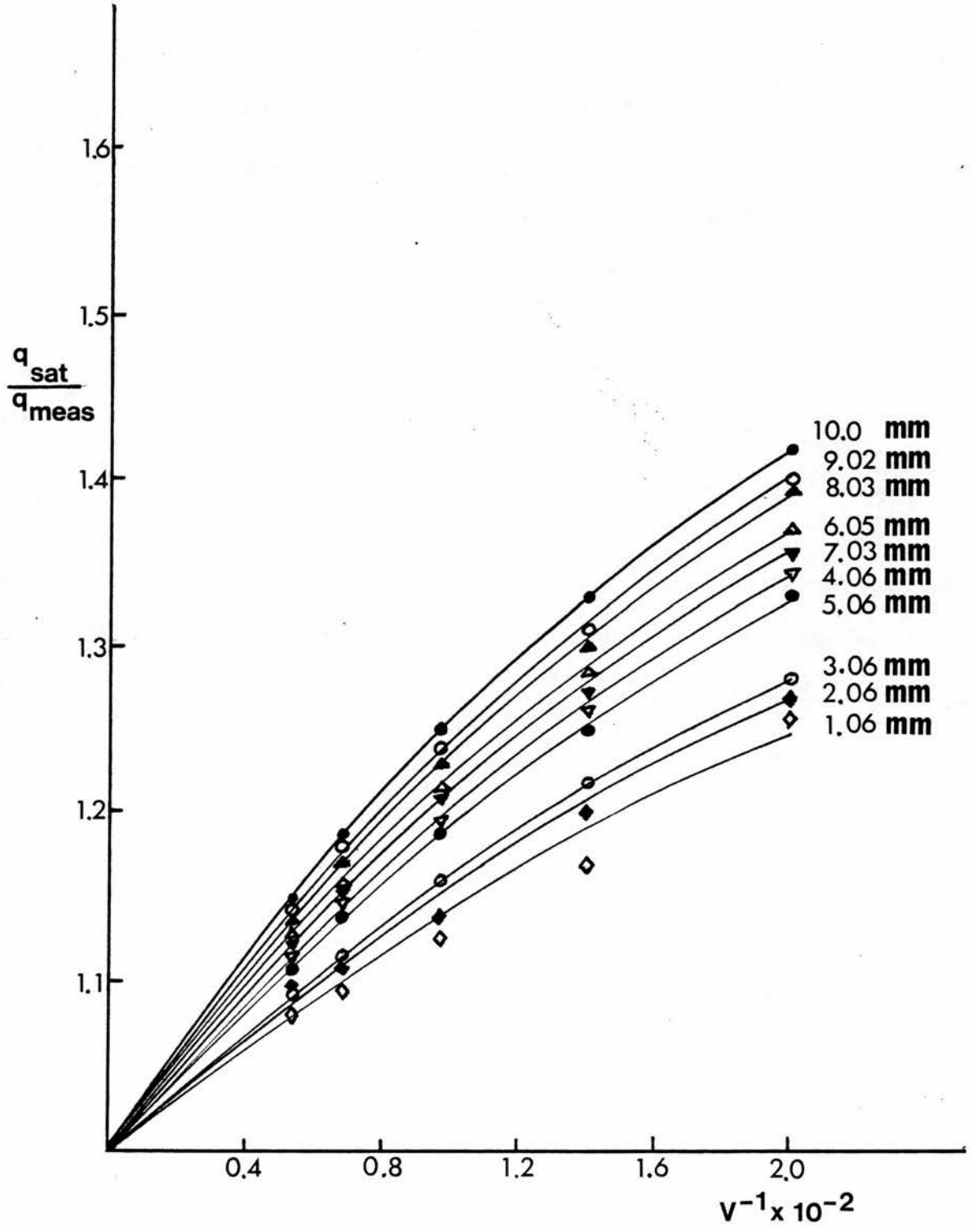

FIGURE 4.8.

FIGURE 4.9 SATURATION CHARACTERISTICS OF GRAPHITE/ CO_2 CHAMBER IN CO_2 ATMOSPHERE, EXPOSED TO d(15MeV) + Be NEUTRONS

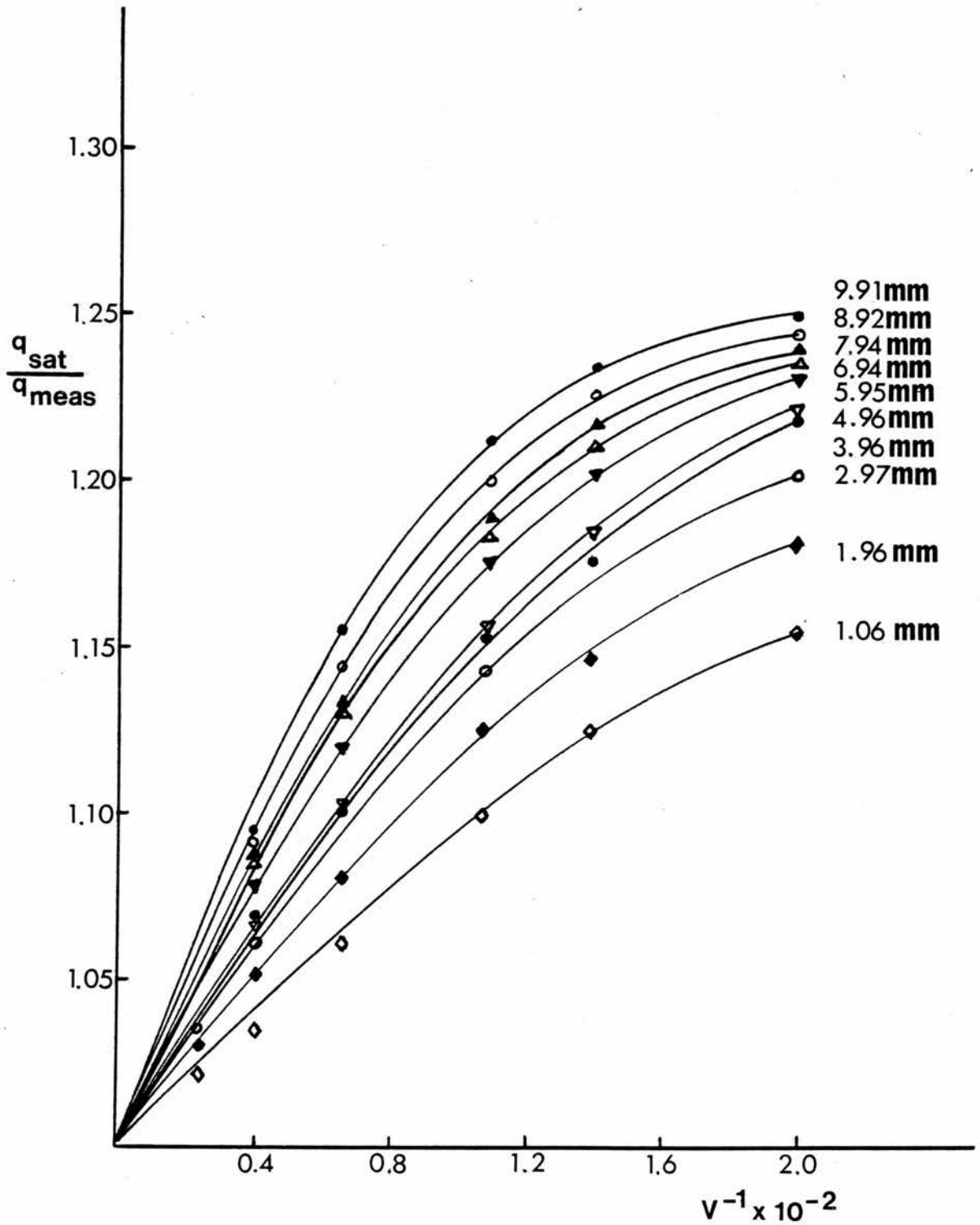

FIGURE 4.9.

FIGURE 4.10 SATURATION CHARACTERISTICS OF GRAPHITE/ CO_2 CHAMBER IN AIR ATMOSPHERE EXPOSED TO d(15MeV) + Be NEUTRONS

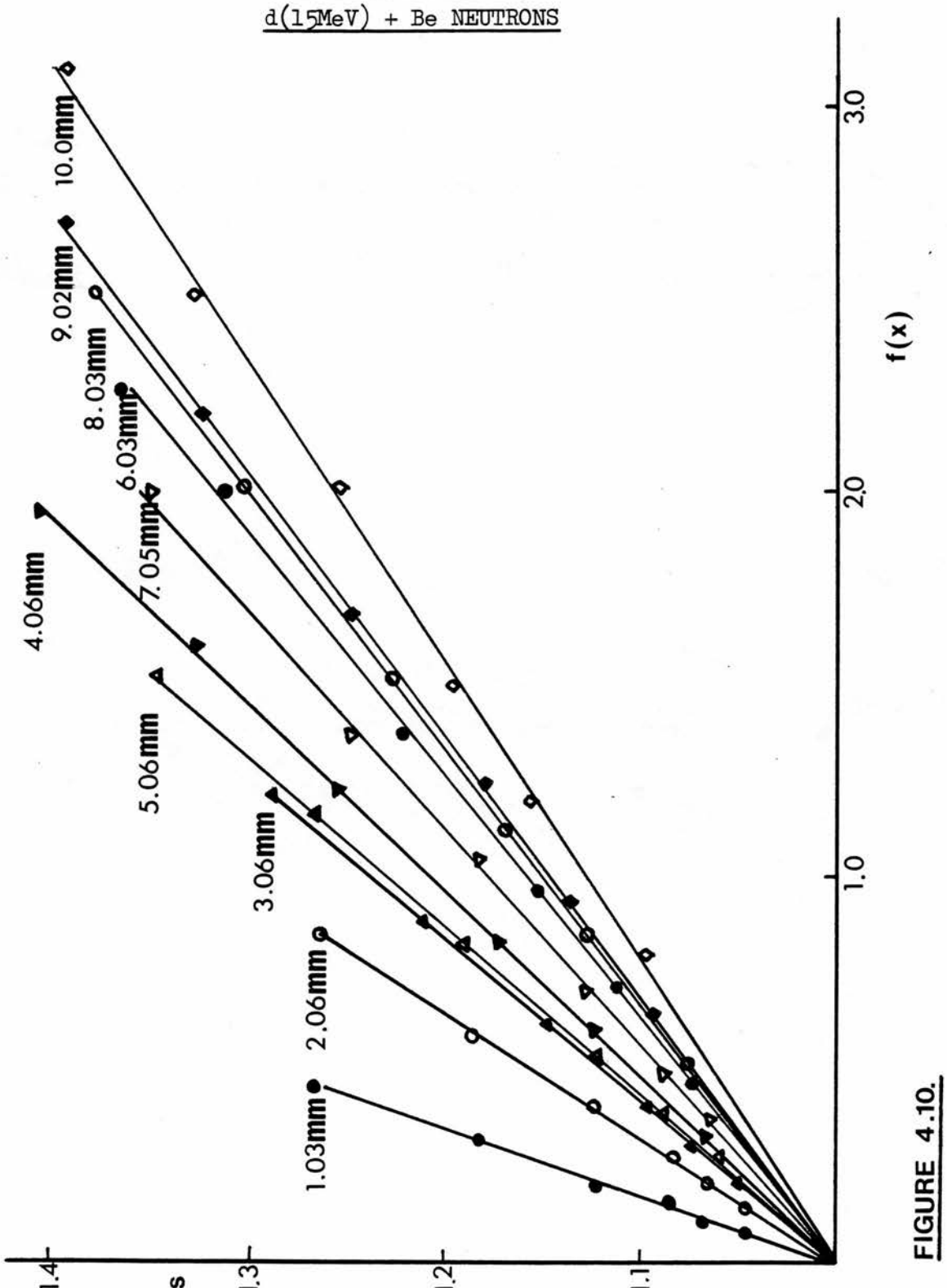

FIGURE 4.10.

FIGURE 4.11 SATURATION CHARACTERISTICS OF GRAPHITE/CO_2 CHAMBER IN CO_2 ATMOSPHERE EXPOSED TO d(15MeV) + Be NEUTRONS

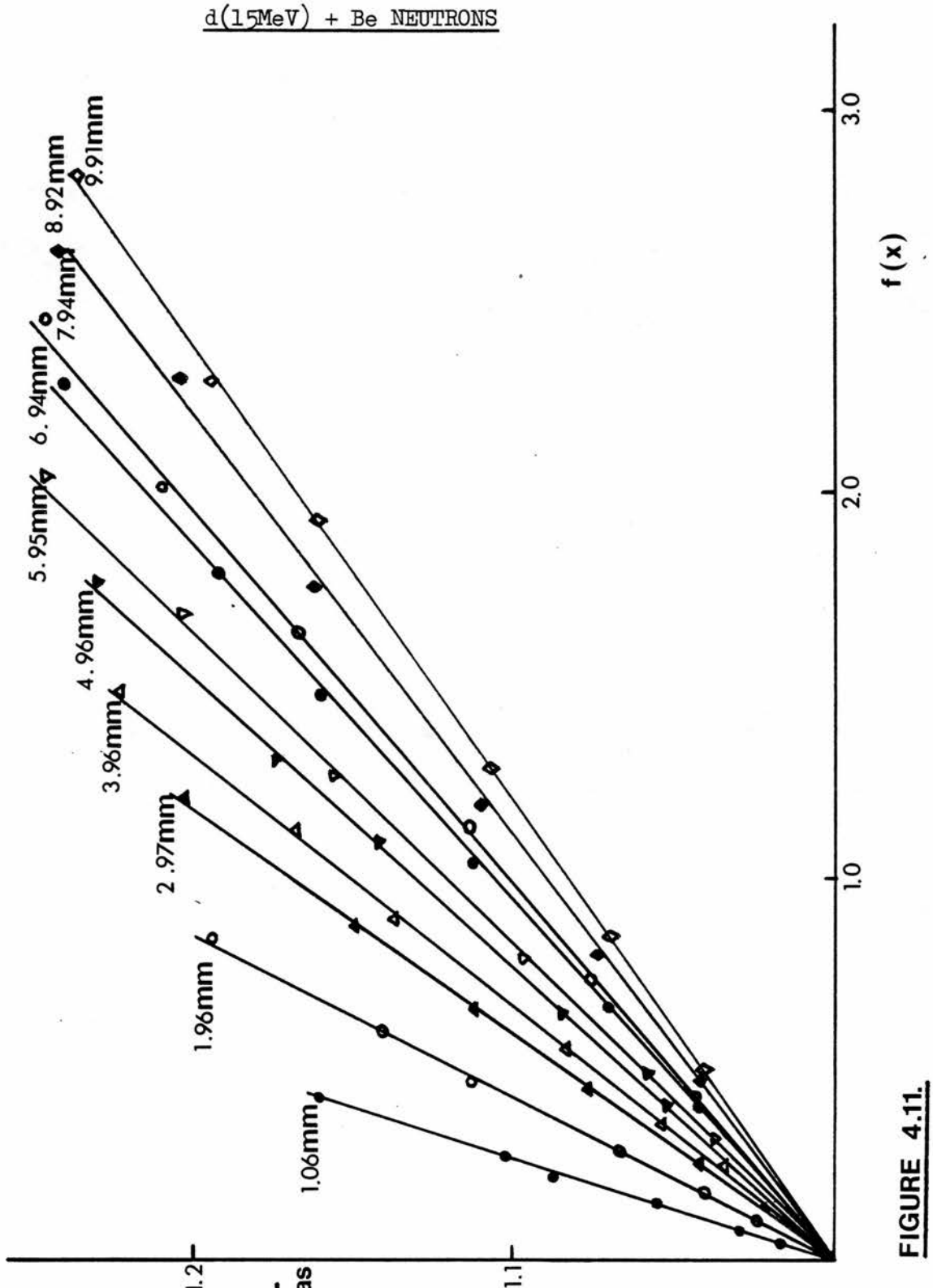

FIGURE 4.11.

CHAPTER 5

IONIZATION MEASUREMENTS AT VARYING PRESSURE

5.1 Experimental Arrangement

When the reduction of plate separation at atmospheric pressure becomes physically inadvisable, e.g. below 1mm, then the equivalent of reduced plate separation can be achieved by reducing the pressure of the gas in the cavity.

The ionization chamber was placed inside the vacuum tight tank (Fig. 5.1), the front face of the chamber being located at 125cm F.S.D. and the plate separation being maintained at a fixed value, d.

For an air cavity, the required equivalent plate separation, d_{eq}, is obtained by pumping the tank from 10^5 to 10 Pa, which on the mercury manometer, corresponds to 0 to $(\rho_{at} - 0.1)$mm Hg, where ρ_{at} is atmospheric pressure in mm Hg, then allowing the introduction of air in the required quantities through the needle valve.
The manometer setting (mm Hg) for a required d_{eq} is -

$$\rho = \rho_{at} - \frac{d_{eq}}{d}\rho_{at}$$

For cavity gases other than air, a gas environment with minimal air contamination is ensured by first pumping the tank down to 10 Pa, filling with the required gas up to atmospheric pressure, then pumping down to 10 Pa. Again, the required gas can be introduced in desired quantities through the needle valve.

5.2 Saturation and Fixed Polarizing Voltage Measurements

The same saturation procedures of ionization measurements at atmospheric pressure are used, namely extrapolation procedures due to the presence of initial recombination. The Jaffé f(x) is again applied in the case of the C/CO_2 chamber.

Saturation curves for TE/air, TE/TE, C/air, C/CO_2 and C/TE configurations of chamber at d_{eq} settings of 0.1 - 2.055mm are shown in Figures 5.2 - 5.6.

q_{sat}/d_{eq} for each d_{eq} was also measured by varying the pressure (hence d_{eq}) while keeping a fixed polarizing voltage on the H.T. electrode, then correcting each q_{meas} for saturation effects. Again, this was done to minimize any errors resulting from saturation curve measurements.

Values of q_{sat}/d_{eq} are shown in Tables 5.1 - 5.5 for both saturation measurements and fixed polarizing voltage measurements for each chamber configuration.

From Tables 5.1 and 5.2, q_{sat}/d_{eq} is constant for TE/air and TE/TE chambers in the range d_{eq} = 0.1 - 2.055mm, to within an experimental error of $\pm$ 1%. There appears to be very good agreement between q_{sat}/d_{eq} measured by a saturation curve, and q_{sat}/d_{eq} obtained at a fixed voltage for the TE/air chamber. For the TE/TE chamber, both sets of results are individually constant, but there is a difference in their average value of 1.5%, which must be due to an error in experimental technique.

For the graphite chamber, (Tables 5.3, 5.4 and 5.5), the saturation measurements at d_{eq} = 0.1 0.2 and 0.3mm involve a large experimental error in comparison with the TE plastic chamber measurements at the same d_{eq}, because of the very small charge measurements involved. These charge measurements can be of the order of 3 x 10^{-11}C for the graphite chamber, compared with 3 x 10^{-10}C for the TE chamber at the same d_{eq}. For this reason, the dose delivered to the graphite chamber at d_{eq} = 0.1, 0.2 and 0.3mm was increased and corrections made accordingly.

From Table 5.3, q_{sat}/d_{eq} for the C/air chamber is constant in the range d_{eq} = 0.3 - 2.055mm to within an experimental error of $\pm$ 1%, and in the range d_{eq} = 0.1 - 2.055mm to within an experimental error of $\pm$ 2%, for both measurement techniques.

From Table 5.4, both measurement techniques show that q_{sat}/d_{eq} for the C/CO_2 chamber is constant in the range d_{eq} = 0.3 - 1.055mm to within an experimental error of $\pm$ 1%, and in the range d_{eq} = 0.1 - 1.055mm to within an experimental error of $\pm$ 1.5%. A reduction of q_{sat}/d_{eq} at d_{eq} = 2.055mm appears to be significant.

From Table 5.5, q_{sat}/d_{eq} for the C/TE chamber is constant in the range d_{eq} = 0.1 - 2.055mm to within an experimental error of $\pm$ 1%, for both measurement techniques.

TABLE 5.1 TE/Air Chamber

Equivalent plate separation d_{eq} (mm)	(a)			(b) V = -80V		
	ρ_{at} (mm Hg)	ρ (mm Hg)	$\frac{q_{sat}}{d_{eq}}$ (10^{-8} Cmm^{-1})	ρ_{at} (mm Hg)	ρ (mm Hg)	$\frac{q_{sat}}{d_{eq}}$ (10^{-8} Cmm^{-1})
0.1	768	731	0.289	747	711	0.285
0.2	768	693	0.289	747	674	0.285
0.3	764	652	0.285	747	638	0.284
0.4	764	615	0.286	747	602	0.285
0.5	764	578	0.286	747	565	0.288
0.6	764	541	0.288	747	529	0.288
0.7	764	504	0.286	747	493	0.289
0.8	764	467	0.288	747	456	0.288
0.9	764	479	0.286	747	420	0.289
1.03	764	381	0.289	747	373	0.288
2.055	764	0	0.286	747	0	0.288

(a) q_{sat}/d_{eq} obtained from saturation curve measurements.

(b) q_{sat}/d_{eq} obtained from fixed polarizing voltage measurements.

TABLE 5.2 TE/TE Chamber

Equivalent plate separation d_{eq} (mm)	(a)			(b) V = -80V		
	ρ_{at} (mm Hg)	ρ (mm Hg)	$\frac{q_{sat}}{d_{eq}}$ (10^{-8} Cmm^{-1})	ρ_{at} (mm Hg)	ρ (mm Hg)	$\frac{q_{sat}}{d_{eq}}$ (10^{-8} Cmm^{-1})
0.1	739	703	0.360	747	711	0.358
0.2	739	667	0.363	747	674	0.360
0.3	739	631	0.364	747	638	0.360
0.4	739	595	0.362	747	602	0.354
0.5	739	559	0.363	747	565	0.356
0.6	739	523	0.361	747	529	0.357
0.7	739	487	0.361	747	493	0.357
0.8	739	451	0.364	747	456	0.357
0.9	739	415	0.362	747	420	0.358
1.03	739	369	0.363	747	373	0.355
2.055	739	0	0.363	747	0	0.357

(a) and (b) as Table 5.1

TABLE 5.3 C/Air Chamber

Equivalent plate separation d_{eq} (mm)	(a)			(b) V = -100V		
	ρ_{at} (mm Hg)	ρ (mm Hg)	$\frac{q_{sat}}{d_{eq}}$ (10^{-8}Cmm^{-1})	ρ_{at} (mm Hg)	ρ (mm Hg)	$\frac{q_{sat}}{d_{eq}}$ (10^{-8}Cmm^{-1})
0.1	733	697	0.0595	751	714	0.0617
0.2	752	679	0.0618	751	678	0.0624
0.3	752	642	0.0610	751	641	0.0603
0.4	752	606	0.0610	751	605	0.0603
0.5	752	569	0.0605	751	568	0.0601
0.6	752	532	0.0607	751	532	0.0602
0.7	733	483	0.0600	751	495	0.0602
0.8	733	448	0.0606	751	459	0.0607
0.9	733	412	0.0609	751	422	0.0608
1.03	733	366	0.0606	751	375	0.0603
2.055	733	0	0.0610	751	0	0.0603

(a) and (b) as Table 5.1

TABLE 5.4 C/CO_2 Chamber

Equivalent plate separation d_{eq} (mm)	(a)			(b) V = -100V		
	ρ_{at} (mm Hg)	ρ (mm Hg)	$\frac{q_{sat}}{d_{eq}}$ $(10^{-8}Cmm^{-1})$	ρ_{at} (mm Hg)	ρ (mm Hg)	$\frac{q_{sat}}{d_{eq}}$ $(10^{-8}Cmm^{-1})$
0.1	765	728	0.0896	751	714	0.0876
0.2	765	691	0.0872	751	678	0.0893
0.3	765	653	0.0882	751	641	0.0881
0.4	751	605	0.0884	751	605	0.0894
0.5	751	568	0.0879	751	568	0.0890
0.6	751	532	0.0894	751	532	0.0889
0.7	751	495	0.0881	751	495	0.0880
0.8	751	459	0.0890	751	459	0.0882
0.9	751	422	0.0883	751	422	0.0882
1.03	751	375	0.0886	751	375	0.0888
2.055	751	0	0.0824	751	0	0.0837

(a) and (b) as Table 5.1

TABLE 5.5 C/TE Chamber

Equivalent plate separation d_{eq} (mm)	(a)			(b) V = -100V		
	ρ_{at} (mm Hg)	ρ (mm Hg)	$\frac{q_{sat}}{d_{eq}}$ (10^{-8} Cmm^{-1})	ρ_{at} (mm Hg)	ρ (mm Hg)	$\frac{q_{sat}}{d_{eq}}$ (10^{-8} Cmm^{-1})
0.1	752	715	0.0747	751	714	0.0747
0.2	752	679	0.0748	751	678	0.0754
0.3	752	642	0.0750	751	641	0.0752
0.4	752	606	0.0751	751	665	0.0754
0.5	752	569	0.0760	751	568	0.0750
0.6	752	533	0.0760	751	532	0.0750
0.7	752	496	0.0760	751	495	0.0754
0.8	752	460	0.0752	751	459	0.0754
0.9	752	423	0.0749	751	422	0.0756
1.03	752	376	0.0755	751	375	0.0757
2.055	752	0	0.0756	751	0	0.0750

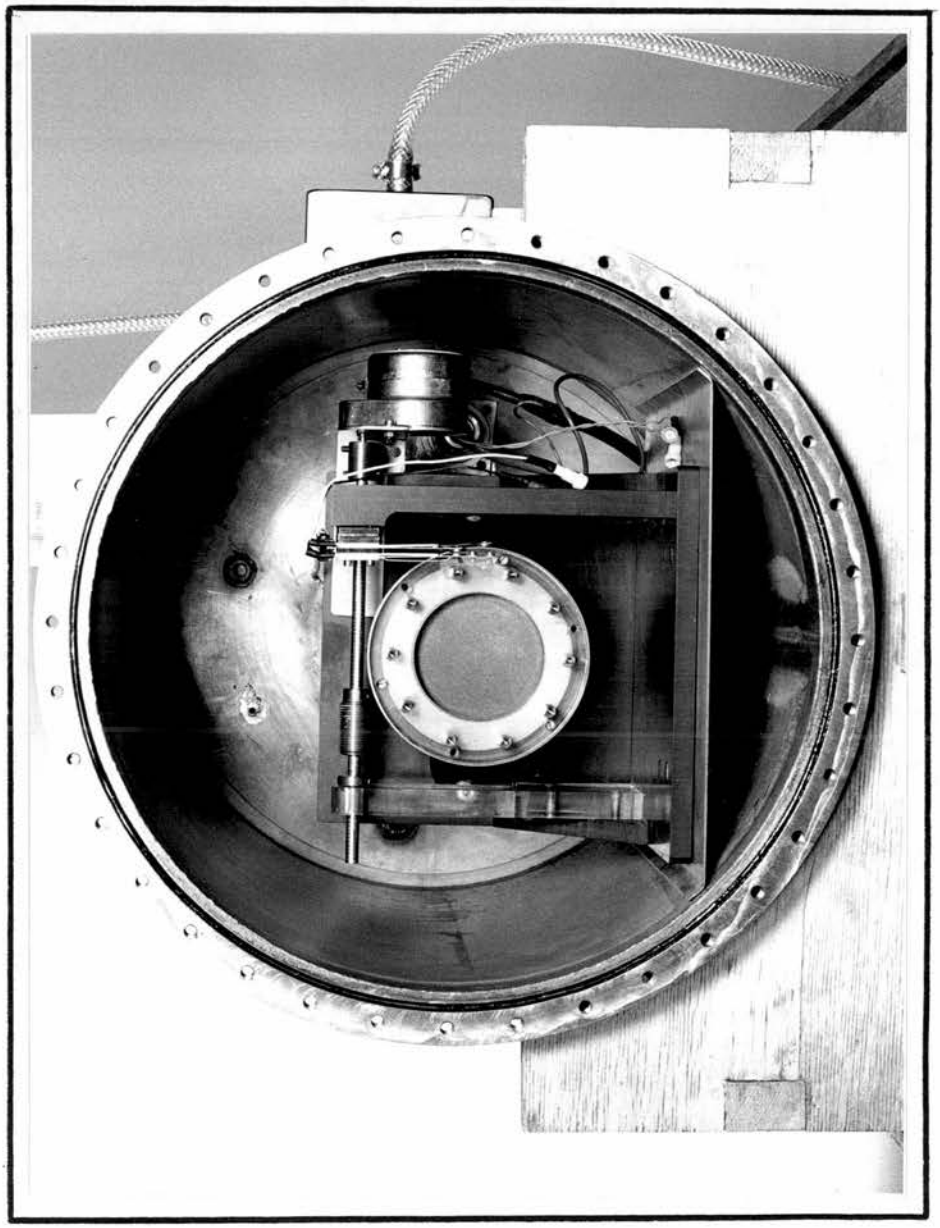

FIGURE 5.1.

FIGURE 5.2 SATURATION CHARACTERISTICS OF TE PLASTIC/AIR AT VARIOUS d_{eq} EXPOSED TO d(15MeV) + Be NEUTRONS

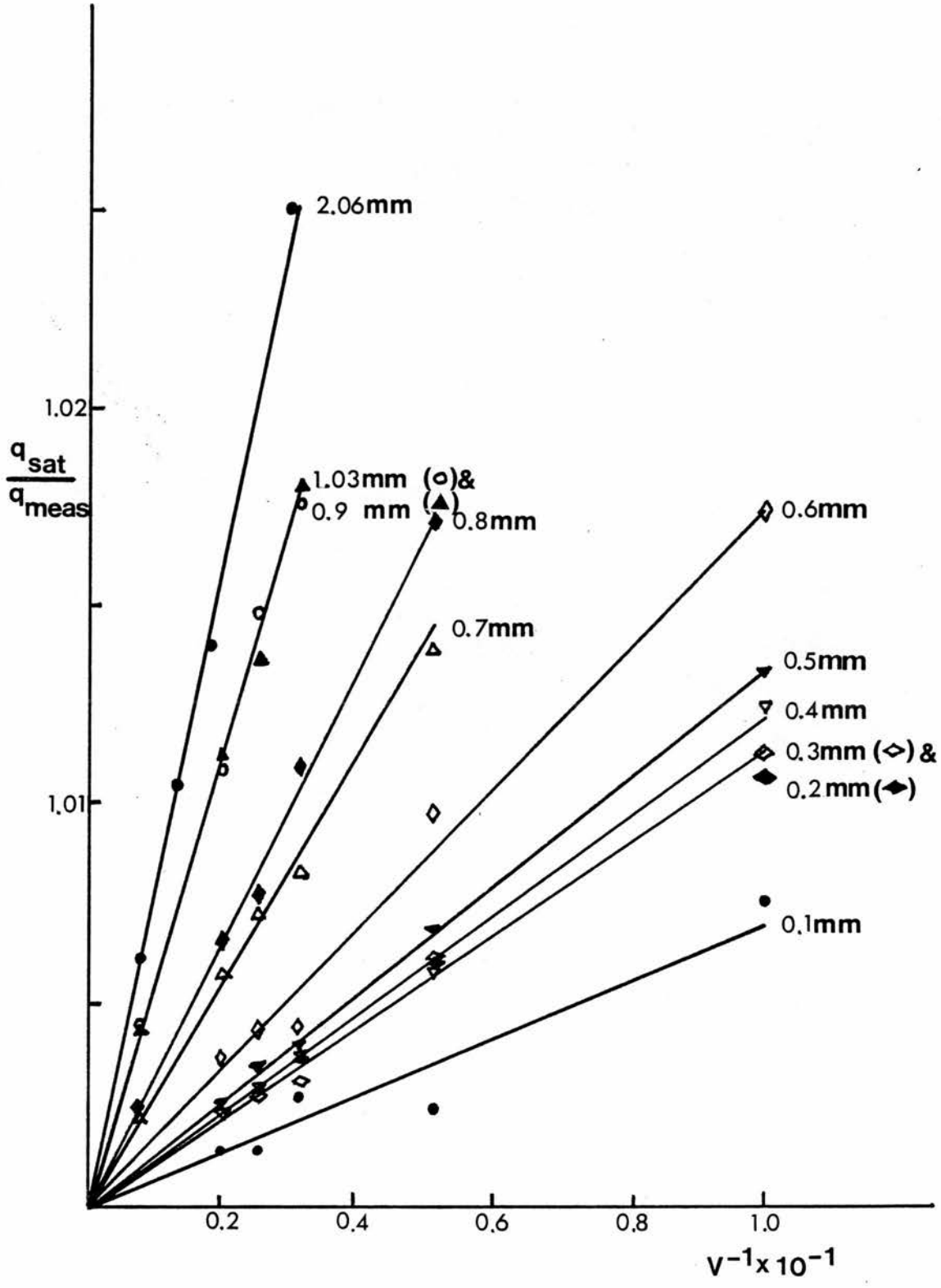

FIGURE 5.2.

FIGURE 5.3 SATURATION CHARACTERISTICS OF TE PLASTIC/ TE GAS AT VARIOUS d_{eq} EXPOSED TO d(15MeV) + Be NEUTRONS

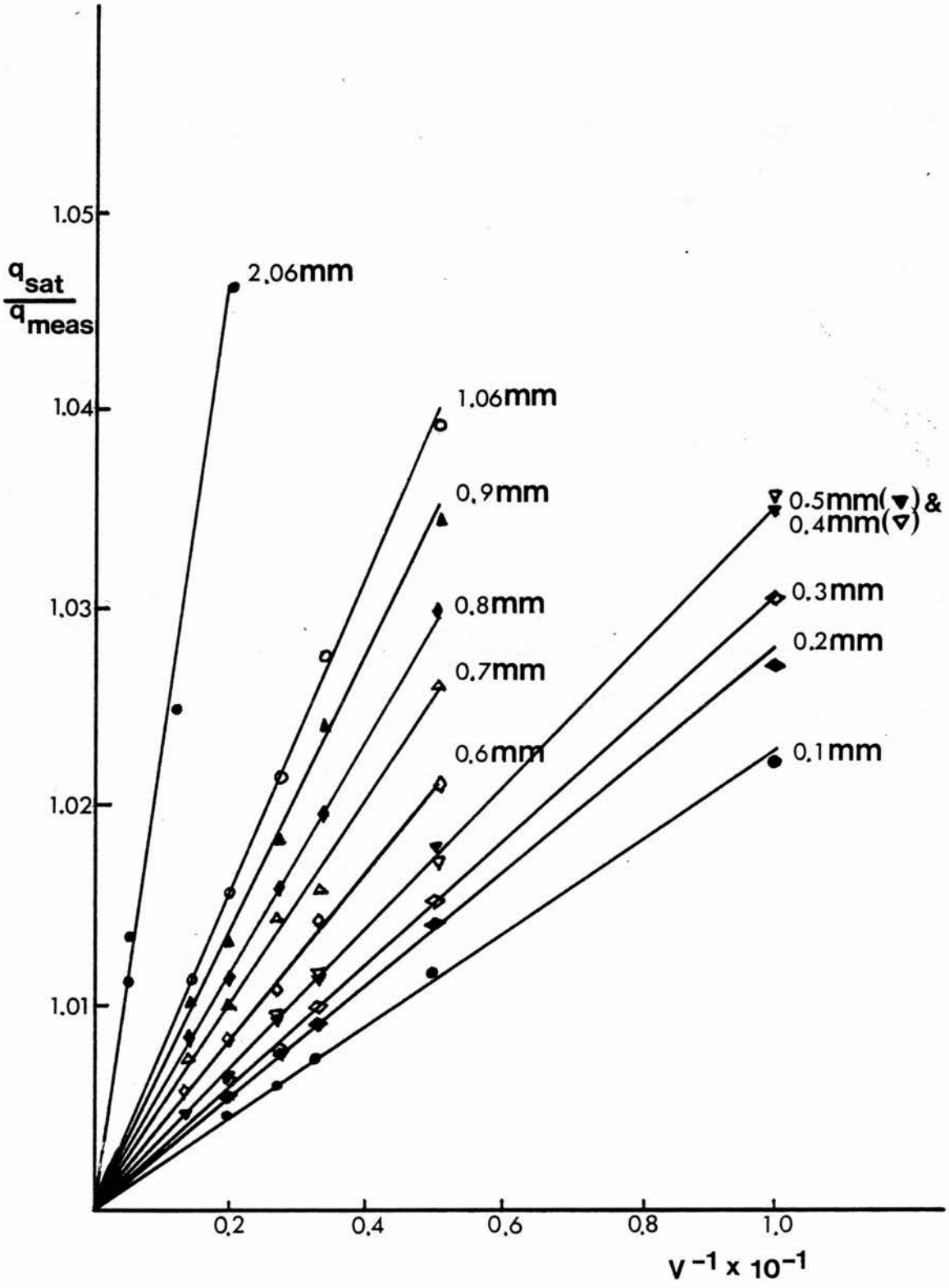

FIGURE 5.3.

FIGURE 5.4 SATURATION CHARACTERISTICS OF GRAPHITE/ AIR CHAMBER AT VARIOUS d_{eq} EXPOSED TO d(15MeV) + Be NEUTRONS

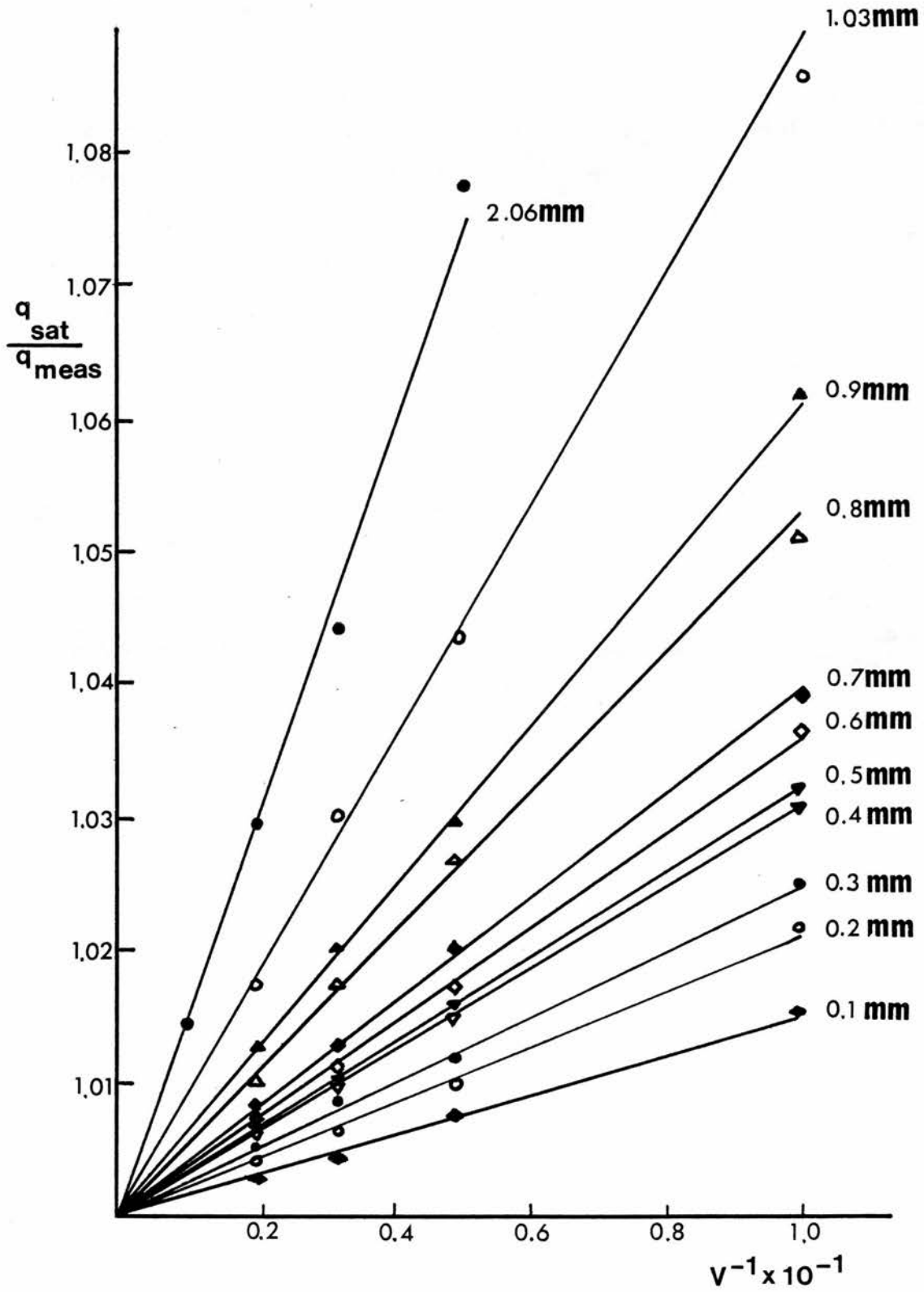

FIGURE 5.4.

FIGURE 5.5 SATURATION CHARACTERISTICS OF GRAPHITE/CO_2 CHAMBER AT VARIOUS d_{eq} EXPOSED TO d(15MeV) + Be NEUTRONS

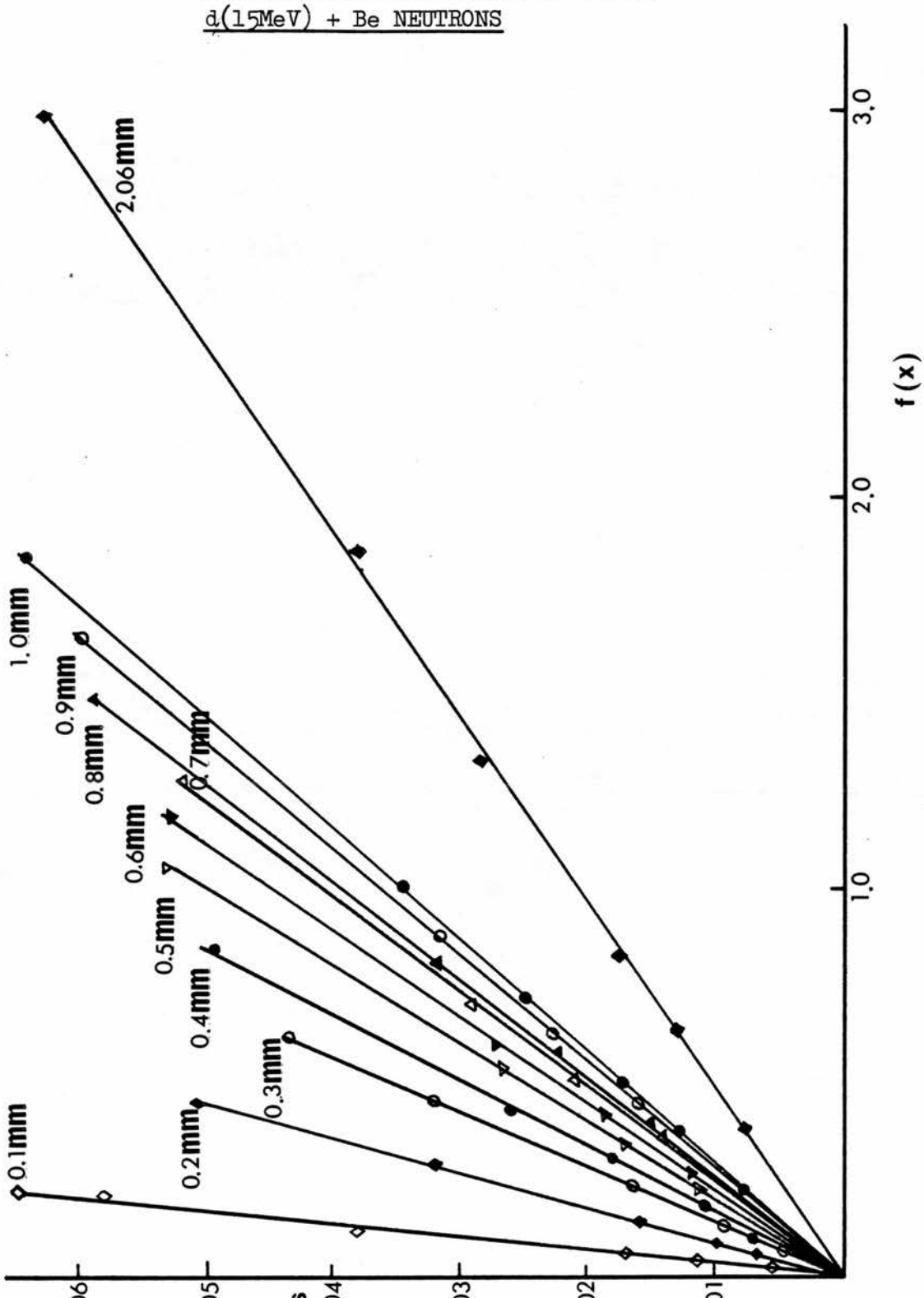

FIGURE 5.5.

FIGURE 5.6 SATURATION CHARACTERISTICS OF GRAPHITE/ T.E. GAS CHAMBER AT VARIOUS d_{eq} EXPOSED TO d(15MeV) + Be NEUTRONS

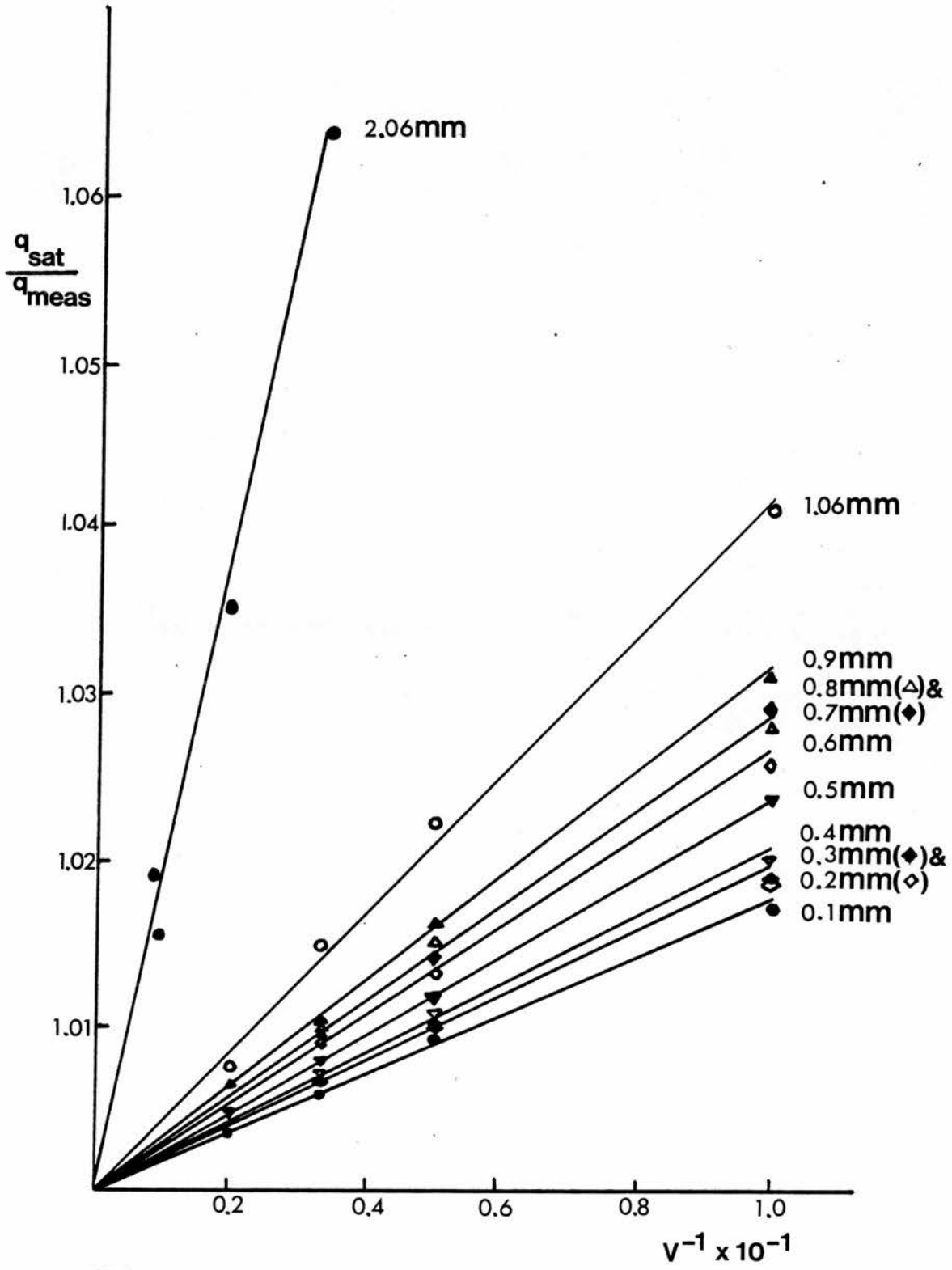

FIGURE 5.6.

CHAPTER 6

SUMMARY OF EXPERIMENTAL RESULTS

By combining the ionization measurements made in Chapters 4 and 5, both at atmospheric and non-atmospheric pressures, the ionization per increment of chamber volume will be obtained for all chamber combinations in the range 0.1 - 18mm of plate separation.

From Chapters 4 and 5, q_{sat}/d is constant for the TE chamber in the range 0.1 - 18mm; $q_{sat}/d = 0.355 \times 10^{-8} Cmm^{-1}$ for TE/TE chamber and $0.285 \times 10^{-8} Cmm^{-1}$ for TE/Air chamber. It must be noted that these charge measurements are not absolute values but are relative to each other. They are normalized by using a polythene/air reference chamber as described in Chapter 2.

Combination of Tables 4.4, 4.5 and 4.6 and Tables 5.3, 5.4 and 5.5 gives the overall increment of ionization per increment of chamber volume for C/Air, C/CO_2 and C/TE chambers as shown in Table 6.1 and Figures 6.1, 6.2 and 6.3. For C/TE chamber (from Table 4.5 and Table 5.5) the ionization measurements at atmospheric and non-atmospheric pressures do not give the same value of q_{sat}/d at the overlap at approximately 1mm. A further experiment had to be carried out to find out if a setting-up error had occurred. A single reading of q_{sat}/d for the chamber at d = 1mm (atmospheric) and a reading taken of q_{sat}/d_{eq} at d_{eq} = 1mm (d = 5mm, ρ = 0.2atm) gave the same value which corresponded to the original atmospheric value. It was therefore concluded that a setting-up error did exist in the case of the non-atmospheric measurements and corrections were made accordingly.

For the C/air chamber, q_{sat}/d is constant in the range 0.1 - 4mm, then it increases in the range 4 - 18mm as shown in Figure 6.1.

For the C/CO_2 chamber, q_{sat}/d is constant in the range 0.1 - 1mm, then it decreases in the range 1 - 7mm; the curve begins to flatten out in the range 7 - 18mm as shown in Figure 6.2.

For the C/TE chamber, q_{sat}/d is constant in the range 0.1 - 5mm, then it increases in the range 5 - 18mm, as shown in Figure 6.3.

6.1 Cavity Theory

There are four categories of charged particles which deposit their energy in a cavity of an ionization chamber (Caswell and Coyne 1972). These fall into the classes of 'starter', 'stopper', 'insider' and 'crosser' as shown in Figure 6.4.

The Bragg-Gray Theory relates the absorbed dose, D_m, in the wall of an ionization chamber to the charge collected, q, by,

$$D_m = \frac{\bar{W}}{e} (S_{m,g}) \left(\frac{q}{m}\right)_{small} \qquad 6.1$$

where $\bar{W}$ is the average energy required to produce an ion pair in the gas due to the particles produced in the wall, e is the electronic charge, $(S_{m,g})$ is the mass stopping power ratio of wall to cavity material for the charged particles produced in the wall; m is the mass of gas in the cavity, and $\left(\frac{q}{m}\right)_{small}$ is the charge collected per unit mass at small plate separations. The plate separation must be small since the theory rests on the basic requirement that the

dimensions of the cavity should be a very small fraction of the range of the particles which cross it i.e. the Bragg Gray Theory holds when 'crossers' only contribute to the ionization. In neutron dosimetry, this situation is impossible to achieve since the heavy recoil ions from the chamber wall are of very short range i.e. the order of a few millimetres. It is assumed, however, that at very small plate separations, the ionization is produced almost entirely by 'crossers' and that 'stoppers' and 'starters' contribute a negligible amount so that a Bragg Gray approximation holds.

Alternatively, at large plate separations i.e. very much greater than the range of the charged particles from the wall, when the charged particle contribution from the wall is responsible for the ionization in what may be described as the 'rind' of the gas volume, the bulk of the ionization is caused by 'insiders', although a few 'stoppers' and 'starters' will also contribute.

The absorbed dose, D_m, now becomes a function of the kerma ratio of wall to gas i.e.

$$D_m = \frac{\bar{W}_2}{e} \frac{K_m}{K_g} \left(\frac{q}{m}\right)_{\text{large}} \qquad 6.2$$

where K_m and K_g are the kerma values in wall and gas respectively. $\bar{W}_2$ in this case is the average energy required to produce an ion pair in the gas due to the particles produced in the gas.

Relating equations 6.1 and 6.2,

$$\frac{\left(\frac{q}{m}\right)_{small}}{\left(\frac{q}{m}\right)_{large}} = \frac{\bar{W}_2}{\bar{W}_1} \frac{K_m}{K_g} (S_{m,g})^{-1}$$

Few data are available on $\bar{W}$ values of protons and charged particles in TE gas, air and CO_2, so the very rough approximation was made that $\frac{\bar{W}_2}{\bar{W}_1} = 1$. This however is only the case if the ionizing particles from wall and gas are the same e.g. for the TE/TE chamber.

For parallel-plate geometry, and if a correction is made for temperature and pressure on all occasions, m is proportional to d, hence

$$\frac{\left(\frac{q}{d}\right)_{small}}{\left(\frac{q}{d}\right)_{large}} = \frac{K_m}{K_g} (S_{m,g})^{-1} \qquad 6.3$$

Kerma values as obtained from computation of data from Coyne (1980), and the neutron spectrum as measured by Bonnet (1979) are shown in Table 6.2; stopping power ratios are obtained as follows from the data of Janni (1966).

6.2 Method for Deriving the Stopping Power Ratio of Heavy Ions from that of Protons

Ziegler (1977) described a method for deriving the stopping power of any ion from that of protons. A reduced stopping power parameter $< S >$ is introduced so that the stopping power S_H (V) of a heavy

ion of velocity V and atomic number Z, may be related to the stopping power S_p (V) of the same substance for protons i.e.

$$S_H (V) = Z_1^2 < S > S_p (V) \qquad 6.4$$

For a heavy ion of initial energy E and mass H, the velocity $V_1 = \left(\frac{2E}{M}\right)^{\frac{1}{2}}$ in the absence of relativistic effects. At this same velocity V_1, the energy of a corresponding proton = $\frac{mE}{M}$, where m = mass of proton. The corresponding stopping power for a proton of this energy may be substituted into equation 6.4 as S_p (V). The stopping power parameter < S >, which is a function of Z and V_1, would be constant for each heavy ion type, so the term Z_1^2 < S > would be eliminated in any stopping power ratio calculation.

Mass and linear stopping powers in the proton energy range 0.1 - 1000MeV for a large number of substances have been obtained from Janni (1966). For proton energies between 0.1 and 1.0MeV, mass stopping power is proportional to (proton energy)^n, where 1 > n > 0. For proton energies less than 0.1MeV, approximate mass stopping powers were obtained by a continuation of this curve to lower energies.

Values of stopping power can also be obtained for TE plastic and TE gas from the data of Janni by calculation of constituent compounds; the percentages by weight of the constituent compounds are shown in Table 6.3. Values of stopping power ratios for a range of proton energies as obtained by the Bragg Additivity Rule are shown in Table 6.4; these ratios differ greatly from the expected ratio of 1.0. This may indicate that the Bragg Additivity Rule is inaccurate,

as is stated by Bichsel (1977). In a publication reviewing the state of Stopping Power Data, Bichsel claims that the Bragg Additivity Rule is valid only with an uncertainty of > 3%.

Since the Bragg Additivity Rule can be applied only with a large uncertainty, the assumption was made, using Janni's data, that $S_{TE\ Plastic} = S_{TE\ Gas} = S_{ICRU\ Muscle}$ (ICRU 26). This procedure has been adopted by several authors e.g. Attix et al (1980) also using Janni's data.

Dennis (1979) describes an effective stopping power ratio $\frac{S_{TE\ Plastic}}{S_{TE\ Gas}} = 1.02$ for neutrons with average energy 8.4MeV, so the assumption that $\frac{S_{TE\ Plastic}}{S_{TE\ Gas}} = 1.0$ may introduce errors of only a few percent.

6.3 Discussion of Bragg-Gray Theory in Relation to Existing Stopping Power, Kerma and Range Data

Table 6.5 shows values of $(q_{sat}/d)_{small}$, $K_{m,g}$ and $S_{m,g}$ for all chamber configurations. (The average energies of the predominant particles produced from the wall, as shown in Table 6.5 are obtained by assuming an average neutron energy E_n of 8.4MeV. This mean neutron energy is based on the energy fluence spectra, obtained from the neutron spectrum as measured by Bonnett (1979) (Fig. 1.1). The maximum recoil energy of the recoil particle is $\frac{4 M_N M_R E_N}{(M_N + M_R)^2}$. Therefore, the mean energy of the particles when first released is $\frac{2 M_N M_R E_N}{(M_N + M_R)^2}$. However, particles emerging from the wall will have all energies from $\frac{2 M_N M_R E_N}{(M_N + M_R)^2}$ down to zero, so will have an average energy of $\frac{M_N M_R E_N}{(M_N + M_R)^2}$.) From these data, values of

$(q_{sat}/d)_{large}$ were calculated and compared with experimental values of $(q_{sat}/d)_{large}$ when obtainable. In order to establish whether $(q_{sat}/d)_{large}$ can be obtained from experiment, a knowledge of the maximum ranges of relevant particles in relevant substances is required. The maximum ranges is tissue of some charged particles as a function of neutron energy are displayed in ICRU 26 (page 15). Taking an average neutron energy of 8.4 MeV, the maximum ranges of protons, α particles, ^{12}C and ^{16}O ions in air, TE gas, CO_2, TE plastic and graphite can be estimated by assuming that range is proportional to $(\text{density})^{-1}$. These estimates are shown in Table 6.6.

From Table 6.6, it is shown that $(q_{sat}/d)_{large}$ cannot be obtained from experiment for any chamber configuration involving the TE plastic wall, as protons produced from the TE plastic wall have estimated maximum ranges of 640, 720 and 400mm in air, TE gas and CO_2 respectively.

As regards the carbon chamber, ^{12}C ions from the wall have ranges in CO_2, air and TE gas of 2.1mm, 3.3mm and 3.7mm respectively. Therefore the carbon ion contribution from the wall is likely to be negligible at a maximum plate separation of 18mm.

However, α particles produced from the carbon wall will have estimated maximum ranges of 25.0mm, 27.9mm and 16.1mm in air, TE gas and CO_2 respectively. Therefore, in the cases of the carbon chamber with air and TE gas, the maximum chamber plate separation of 18mm is too small to obtain a situation whereby 'stoppers' contribute a negligible amount.

In the case of C/CO_2, the maximum range of the α particles from the wall is less than the maximum plate separation, but not considerably less, so that α particle 'stoppers' may not be negligible. $(q_{sat}/d)_{large}$ for C/CO_2 as obtained by experiment and $(q_{sat}/d)_{large}$ as obtained by calculation are shown in Table 6.5, the difference being 6.02% for 0.6 MeV ^{12}C ions.

For the remainder of the chamber configurations, the values of $(q_{sat}/d)_{large}$ obtained from calculation will be the same for different chamber walls and same gases in the absence of attenuation effects, since at very large plate separation, there will be negligible ionization resulting from the particles produced in the wall.

Comparing TE/TE chamber with C/TE chamber, $(q_{sat}/d)_{large}$ values show a difference of approximately 3.8% for 0.6 MeV ^{12}C ions; comparing TE/Air chamber with C/Air chamber, $(q_{sat}/d)_{large}$ values show a difference of approximately 5.0% for 0.6 MeV ^{12}C ions.

It must be noted that these observations are dependent on the reliability of the stopping power, kerma and range data used. Two major sources of error are:

1. The calculations of $(q_{sat}/d)_{large}$ for carbon chambers involve a stopping power ratio calculated for ^{12}C ions, which are the predominant particles produced in the wall. These stopping power ratios do not take the α particles produced from the wall into account. These α particles will be discussed in more detail in Chapter 7.

2. The assumption that $\frac{\overline{W}_1}{\overline{W}_2} = 1$. $\overline{W}$ values will be discussed in more detail in Chapters 7 and 8.

6.4 Comparison with Results of Makarewicz and Pszona (1981)

Makarewicz and Pszona have calculated a dose conversion factor for TE/TE and C/CO_2 ionization chambers as a function of plate separation. Their dose conversion factor was defined as

$$r = \frac{D_g}{D_w}$$

where D_g and D_w are the absorbed doses in the gas and wall of an ionization chamber respectively. To express in terms of measurable quantities,

$$r = \frac{D_g^{\,g} + D_g^{\,w}}{K_w}$$

where $D_g^{\,g}$ and $D_g^{\,w}$ are the absorbed doses in gas by charged particles created in gas and wall respectively. Therefore

$$r = \frac{(Q/m)_1 \, \overline{W}_1/e + \left[(Q/m)_2 \, \overline{W}_2/e \;\; S_{g,m}\right]}{K_w} \qquad 6.5$$

where $(Q/m)_1$ and $(Q/m)_2$ are the charge per unit mass due to

particles produced in gas and wall respectively, $\overline{W}_1$ and $\overline{W}_2$ are the average energy required to produce an ion pair in the gas due to gas and wall particles respectively and $S_{g,m}$ is the stopping power ratio of gas to wall. Equation 6.5 can be rewritten as

$$r = \frac{(Q/m)_{large}\ \overline{W}_1/e}{K_w} + \frac{(Q/m)_{small}\ \overline{W}_2/e\ S_{g,m}}{K_w} \qquad 6.6$$

where $(Q/m)_{small}$ and $(Q/m)_{large}$ are as previously defined in this chapter.

For infinitesimal plate separations, first term of Equation 6.6 approaches zero, $(Q/m)_{small}\ \overline{W}_2 = K_w$, therefore $r = S_{g,m}$.

For infinite plate separations, second term approaches zero, $(Q/m)_{large}\ \overline{W}_1/e = K_g$, therefore $r = K_g/K_w$.

This is in agreement with the theory given in this chapter.

For TE/TE chamber, the approximation is made that $S_{m,g} = 1.0$ Assuming that similar particles are produced in both TE plastic wall and TE gas, the approximation is made that $\overline{W}_1 = \overline{W}_2$. Therefore

$$r \simeq \frac{\overline{W}}{K_w}\left[(Q/m)_{large} + (Q/m)_{small}\right]$$

Since $\frac{\overline{W}}{K_w}$ is a constant, $r \propto (Q/m)_{total}$.

For TE/TE chamber, Makarewicz and Pszona have shown that r is constant to within $\pm$ 2.5% with increasing plate separation in the range 0.1 - 20mm.

This is in agreement with the experiments of Chapters 4 and 5 which have shown that q_{sat}/d for TE/TE chamber is constant in the range 0.1 - 18mm.

TABLE 6.1 Increment of Ionization per Increment of Chamber Volume for C/Air, C/CO_2 and C/TE Chambers

Plate Separation d (mm)	q_{sat}/d (10^{-8} Cmm^{-1})		
	C/Air	C/CO_2	C/TE
0.1	0.0617	0.0876	0.0814
0.2	0.0624	0.0893	0.0821
0.3	0.0603	0.0881	0.0819
0.4	0.0603	0.0894	0.0821
0.5	0.0601	0.0890	0.0817
0.6	0.0602	0.0889	0.0817
0.7	0.0602	0.0880	0.0821
0.8	0.0607	0.0882	0.0821
0.9	0.0608	0.0882	0.0823
1.055	0.0606	0.0888	0.0817
2.055	0.0606	0.0837	0.0815
3.055	0.0603	0.0834	0.0824
4.055	0.0605	0.0814	0.0817
5.055	0.0608	0.0792	0.0814
6.048	0.0611	0.0779	0.0822
7.033	0.0613	0.0785	0.0830
8.029	0.0615	0.0778	0.0841
9.018	0.0616	0.0775	0.0853
10.000	0.0623	0.0781	0.0867
11.0	0.0632	0.0775	0.0883
12.0	0.0637	0.0780	0.0901
13.0	0.0640	0.0775	0.0920
14.0	0.0641	0.0780	0.0933
15.0	0.0647	0.0786	0.0950
16.0	0.0649	0.0780	0.0961
17.0	0.0650	0.0780	0.0970
18.0	0.0653	0.0777	0.0997

TABLE 6.2 Kerma Values Obtained from Data of Coyne (1980) for the Neutron Spectrum as Measured by Bonnett (1980)

Material	Kerma Value ($Gycm^2$)
Air	1.053×10^{-11}
CO_2	0.743×10^{-11}
TE Gas	0.463×10^{-10}
TE Plastic	0.466×10^{-10}
Graphite	0.829×10^{-11}

TABLE 6.3 Compositions (% by weight) of A-150 TE Plastic and Methane-Based TE Gas

Material	Composition (% by weight)	
TE Plastic (A-150)	45.14%	Polyethylene (C_2H_4)
	35.22%	Nylon
	16.06%	Carbon (C)
	3.58%	Calcium Fluoride (CaF)
TE Gas (Methane-Based)	64.4%	Methane (CH_4)
	32.4%	CO_2
	3.2%	N_2

TABLE 6.4 Stopping Power Values for Constituent Compounds of TE Plastic and TE Gas and Resultant Stopping Power Ratios of TE Plastic/TE Gas for Protons in the Range 0.1 - 3.2 MeV

Proton Energy (MeV)	MASS STOPPING POWER VALUES (MeV $cm^2 g^{-1}$)									Stopping Power Ratio
	$(C_2H_4)_n$	NYLON	C	CaF	CH_4	CO_2	N_2	T.E. PLASTIC	T.E. GAS	
0.1	1204.9	1031.5	822.90	545.50	1490.9	668.68	774.81	1058.87	1201.59	0.881
0.5	484.36	438.27	367.65	263.60	571.73	343.65	344.76	441.48	490.57	0.900
1.0	294.19	269.29	230.88	174.33	343.15	219.17	222.58	270.96	299.12	0.906
1.5	219.75	201.82	174.70	134.29	254.52	165.82	168.26	203.14	223.02	0.911
2.0	176.95	162.91	141.89	110.52	203.97	134.71	136.71	163.99	179.38	0.914
2.5	149.59	138.00	120.65	94.84	171.89	114.68	116.37	138.90	151.58	0.916
3.0	129.90	120.04	105.22	83.365	148.90	100.16	101.62	120.80	131.60	0.918
3.2	123.57	114.25	100.24	79.636	141.53	95.472	96.852	114.97	125.18	0.918

TABLE 6.5 Comparison of (q_{sat}/d) Obtained by Experiment to (q_{sat}/d) Obtained by Calculation of Existing Data

Chamber Combination	$(q_{sat}/d)_{small}$ $(10^{-8}Cmm^{-1})$	$(K_{m,g})$	$(S_{m,g})$	Energy of Relevant Particle	$(q_{sat}/d)_{large}$ Theory $(10^{-8}Cmm^{-1})$	$(q_{sat}/d)_{large}$ Experiment $(10^{-8}Cmm^{-1})$
TE/TE	0.355	1.000	1.000	2.1 MeV Proton	0.355	-
TE/Air	0.285	4.397	1.176	2.1 MeV Proton	0.076	-
C/TE	0.081	0.179	0.816	0.6 MeV ^{12}C Ion	0.369	-
C/Air	0.060	0.787	1.046	0.6 MeV ^{12}C Ion	0.080	-
C/CO_2	0.090	1.116	1.058	0.6 MeV ^{12}C Ion	0.083	0.078

TABLE 6.6 Estimation of Maximum Ranges of Protons, α Particles, ^{12}C and ^{16}O Ions, in Various Substances, from ICRU 26, for 8.4 MeV Neutron Reactions

Particle	ESTIMATED MAXIMUM RANGE (mm)					
	Tissue	Air	TE Gas	TE Plastic	Graphite	CO_2
Proton	0.8	64.0	72.0	0.72	0.35	40.0
α Particle	0.030	27.9	27.9	0.028	0.015	16.1
^{12}C	0.004	3.3	3.7	0.0038	0.0018	2.1
^{16}O	0.003	2.5	2.8	0.0028	0.0014	1.6

FIGURE 6.1 GRAPHITE/AIR: SATURATION CHARGE PER UNIT PLATE SEPARATION

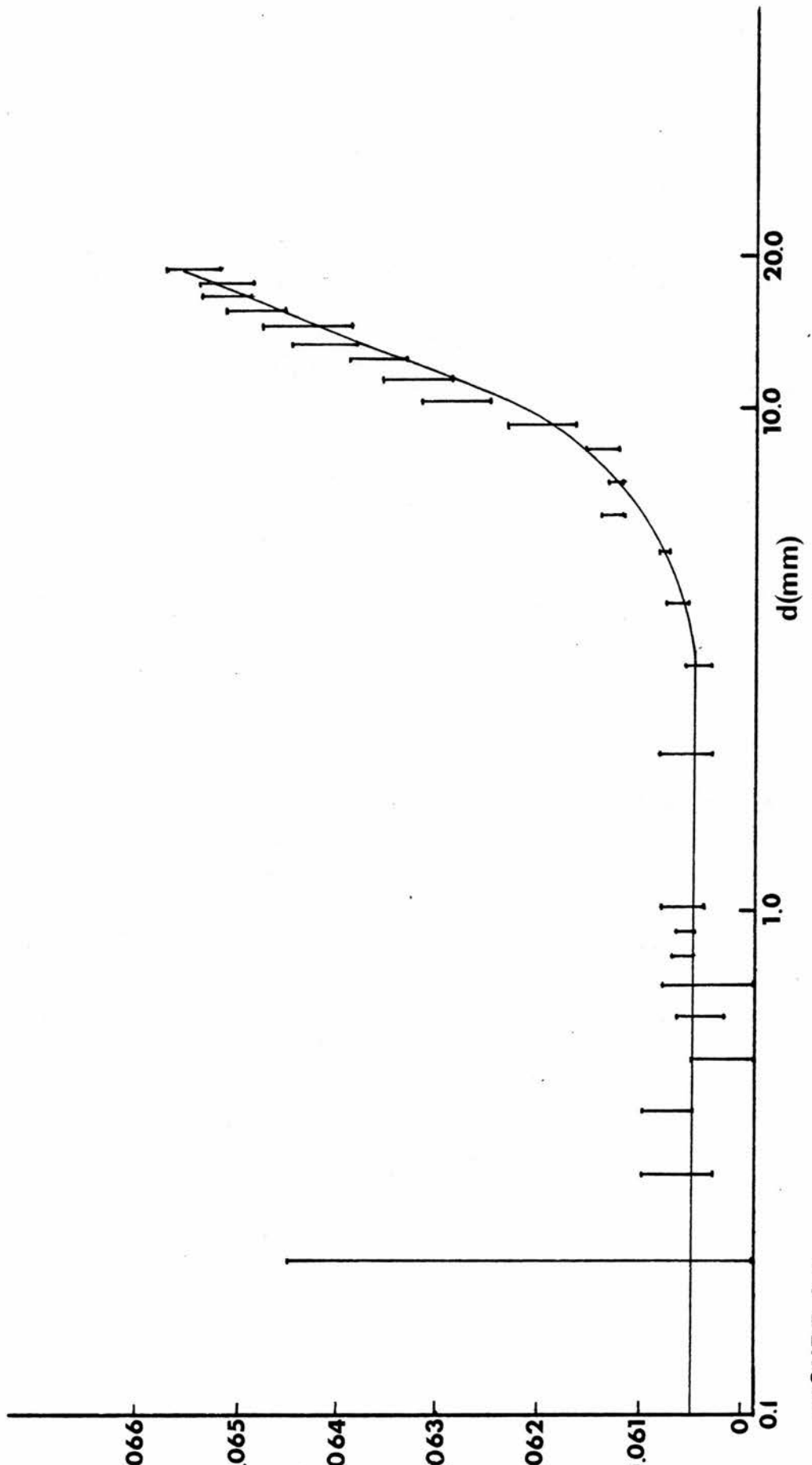

FIGURE 6.1.

FIGURE 6.2 GRAPHITE/CO2: SATURATION CHARGE PER UNIT PLATE SEPARATION

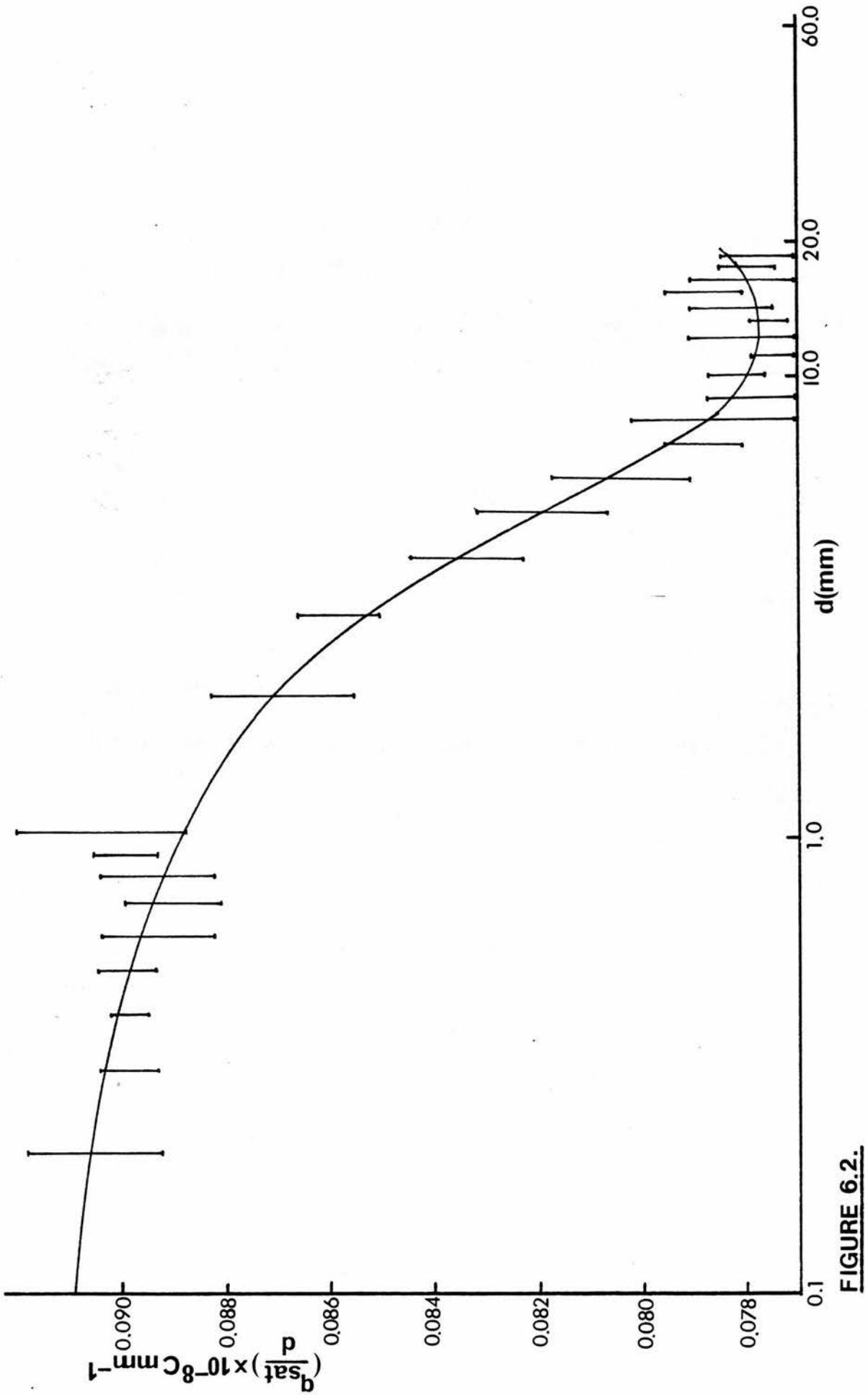

FIGURE 6.2.

FIGURE 6.3 GRAPHITE/T.E. GAS; SATURATION CHARGE PER UNIT PLATE SEPARATION

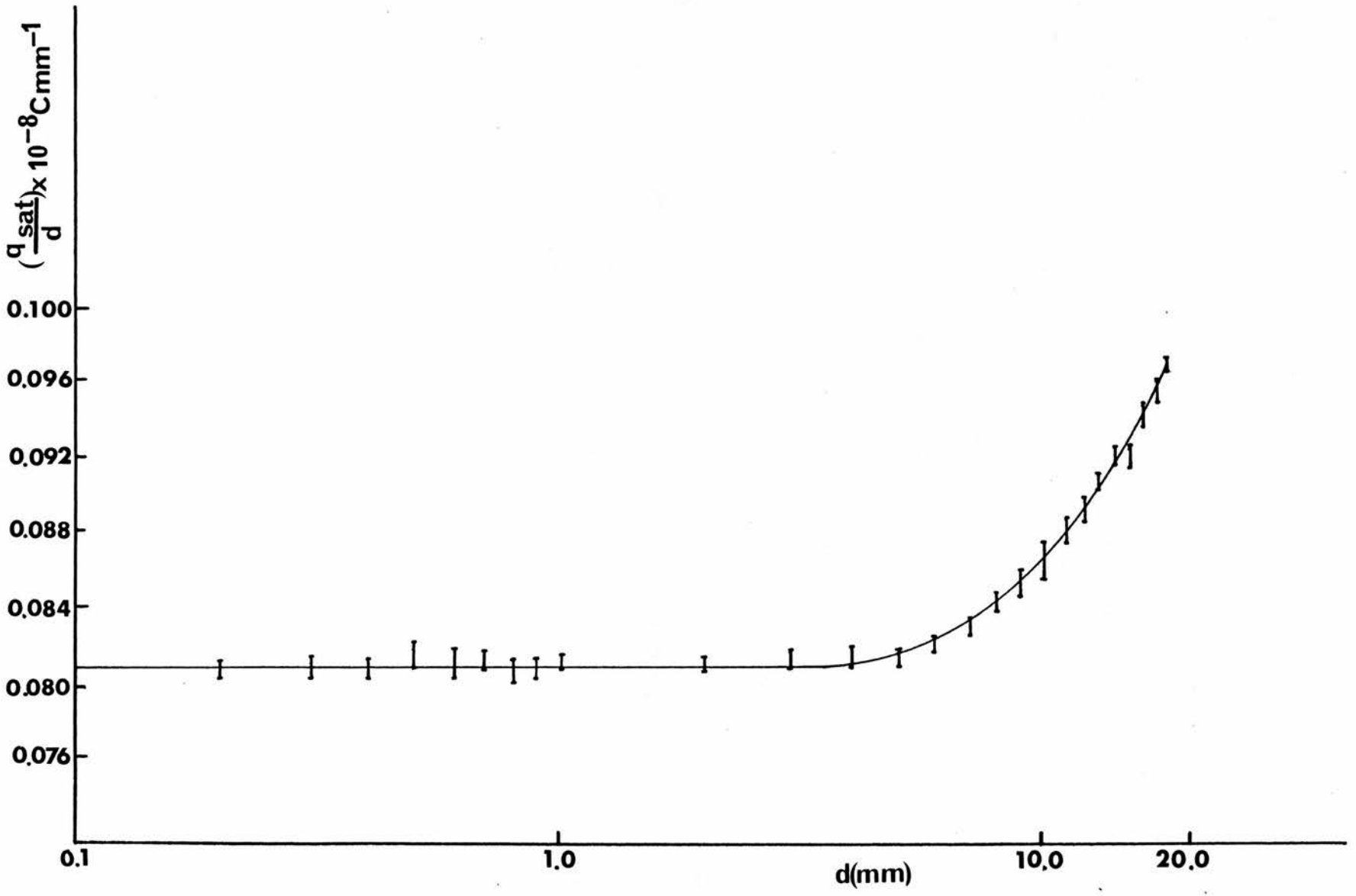

FIGURE 6.3.

FOUR CLASSES OF RECOIL INTERACTIONS IN A CAVITY

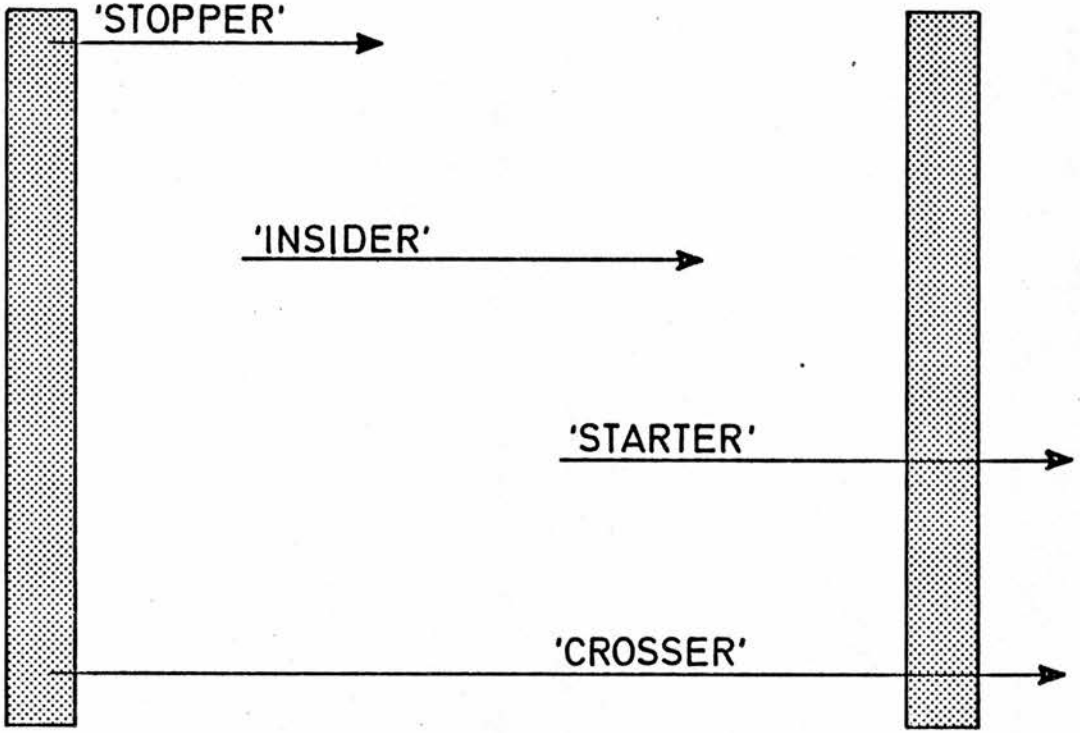

FIGURE 6.4.

CHAPTER 7

ESTIMATION OF THE RELATIVE CHARGED PARTICLE CONTRIBUTION IN VARIOUS GASES FROM WALL AND GAS PARTICLES

7.1 Introduction

The experimental results of Chapter 6 have established that the variation of q_{sat}/d with d in the range 0.1 - 18mm for TE/TE, TE/Air, C/CO_2, C/TE and C/Air chambers is in agreement with established kerma, stopping power and range data. The aim of this chapter is to estimate the relative charged particle contribution in the gases of the above chambers due to the individual particles produced both in the wall and in the gas of the ionization chambers. A theoretical analysis will be developed and the calculated results will be compared with experimental results accumulated in Chapter 6.

The theoretical model is based on the assumption that the fluence of the charged particles liberated in the gas will be attenuated exponentially in the gas as will the fluence of charged particles liberated in the wall which enter the gas.

The theoretical absorbed dose in the gas of the ionization chambers will be divided into the doses from wall and gas particles (Equations 7.1 and 7.3) then subdivided into the ionization due to the constituent particles which are produced in the wall and gas respectively (Equations 7.10 and 7.11).

The final contribution to the ionization of each particle is based on its linear attenuation coefficient, average energy, stopping

power, fraction of kerma allocated etc, each of which will be developed in turn.

7.2 Charged Particles Liberated in the Gas

If negligible attenuation of neutrons in distances equal to the ranges of the secondary charged particles is assumed, then the neutron energy fluence is constant within this range and equal to ψ_N. This neutron energy fluence will release, in the gas, a charged particle energy fluence $\psi_N ((\mu_{tr})_N)_g dx$ in a thickness dx at a depth x, where $((\mu_{tr})_N)_g$ is the linear energy transfer coefficient of the gas for neutrons.

In travelling to a depth x_1, the assumption is made that the fluence of the charged particles liberated in dx will decay exponentially i.e. the charged particle energy fluence will be attenuated to $\psi_N ((\mu_{tr})_N)_g \, dx \exp\left[-(\mu_{gcp})_g (x_1 - x)\right]$. At x_1, a fraction $(\mu_{gcp})_g \, dx$ will be absorbed in thickness dx, where $(\mu_{gcp})_g$ is the linear attenuation coefficient of the charged particles released in the gas. Therefore, at x_1, the absorbed dose in a volume of unit area, thickness dx and density ρ, due to charged particles originating in the gas is given by

$$Dx_1 = \psi_N \frac{((\mu_{tr})_N)_g}{\rho} (\mu_{gcp})_g \int_0^{x_1} \exp\left[-(\mu_{gcp})_g (x_1 - x)\right] dx$$

$$\psi_N \frac{((\mu_{tr})_N)_g}{\rho} \left[1 - \exp\left(-(\mu_{gcp})_g x_1\right)\right]$$

The quantity $\psi_N \frac{((\mu_{tr})_N)_g}{\rho}$ is the kerma in the gas, K_g, therefore

$$Dx_1 = K_g \left[1 - \exp\left(-(\bar{\mu}_{gcp})_g x_1\right)\right] \qquad 7.1$$

7.3 Charged Particles Liberated in the Wall

Particles released in the wall will give rise to an absorbed dose in the gas which will be a maximum at $x_1 = 0$, and for increasing x_1 the charged particle energy fluence will be attenuated.

In the wall, the energy released by the neutrons will be $\psi_N \frac{((\mu_{tr})_N)}{\rho_W}$ per unit mass, or $\psi_N ((\mu_{tr})_N)_W$ per unit length and cross-section.

In a thickness dx within the wall, and having unit cross-section perpendicular to the radiation beam, an energy transfer of $\psi_N ((\mu_{tr})_N)_W$ dx takes place.

For charged particle equilibrium, this must also be the charged particle energy deposited in dx =

$$\psi_{cp} (\bar{\mu}_{wcp})_W \, dx$$

where $(\bar{\mu}_{wcp})_W$ is the linear attenuation coefficient of the wall for charged particles originating in the wall. Thus

$$\psi_{cp} (\bar{\mu}_{wcp})_W = \psi_N ((\mu_{tr})_N)_W$$

$$\therefore \psi_{cp} = \psi_N \frac{((\mu_{tr})_N)_W}{(\bar{\mu}_{wcp})_W}$$

It is this charged particle energy fluence that issues from the chamber wall and enters the gas.

At a distance x_1 into the gas, it will give rise to an absorbed dose

$$Dx_1 = \psi_N \frac{((\mu_{tr})_N)_W}{(\mu_{wcp})_W} \frac{(\mu_{wcp})_g}{\rho_g} \exp\left(-(\mu_{wcp})_g\ x_1\right)$$

This can be rewritten as,

$$Dx_1 = \psi_N \frac{((\mu_{tr}/\rho)_N)_W}{(\mu_{wcp}/\rho)_W} \frac{(\mu_{wcp})_g}{\rho_g} \exp\left(-(\mu_{wcp})_g\ x_1\right) \qquad 7.2$$

$$Dx_1 = K_W \frac{(\mu_{wcp}/\rho)_g}{(\mu_{wcp}/\rho)_W} \exp\left(-(\mu_{wcp})_g\ x_1\right)$$

where $(\mu_{wcp}/\rho)_g$ and $(\mu_{wcp}/\rho)_W$ are the mass attenuation coefficient for wall charged particles in gas and wall respectively.

But $$\frac{(\mu_{wcp}/\rho)_g}{(\mu_{wcp}/\rho)_W} = (S_{wcp})_{g,W} = S_{g,m}$$

$$\therefore \quad Dx_1 = K_W\ S_{g,m} \exp\left(-(\mu_{wcp})_g\ x_1\right) \qquad 7.3$$

The method of calculation of the constituent terms of Equations 7.1 and 7.3 for individual particles will be developed in the following sections.

7.4 Calculation of μ_g from Stopping Power

The value of μ_g, the linear attenuation coefficient, for each particle type in each gas can be obtained by calculating the linear stopping power for each particle type and dividing by the energy of the particle.

7.4.1 Method for Deriving the Stopping Power of Heavy Ions from that of Protons

As mentioned in the preceding chapter, Dennis (1979) gives a method for deriving the stopping power of any ion from that of protons by means of a reduced stopping power parameter <S>, so that the stopping power $S_H(V)$ of a heavy ion of velocity V and atomic number Z may be related to the stopping power $S_p(V)$ of the same substance for protons by

$$S_H(V) = Z^2 \langle S \rangle S_p(V) \qquad 7.4$$

In this case, the actual stopping powers $S_H(V)$ are required, therefore the terms Z^2 <S> do not cancel as in the case of the ratio calculations.

From Dennis (1979), the stopping parameter <S> is given by

$$\langle S \rangle = 1 - (1.034 - 0.1777 \exp(-0.08114Z)) \exp -(V_2)^2$$

where $V_2 = V_1 = 0.0378 \sin(\frac{V_1 \pi}{2})$

$$V_1 = 0.886 \ (V/V_o) \ Z^{\frac{2}{3}}$$

and $V_o = c^2/h = 2.188 \times 10^6 ms^{-1}$

In the absence of relativistic effects, a heavy ion has velocity = $(\frac{2E_R}{M_R})^{\frac{1}{2}}$ where E_R = average recoil energy of ion as stated previously. A proton with velocity $(\frac{2E_R}{M_R})^{\frac{1}{2}}$ will have energy = $(\frac{mE_R}{M_R})$ where m = mass of proton. Therefore, $S_p(V)$ can be obtained for a proton of energy $(\frac{mE_R}{M_R})$ and substituted into Equation 3 to obtain $S_H(V)$ for a heavy ion of energy E_R.

Proton stopping power values were obtained from Janni (1966) as stated in the preceding chapter.

This procedure assumes that the charge on the heavy ions is the same as the charge on a proton.

7.4.2 Stopping Power of α Particles

As stated by Dennis, the procedure described in Section 7.3.1, does not apply to α particles, presumably because equation 7.4 makes no allowance for a difference in charge. For this reason, estimates for stopping powers of α particles in various gases are taken from a report prepared for the ICRU Stopping Power Committee by Powers (1978).

7.5 Analysis of C/CO_2 Chamber

The predominant reactions produced from neutron bombardment in both carbon and oxygen are elastic scattering and α particle production. Each important reaction will be dealt with individually.

7.5.1 Reactions in Carbon

The relative percentages of carbon recoils and α particles produced from neutron reactions in carbon are obtained from ICRU 26, Appendix A, Figure A2 which displays the fraction of energy transferred by any given mechanism against neutron energy. The fraction of carbon recoils (f_c) and α particles (f_α) for the neutrons used is estimated as 66% and 34% respectively.

7.5.1.1 Carbon Recoils

Since the majority of the carbon recoils are produced from elastic scattering, then the maximum energy of the carbon recoils =

$$\frac{4\, M_N\, M_R\, E_N}{(M_N + M_R)^2}$$

where M_N = mass of neutron

M_R = mass of recoil

E_N = average energy of neutron

The average recoil energy is therefore

$$\frac{2\, M_N\, M_R\, E_N}{(M_N + M_R)^2} \qquad 7.5$$

Since the average neutron energy is 8.4MeV obtained from the neutron energy fluence spectrum of Figure 1.1, then the average carbon recoil energy is 1.2MeV. Therefore 66% of the ionization in carbon is due to carbon recoils of average energy 1.2MeV.

7.5.1.2 α Particles

There are two prominent neutron reactions in carbon, producing α particles i.e.

1. ^{12}C (n, α)^{9}Be
2. ^{12}C (n, n'3α)

The fraction of neutron energy transferred by each mechanism f_α is shown in ICRU 26, Appendix A, Figure A2. The average α particle energy from neutron reactions in carbon can be estimated using the following procedure.

The neutron spectrum of Figure 1.1 is multiplied by $f_\alpha E\, N(E)$ to obtain the neutron energy fluence spectrum as shown in Figure 7.1. The mean neutron energy E_N for both reactions can be obtained; from E_N, the mean emitted particle energy can be estimated.

The predominant reaction in the production of α particles from carbon is obviously the ^{12}C (n, α)^{9}Be reaction; the mean neutron energy estimated from Figure 7.1 is 10.2MeV.

The average energy of the emitted particle is given by

$$E_\alpha = \left(\left(1 - \frac{m_\alpha}{m_\alpha + m_2}\right)\left(\frac{M_R E_N}{M_N + M_R} + (Q - E_1^* - E_2^*)\right) + \frac{M_N m_\alpha}{(M_R + M_N)^2}\right) \quad 7.6$$

See Appendix B.

where E_α = energy of α particle

m_α = mass of α particle

m_2 = mass of ^{9}Be particle

M_R = mass of ^{12}C recoil

M_N = mass of neutron

Q = reaction energy

E_1^* = residual energy of α particle

E_2^* = residual energy of ^{9}Be ion

E_N = energy of neutron

The reaction energy for the ^{12}C (n, α)^{9}Be reaction is - 5.704MeV from Dennis (1973) and Caswell and Coyne (1972).

Possible energies of E_2^* i.e. possible energy levels of ^{9}Be = 0, 1.67MeV, 2.43MeV, 3.03MeV, 4.70MeV and 6.66MeV, from Caswell and Coyne (1972).

Possible energies of E_1^* = 0, and 2.43MeV.

Possible combinations of E_1^* and E_2^*, reaction cross-sections and the resultant α particle energies as calculated from Equation 7.6, are shown in Table 7.1.

Taking the reaction cross-sections as being a measure of the probability of each reaction, then the average α particle energy E_α is calculated as being = 1.77MeV.

Of the possible combinations of E_1^* and E_2^* of Table 7.1, sequential 2-body decays can occur e.g.

$$n + {}^{12}C \rightarrow \alpha + {}^{9}Be\ (2.43MeV)$$
$${}^{9}Be\ (2.43MeV) \rightarrow {}^{8}Be\ (\text{ground state}) + n$$
$${}^{8}Be\ (\text{ground state}) \rightarrow 2\alpha$$

These sequential 2-body decays can be incorporated in the determination of the average energy of the α particles from the ^{12}C (n, n'3α) reactions.

The mean neutron energy associated with the ^{12}C (n, n'3α) reaction of Figure 7.1 is 12.9MeV. This reaction is more complicated in that it is divided into 8 modes of interaction as shown by Caswell and Coyne (1972). Their analysis is for 14MeV neutrons but since all reaction channels are also open at 12.9MeV, the resultant initial energy spectrum of Figure 3 of this publication for ^{12}C (n, n'3α) reaction should not be too different for 12.9MeV neutrons. A rough calculation of N_p at 1, 2, 3, 4, 5 and 6MeV

gives an average α particle energy of approximately 1.85MeV, which is not too different from that obtained from the ^{12}C (n, α) ^{9}Be reaction.

Therefore an average initial energy of α particles emitted from carbon is estimated as $(E_\alpha)_c$ = 1.80MeV.

7.5.1.3 ^{9}Be Recoils

Due to the significant effect of the ^{12}C (n, α) ^{9}Be reaction, the ^{9}Be contribution to the ionization cannot be ignored.

To estimate the average energy of the ^{9}Be recoils, the same procedure was followed as that described by Equation 7.6 i.e.

$$E_B = \left(\left(1 - \frac{m_B}{m_B + m_\alpha}\right)\left(\frac{M_R E_N}{M_N + M_R} + (Q - E_1^* - E_2^*)\right) + \frac{M_N m_B}{(M_R + M_N)^2} E_N\right) \quad 7.7$$

The resultant ^{9}Be energies as calculated from Equation 7.7 are also shown in Table 7.1. Taking the reaction cross-sections as being a measure of the probability of each reaction, then the average ^{9}Be recoil energy E_B is calculated as being 1.27MeV.

A summary of the relative percentages and the average energies of the particles produced in carbon are described in Section 7.5.1.4 and given in Table 7.2.

7.5.1.4 Summary of the Percentages of Total Kerma

A summary of the percentages of the total kerma transferred to the particular particles (f_i) in carbon is given in Table 7.2. These were obtained as follows.

f_i for individual elements is obtained by multiplying the kerma data from Table 7.8 (Coyne et al 1980), and the relative masses of each element present and adjusting to a total of 1.

For each element, in this case, carbon, f_i is divided between the different reactions with that element using data from ICRU 26, Figure A2. For each reaction, this fraction of kerma is divided between the particles in the ratio of their mean energies. Therefore, in the case of a carbon recoil (only one particle), it gains all the energy; in the case of ^{12}C (n, α) ^{9}Be, the kerma is divided in the ratio of mean energies; in the case of ^{12}C (n, n' 3α), the α particles are assumed to gain all the energy.

In carbon, f_i for carbon recoils is assumed to be 66%. Of the remaining 34%, it is assumed that the ^{12}C (n, α) ^{9}Be reaction yields 76% of α particles, and the ^{12}C (n, n' 3α) reaction yields 24% from Figure 7.1. Therefore, by taking the ratio of mean energies of the α particles and ^{9}Be recoils from the former reaction, it is assumed that α particles constitute 15.2% of total kerma, and ^{9}Be recoils 10.6%. Therefore, α particles from ^{12}C (n, n' 3α) reaction constitute 8.2% of the total kerma transferred to carbon.

7.5.2 Reactions in Oxygen

The relative percentages of oxygen recoils and α particles produced from neutron reactions in oxygen are obtained from ICRU 26, Appendix A, Figure A2, which displays the fraction of energy transferred by any given mechanism against neutron energy. The fraction of the energy transferred to oxygen recoils (f_o) and to α particles reactions $(f_\alpha)_o$ is estimated as 50% and 48% respectively, the other 2% being for other reactions such as (n, p) reactions.

7.5.2.1 Oxygen Recoils

Since the majority of oxygen recoils are produced from elastic scattering, the average energy of oxygen recoils is given by Equation 7.5. For an average neutron energy of 8.4MeV, an average oxygen recoil energy is calculated as 0.94MeV.

7.5.2.2 α Particles

There are two prominent neutron reactions in oxygen, producing α particles i.e.

1. ^{16}O (n, α) ^{13}C
2. ^{16}O (n, n'α) ^{12}C

The fraction of energy transferred by each mechanism f_α is again obtained from ICRU 26, Appendix A, Figure A2. The average α particle energy from neutron reactions in oxygen can be estimated via the neutron energy fluence spectrum as described in Section 7.5.1.2.

The predominant reaction in the production of α particles in oxygen is obviously the ^{16}O (n, α) ^{13}C reaction; the mean neutron energy estimated from Figure 7.2 is 9.47MeV.

The average energy of the emitted particle is given by Equation 7.6, where m_2 = mass of ^{13}C recoil and M_R = mass of ^{16}O recoil.

The reaction energy for the ^{16}O (n, α) ^{13}C reaction is - 2.215MeV (from Dennis (1973)). Possible energies of E_1^* are 0, 3.09 and 3.77MeV from Caswell and Coyne (1972). In the case of ^{13}C recoils, a neutron energy above 7.3MeV results in the ^{13}C recoil becoming excited to 3.09 and 3.77MeV levels and thereafter emitting gamma rays of these energies. Therefore possible values of E_2^* are 0, 3.09 and 3.77MeV also.

Possible combinations of E_1^* and E_2^*, reaction cross-sections, and the resultant α particle energies as calculated from Equation 7.6, are shown in Table 7.3.

Taking the reaction cross-sections as being a measure of the probability of each reaction, then the average α particle energy E_α is calculated as being 1.63MeV.

Very few data are to be found on the ^{16}O (n, n'α) ^{12}C reaction. It is however completely overshadowed by the ^{16}O (n, α) ^{13}C reaction. Therefore, since the mean neutron energy estimated for the ^{16}O (n, n'α) ^{12}C is 14MeV, and some of this energy is used in the neutron inelastic scattering reaction, then an overall α particle energy of 1.63MeV obtained from the ^{16}O (n, α) ^{13}C reaction is estimated.

7.5.2.3 ^{13}C Recoils

Due to the significant effect of the ^{16}O (n, α) ^{13}C reaction, the ^{13}C contribution to the ionization cannot be ignored.

To estimate the average energy of the ^{13}C recoils, the same procedure was followed as that described by Equation 7.6, where m_2 = mass of ^{16}O recoil and M_R = mass of ^{13}C recoil.

The resultant ^{13}C energies as calculated from Equation 7.6 are also shown in Table 7.3. Taking the reaction cross-sections as being a measure of the probability of each reaction, then the average ^{13}C recoil energy is calculated as being 0.9MeV.

7.5.2.4 Summary of Particles Produced in C/CO_2 Chamber

The percentages of the total energy carried by the particle and the average energies of the particles produced in CO_2 are given in Table 7.4. These are obtained by following the same procedure as discussed in Section 7.5.1.4 for reactions in carbon only.

7.5.3 Energies of Wall and Gas Particles

Having established the energies of particles produced both in carbon and oxygen as shown in Tables 7.2 and 7.4, a distinction must be made between particles produced in the wall and particles produced in the gas. If a particle is released in the wall, it will have all energies from its energy at production down to zero. Therefore, the assumption is made that the mean energy of the particles issuing from the wall is equal to half the initial energy.

For particles released in the gas, the assumption is made that the particle will have its initial energy.

7.6 Comparison of Theory and Experiment of the Relative Charged Particle Distribution in a C/CO_2 Chamber

The mean energies and the percentages of the total energy carried by particles produced both in the wall and the gas of the C/CO_2 chamber have been established in the preceding sections. The method of calculating μ has been dealt with in Section 7.4; values of μ for particles produced both in wall and gas are shown in Table 7.5. Therefore, these parameters must now be related to Equations 7.1 and 7.3 which in turn must be related to experiment.

Equations 7.1 and 7.3 are expressed in terms of absorbed dose, whereas experimental measurements are made in terms of charge

per unit volume. The proportionality between these two parameters is $\frac{\overline{W}}{e}$. Therefore, equation 7.1 can be expressed as

$$\left(\frac{Q}{m}\right)_x = \frac{eK_g}{\overline{W}_1} \; 1 - \exp\left(-(\mu_{gcp})\, x_1\right) \qquad 7.8$$

for charged particles liberated in the gas, Equation 7.3 can be expressed as

$$\left(\frac{Q}{m}\right)_x = \frac{eK_w}{\overline{W}_2} \; S_{g,m} \exp\left(-(\mu_{wcp})_g\, x_1\right) \qquad 7.9$$

for charged particles liberated in the wall. As regards $\overline{W}_1$ and $\overline{W}_2$ the average energy required to produce an ion pair in the gas due to particles liberated in the gas and wall respectively, $\overline{W}$ values due to gas and wall particles are taken from ICRU 31 and Nguyens et al (1980) and are shown in Table 7.6. It would seem inappropriate to perform this analysis using individual $\overline{W}$ values for each particle because no data are available on the $\overline{W}$ values of ^{9}Be recoils in CO_2. Therefore, an effective $\overline{W}$ value ($\overline{W}_{eff}$), is calculated for both wall and gas by taking the percentages of available $\overline{W}$ values for carbon and oxygen recoils in wall and gas respectively. The resulting ratio $\overline{W}_1/\overline{W}_2$ = 1.02 i.e. a difference between $\overline{W}_1$ and $\overline{W}_2$ of approximately 2%. Because errors are associated with individual $\overline{W}$ values e.g. in the case of 0.9, 1.8

and 1.63MeV α particles, $\bar{W}$ values are estimated from 5.3MeV α particles, and because no data are available for ^{9}Be recoils, the assumption is made that $\bar{W}_1 = \bar{W}_2$ for the purposes of simplifying calculations.

An overall stopping power ratio for C/CO_2 can be calculated from the stopping powers in carbon and CO_2, of carbon recoils, α particles, and ^{9}Be recoils produced in the wall.

Table 7.6 shows the stopping power ratios of 0.6MeV carbon recoils, 0.9MeV α particles and 0.64MeV ^{9}Be recoils for a C/CO_2 chamber. Assuming their relative abundances to be 66%, 21% and 13% respectively, the overall stopping power ratio $S_{m,g}$ for C/CO_2 chamber for the purposes of this calculation is estimated to be 1.115.

This estimate can be compared with the data of Bichsel and Rubach (1978). They give values of $S_{m,g}$ for α particles and ^{12}C ions for an infinitesimal Bragg-Gray chamber and a neutron energy of 14MeV. Assuming relative abundances of α particles and ^{12}C ions of 34% and 66% respectively, the value of $S_{m,g}$ is calculated as 0.99 ± 0.13 which incorporates the calculated value from Janni.

The estimate from Janni can also be compared with the stopping power ratio calculated from Edwards (1978). The value of $S_{m,g}$ is estimated as 1.13 ± 0.06 which agrees within the uncertainties with the estimated value of Janni.

7.6.1 Summary of the Relative Contribution to Ionization from Wall and Gas

The total ionization from wall particles is taken from Equation 7.9 i.e. the charge per unit mass is given by -

$$\left[\left(\frac{Q}{m}\right)_x\right]_w = \sum_{i = a,b,c} \frac{e\, f_i\, S_{g,m}\, K_w \exp\left(-\left((\mu_{wcp})_g\right)_i\, x\right)}{\overline{W}_2} \qquad 7.10$$

where a, b, and c refer to 0.6MeV carbon recoils, 0.9MeV α particles and 0.64MeV ^{9}Be recoils from the wall respectively; f_i refers to the fraction of energy due to these particles respectively, taken from Table 7.2

The total ionization from gas particles is taken from Equation 7.8 i.e. the charge per unit mass is given by -

$$\left[\left(\frac{Q}{m}\right)_x\right]_g = \sum_{i = d,e,f,g,h,j} \frac{e\, f_i\, K_g \left(1 - \exp\left(-\left((\bar{\mu}_{gcp})_g\right)_i\, x\right)\right.}{\overline{W}_1} \qquad 7.11$$

where d, e, f, g, h, and j refer to 1.2MeV carbon recoils, 1.8MeV α particles, 1.27MeV ^{9}Be recoils, 0.94MeV ^{16}O recoils, 1.63MeV α particles and 0.9MeV carbon recoils respectively; f_i refers to the fraction of energy due to the particles, respectively, taken from Table 7.4.

Individual contributions to the wall and gas ionization as described by Equations 7.10 and 7.11 are shown in Figure 7.4, assuming

$\overline{W}_1 = \overline{W}_2$ (as has been discussed), and displaying 1.12 for the wall particle contributions. The individual total wall and gas contributions are shown in Figure 7.5.

The total ionization in the C/CO_2 chamber is given by the sum of Equations 7.10 and 7.11 i.e.

$$\left[\left(\frac{Q}{m}\right)_x\right]_T = \left[\left(\frac{Q}{m}\right)_x\right]_W + \left[\left(\frac{Q}{m}\right)_x\right]_g \qquad 7.12$$

as shown in Figure 7.6.

$\left[(Q/m)_x\right]_T$ describes the incremental ionization in an increment of chamber volume, since density of CO_2 remains constant. The experiments of Chapters 4, 5 and 6 are displayed in terms of q_{sat}/d where q_{sat} is the integrated charge over the total chamber volume.

Therefore to relate theory and experiment, Equations 7.10 and 7.11 must be integrated with respect to x from x = 0 to x = d, and then divided by d i.e.

$$\left(\frac{q_{sat}}{d}\right)_{theory} = \frac{\int_o^d \left[\left(\frac{Q}{m}\right)_x\right]_w + \int_o^d \left[\left(\frac{Q}{m}\right)_x\right]_g}{d} \qquad 7.13$$

Theory and experiment can be compared by normalising both $(q_{sat}/d)_{expt}$ from Chapter 6 and $(q_{sat}/d)_{theory}$ from Equation 7.13 as is shown in Figure 7.7

As is shown in Figure 7.7, in the range 0 - 8mm, theory predicts a more rapid decrease in (q_{sat}/d) with plate separation to a lower value, than is shown by experiment. Theory predicts a rise in q_{sat}/d in the range greater than 8mm whereas experiment shows q_{sat}/d to begin to flatten out.

Unfortunately, the scope of the C/CO_2 chamber is such that the $(q_{sat}/d)_{expt}$ contribution beyond 18mm cannot be obtained. $(q_{sat}/d)_{theory}$, can, however, be continued to higher plate separations, and with increasing d, $(q_{sat}/d)_{theory}$ approaches a value equal to the value of $(q_{sat}/d)_{theory}$ as $d \rightarrow 0$, i.e. $\left[\frac{(q_{sat}/d)_{small}}{(q_{sat}/d)_{large}}\right]_{theory} = 1.0.$

The predictions of Chapter 6, Section 6.1, Equation 6.3 states that

$$\frac{(q_{sat}/d)_{small}}{(q_{sat}/d)_{large}} = \frac{K_m}{K_g} \quad (S_{m,g})^{-1}$$

where K_m/K_g = ratio of kerma in wall and gas. We have chosen a value of $(S_{m,g})$ = 1.12 earlier in this chapter. From Table 6.5, the ratio of kerma is calculated as 1.116. Therefore the value of $\frac{(q_{sat}/d)_{small}}{(q_{sat}/d)_{large}}$ = 1.0 is in good agreement with the value as calculated previously.

7.7 Analysis of C/Air Chamber

The elemental composition of air is shown in Table 7.9. The predominant reactions produced from neutron bombardment in oxygen have been discussed in Section 7.5. Reactions in nitrogen have been mentioned and will now be discussed in detail.

7.7.1 Reactions in Nitrogen

The relative percentages of nitrogen recoils, protons, deuterons and α particles produced in nitrogen are obtained from ICRU 26, Appendix A, Figure A2, which displays the fraction of energy transferred by any given mechanism against neutron energy. The fractions of nitrogen recoils, protons, deuterons, α particles and other reactions for the neutrons used are estimated as 40%, 22%, 4%, 31% and 3% respectively.

7.7.1.1 Nitrogen Recoils

The average energy of the resultant nitrogen recoils are given by Equation 7.5 and is calculated as 1.05MeV.

7.7.1.2 Deuterons

The predominant neutron reactions in nitrogen producing deuterons is the $^{14}N(n, d)\ ^{13}C$ reaction. The fraction of neutron energy transferred by this mechanism, f_d, is shown in ICRU 26, Appendix A Figure A2. The average deuteron energy from neutron reactions in nitrogen can be estimated via the neutron energy fluence spectrum (Figure 7.3) as described in Section 7.5.1.2; the mean neutron energy estimated from Figure 7.3 is 10.6MeV. The average energy of the emitted particle is given by Equation 7.6 where m_2 = mass of ^{13}C recoil and M_R = mass of ^{14}N recoil. The reaction energy for the $^{14}N(n, d)\ ^{13}C$ reaction is - 5.326MeV (from Dennis 1973).

Possible values of E_1^* and E_2^* are 0 and 3.68MeV (from Caswell and Coyne 1972).

Possible combinations of E_1^* and E_2^*, reaction cross-sections, and the resultant deuteron energies as calculated from Equation 7.6 are shown in Table 7.10.

Taking the reaction cross-sections as being a measure of the probability of each reaction, then the average deuteron energy E_d is calculated as 1.6MeV.

7.7.1.3 ^{13}C Recoils

The ^{13}C recoil contribution from the $^{14}N(n, d)\ ^{13}C$ reaction must be considered. To estimate the average energy of ^{13}C recoils,

the same procedure was followed as that described by Equation 7.6, where m_2 = mass of ^{14}N recoil and M_R = mass of ^{13}C recoil.

The resultant ^{13}C recoil energies as calculated from Equation 7.6 are also shown in Table 7.10. Taking the reaction cross-section as being a measure of the probability of each reaction, then the average ^{13}C recoil energy is calculated as 0.302MeV.

7.7.1.4 α Particles

The predominant neutron reaction in nitrogen producing α particles is the $^{14}N(n, \alpha)\ ^{11}B$ reaction. The fraction of energy transferred by this mechanism is again obtained from ICRU 26, Appendix A, Figure A and the average α particle energy is again obtained via the neutron energy fluence spectrum; the mean neutron energy for this reaction is estimated as 7.8MeV. The average energy of the emitted α particle is given by Equation 7.6. The reaction energy for this reaction is - 0.157MeV (Dennis 1973). Possible energies of E_1^* and E_2^* are 0, 2.214MeV, 4.444MeV and 5.019MeV (Caswell and Coyne 1972). Possible combinations of E_1^* and E_2^*, reaction cross sections, and the resultant α particle energies as calculated from Equation 7.6 are shown in Table 7.11. Taking the reaction cross-sections as being a measure of the probability of each reaction, then the average α particle energy is calculated as 2.62MeV.

7.7.1.5 ^{11}B Recoils

The ^{11}B recoil contribution from the $^{14}N(n, \alpha)\ ^{11}B$ reaction must be considered. The same procedure as has been followed during the course of this chapter has been employed, resulting in an average ^{11}B recoil energy of 1.07MeV (Table 7.11).

7.7.1.6 Protons

There are two prominent neutron reactions in nitrogen producing protons i.e. $^{14}N(n, p)\ ^{14}C$ and $^{14}N(n, n'p)\ ^{14}C$. The same procedure is followed as has been described during the course of this chapter. For the $^{14}N(n, p)\ ^{14}C$ reaction, the mean neutron energy estimated from Figure 7.3 is 8.13MeV; the reaction energy is 0.626MeV; possible energies of E_1^* and E_2^* are 0, 6.78MeV and 8.32MeV (Ajzenberg-Selove 1970). Resultant proton energies as calculated from Equation 7.6 are shown in Table 7.12; the average proton energy is calculated as 4.5MeV.

Very little information is available on the $^{14}N(n, n'p)\ ^{13}C$ reaction, which is secondary in importance to the $^{14}N(n, p)\ ^{13}C$ reaction. Therefore, since the mean neutron energy estimated for the $^{14}N(n, n'p)\ ^{13}C$ reaction is 12.7MeV, and some of this energy is used in the neutron inelastic scattering reaction, then an overall proton energy of 4.5MeV obtained from the $^{14}N(n, p)\ ^{14}C$ reaction is estimated.

7.7.1.7 ^{14}C Recoils

The ^{14}C recoil contribution from the $^{14}N(n, p)\ ^{14}C$ and $^{14}N(n, n'p)\ ^{14}C$ reactions must be considered. Using the same procedure as previously, an average ^{14}C recoil energy of 0.39MeV is estimated (Table 7.12).

7.7.2 Summary of Relative Contributions in C/Air Chamber

Summaries of the relative percentages and the average energies of the particles produced in carbon and air are given in Tables 7.2 and 7.13 respectively.

Values of μ for both wall and gas particles are shown in Table 7.14; calculation of μ is based on the method outlined in Section 7.3.

The total ionization from wall and gas particles is again given by Equations 7.10 and 7.11, respectively, where $S_{g,m}$ now represents the stopping power ratio of air and carbon, $\overline{W}_1$ is the average energy required to produce an ion pair in air due to particles produced in air, and $\overline{W}_2$ is the average energy required to produce and ion pair in air due to particles produced in the wall.

Very few data are available on the $\overline{W}$ values of the individual particles emanating from both wall and gas. Therefore the assumption is made that $\overline{W}_1 = \overline{W}_2$.

An overall stopping power ratio can be calculated from the stopping powers in air of carbon recoils, α particles and ^{9}Be

recoils issuing from the wall. Table 7.15 shows the stopping power ratios of 0.6MeV ^{12}C recoils and 0.64MeV ^{9}Be recoils as taken from Janni (1966) and of 0.9MeV α particles from Powers (1980). Assuming the relative abundances from Table 7.2, the overall stopping power ratio $S_{m,g}$ for C/Air chamber is estimated to be 1.05. Kerma values are shown in Table 7.8. Individual contributions to the ionization in the C/Air chamber are shown in Figure 7.8, assuming $S_{m,g} = 1.118$. Individual total contributions from wall and gas are shown in Figure 7.9: $\left[(Q/m)_x\right]_T$ from Equation 7.12 is shown in Figure 7.10.

With $S_{m,g} = 1.05$, the wall contribution is too large compared to the gas contribution contrary to experimental results. A value of $S_{m,g} = 1.18$ gives very good agreement with experiment in the range 0 - 18mm, as is shown in Figure 7.11.

A continuation of $(q_{sat}/d)_{theory}$ to higher plate separations results in a value of $\left[\frac{(q_{sat}/d)_{small}}{(q_{sat}/d)_{large}}\right]_{theory} = 0.68.$

This is in good agreement with Equation 6.3: a combination of $S_{m,g} = 1.18$ and $(K_{m,g}) = 0.787$ from Table 6.5 results in a value of $\frac{(q_{sat}/d)_{small}}{(q_{sat}/d)_{large}} = 0.667.$

7.8 Analysis of C/TE Chamber

The elemental composition of TE gas is shown in Table 7.16. The predominant reactions produced from neutron bombardment in both carbon and oxygen have been discussed in Section 7.5. The predominant reaction in hydrogen is elastic scattering i.e. recoil proton production. The predominant reaction in nitrogen is assumed to be elastic scattering although α particle and proton production would also contribute; the reason for this omission is because nitrogen is only a 3.5% fraction of the elemental composition of TE gas by weight, therefore a more detailed analysis would not affect the final result significantly. The average energies of the resultant protons and nitrogen recoils are calculated from Equation 7.5.

Summaries of the relative percentages and the average energies of the particles produced in carbon and TE gas are given in Tables 7.2 and 7.17 respectively. These energies are based on the assumption that the average energy of the wall particles is half the initial energy, and the average energy of the gas particles is the initial energy, as discussed in Section 7.5.3.

Values of μ for both wall and gas particles are shown in Table 7.8; calculation of μ is based on the method outlined in Section 7.3. The total ionization from wall and gas particles is again given by Equations 7.10 and 7.11 respectively, where $S_{g,m}$ now represents the stopping power ratio between TE gas and carbon, $\overline{W}_1$ is the average energy required to produce an ion pair in the TE gas due to particles produced in the gas, and $\overline{W}_2$ is the average energy required to produce an ion pair in the TE gas due to particles produced in the wall. For wall particles (Equation 7.10), i = a, b, c where a, b and c again refer to 0.6MeV ^{12}C recoils, 0.9MeV α particles and 0.64MeV ^{9}Be recoils respectively. For gas particles (Equation 7.11), i = d, e, f, g, h, j, k, l where d, e, f, g, h, j, k and l refer to 4.2MeV protons, 1.2MeV ^{12}C recoils, 1.8MeV α particles, 1.27MeV ^{9}Be recoils, 1.05MeV ^{14}N recoils, 0.94MeV ^{16}O recoils, 1.63MeV α particles and 0.9MeV ^{13}C recoils respectively.

Values of $\overline{W}_1$ and $\overline{W}_2$ for particles liberated in both gas and wall are taken from ICRU 31 and Nguyens et al (1980) and are shown in Table 7.9. Again, it would seem inappropriate to use individual $\overline{W}$ values for each particle because no data are available on the $\overline{W}$ values of ^{9}Be recoils in TE gas. Therefore, effective $\overline{W}$ values ($\overline{W}_{eff}$) are calculated for both wall and gas by taking the percentages of available $\overline{W}$ values for particles produced in wall and gas respectively. The resulting ratio $\overline{W}_1/\overline{W}_2$ = 1.03 i.e. a difference between $\overline{W}_1$ and $\overline{W}_2$ of approximately 3%. Again, because of errors associated with individual $\overline{W}$ values and the lack of data for ^{9}Be recoils, the assumption is made that $\overline{W}_1 = \overline{W}_2$ for the purposes of simplifying calculations.

An overall stopping power ratio for C/TE can be calculated from the stopping powers in carbon and TE gas of carbon recoils, α particles and ^{9}Be recoils produced in the wall. Table 7.20 shows the stopping power ratios of 0.6MeV ^{12}C recoils and 0.64MeV ^{9}Be recoils as taken from Janni (1966) and of 0.9MeV α particles from Powers (1978). Assuming the relative abundances from Table 7.2, the overall stopping power ratio $S_{m,g}$ for C/TE chamber is estimated to be 0.66.

Kerma values are shown in Table 7.8.

To relate theory and experiment, $(q_{sat}/d)_{theory}$ is again given by Equation 7.13 and $(q_{sat}/d)_{expt}$ is taken from Chapter 6, Figure 6.2; for comparison, $(q_{sat}/d)_{theory}$ and $(q_{sat}/d)_{expt}$ are both normalised.

Using a value of $S_{m,g} = 0.66$, $(q_{sat}/d)_{theory}$ does not agree with $(q_{sat}/d)_{expt}$, in that experiment shows q_{sat}/d to increase to approximately 18% at large plate separations, whereas theory predicts q_{sat}/d to fall to approximately 35% at large plate separations.

Theory and experiment would agree if a combination of $S_{m,g}\ \bar{W}_1/\bar{W}_2 = 1.33$, which is a complete contradiction to the value of 0.66 calculated from Janni. A value of $S_{m,g} = 1.33$ indicates that the stopping power of carbon is greater than that of TE gas. In fact,

the stopping power of TE gas is larger than that of carbon because of the large stopping power of methane, a constituent compound of TE gas. (This large value of S_{CH_4} is confirmed in Chapter 8, where $\overline{W}$ values are discussed). Therefore, merely choosing a suitable value of $S_{m,g}$ to fit experiment does not appear to be the solution in this case.

The major difference in the C/TE chamber from the C/CO_2 and C/Air cases is the introduction of hydrogen into the calculations. C/CO_2 and C/Air give good results because we are dealing with heavy recoils and α particles only, with the same order of magnitude in values of kerma, stopping power, energy, μ values, range, etc.

However, the parameters in similar calculations with protons involve energies of the order of 4 times those of the heavy recoils and α particles, kerma values of hydrogen of the order of 10 times that of carbon, oxygen and nitrogen, accumulating in a μ value of the order of 100 times smaller than the μ values of the heavy recoils and α particles.

It may be assumed that the heavy recoil and α particle contributions of Figure 7.8 are reasonably accurate, since C/CO_2 and C/Air chambers give good agreement between theory and experiment.

Clearly, the disagreement between theory and experiment in the C/TE case lies primarily in the theoretical proton gas contribution not building up quickly enough with respect to plate separation

i.e. the value of μ assigned to protons is too low. In fact a value of μ of $0.21cm^{-1}$, a value 10 times that of the predicted value, allows a build up of protons which results in the theoretical curve of Figure 7.12. Individual contributions to the ionization in the C/TE chamber are shown in Figure 7.13, assuming $S_{m,g}$ = 0.66 and μ_g for protons = $0.21cm^{-1}$. The individual total wall and gas contributions are shown in Figure 7.14; the total ionization as given by Equation 7.12 is shown in Figure 7.15.

A value of $\mu = 0.21cm^{-1}$ indicates,

1. The protons to have a lower average energy than 1.2MeV, in this case, an energy of approximately 2.0MeV; or

2. The angular distribution to be other than a generally forward distribution i.e. a more isotropic distribution may be assumed.

The situation in reality is likely to be a combination of both cases, since a small change in either energy or angular distribution results in a large change in μ.

As was discussed for the C/CO_2 chamber, $(q_{sat}/d)_{expt}$ cannot be continued to higher plate separations. However, a continuation of $(q_{sat}/d)_{theory}$ results in a flattening of the curve at a value of $(q_{sat}/d)_{theory}$ corresponding to a ratio of $\left[\frac{(q_{sat}/d)_{small}}{(q_{sat}/d)_{large}}\right]_{theory} = 0.27$.

This result is in good agreement with Chapter 6, Equation 6.3; a combination of a value of $S_{m,g} = 0.66$ as used in this analysis and a kerma ratio of 0.179 obtained from Table 6.5 results in a value of $\left[\frac{(q_{sat}/d)_{small}}{(q_{sat}/d)_{large}}\right]_{theory} = 0.271$.

7.9 Summary

The relative charged particle contribution in CO_2, TE gas, and air from the wall and gas particles in C/CO_2, C/TE, and C/Air chambers, respectively, has been estimated.

In all three analyses, there have been obvious shortcomings in the theory, exhibiting themselves in different ways.

The general shortcomings common to all three situations can be summarised as follows -

7.9.1 Neutrons are assigned one average energy per individual reaction, as calculated from the particle energy fluence spectrum, when in fact, the neutrons have a range of energies.

7.9.2 The individual particle energies are calculated from this one average neutron energy, and in turn, the various particles are assigned one average energy.

7.9.3 The fraction of energy transferred by a given mechanism is calculated from Appendix A, Figure A2, ICRU 26, which is as the fraction of energy transferred per 0.5MeV energy interval. Calculations in this chapter use the mean energy fraction transferred by each mechanism over the energy range 0 - 20MeV.

7.9.4 Relatively unimportant reactions are ignored e.g.

a) In the case of reactions in oxygen, 2% of reactions other than ^{16}O recoil and α particle production, are not included.

b) The ^{16}O (n, n'α) ^{12}C reaction is included in the calculation involving the ^{16}O (n, α) ^{13}C reaction.

7.9.5 The factor μ is calculated using a single average particle energy, and assuming a generally forward distribution. No provision is made for differing μ values with differing energy, or differing angular distribution with each particle type.

7.9.6 The stopping power values as used in the calculation of μ for each particle type, and $S_{m,g}$ were calculated approximately from an empirical formula given by Dennis (1979) for heavy recoils. The stopping power values of protons of the same velocity as each particle type, also involved in this calculation, were taken from an extrapolation of the data of Janni (1966). This is not so important in the case of $S_{m,g}$, as any discrepancy in the calculation of $\langle S \rangle$ and Z^2 will cancel in any ratio calculations.

7.9.7 Wall and gas particles are assigned an average energy which is half their initial energy, and their initial energy, respectively. This is perhaps the assumption which has the greatest effect on the disagreement between theory and experiment.

It may be that the wall particles produced near the wall/gas interface contribute most to the ionization and would therefore not have lost a great deal of their initial energy when entering the gas; the wall particles produced deep in the wall may have been stopped before entering the gas. This would result in wall particles having an average energy somewhere between their initial and half their initial energy.

Also, the gas particles produced at lower plate separations would have lost some of their energy before reaching higher plate separations, so would have energies lower than their initial energies.

Shortcomings specific to individual chamber analyses can be summarised as follows -

7.9.8 C/CO_2 Chamber - Limitations

The calculation of an overall $\overline{W}$ value for both wall and gas, involved extrapolations from the data given by Nguyens et al (1980) for recoil particles, when available, and from ICRU 31 for α particles. No data were available for ^{9}Be recoils. Since an overall $\overline{W}_{eff}$ ratio for C/CO_2 resulted in a value differing by only a few percent from 1.0, the approximation was made that $\overline{W}_1/\overline{W}_2 = 1.0$.

7.9.9 C/TE Chamber - Limitations

7.9.9.1 For reactions in nitrogen, it was assumed that the predominant reaction of elastic scattering was the only reaction, although α particle and proton production would also contribute.

7.9.9.2 In order to calculate the stopping powers in TE gas, the stopping powers in the constituent compounds i.e. CH_4, CO_2 and N_2, were obtained and an overall stopping power was calculated using the Bragg Additivity Rule; Bichsel (1977) claims that the Bragg Additivity Rule can only be applied with an uncertainty exceeding 3%.

7.9.9.3 The only approximation obtained for $S_{m,g}$ was that calculated from Janni. No other data on the $S_{m,g}$ for C/TE chamber could be obtained.

7.9.10 C/Air Chamber - Limitations

7.9.10.1 Deuterons and ^{13}C recoils are not included in the final overall contribution as they each contribute less than 2% to the ionization in N_2.

7.9.10.2 4% of the reactions in N_2, which are other than those dealt with in detail, have been omitted in the final contribution.

7.9.10.3 The approximation was made that $\overline{W}_1 = \overline{W}_2$, due to the lack of available data.

Taking the 3 cases described as a whole, theoretical conditions ascribed to all chambers are those which give best agreement between theory and experiment. For example, it may be the case that a slight change in theory may benefit agreement between theory and experiment in the case of the C/CO_2 chamber, but would result in complete disagreement in the case of the C/Air chamber.

The results as shown are, in fact, the best compromise of the outlined theory to give balanced results in all three cases.

7.10 Conclusion and Comparison with the Results of Makarewicz and Pszona (1981)

It must be concluded that an accurate picture of the relative charged partical contribution in an ionization chamber is very difficult, if not impossible, to achieve with existing theory.

It is therefore a series of estimations, based on some broad assumptions, which are presented in this thesis.

Makarewicz and Pszona describe partial conversion factors for gas and wall given by

$$r_g = \left[\frac{1}{1 + cR/d}\right] \frac{K_g}{K_w}$$

for gas conversion factors and

$$r_w = 1 - \frac{1}{1 + cR/d} S_{g,m}$$

for wall conversion factors where R = range of individual particles in the gas of interest.

For C/CO_2 chamber, Makarewicz and Pszona display their results as R/d against r for both wall and gas particles, using a value of c = 0.31.

In order to compare their results with the results given in this thesis, the range of particles in a C/CO_2 chamber can be calculated from $1/\mu$ where μ has been described as the linear attenuation coefficient for each particle type in a particular gas. Values of μ for C/CO_2 chamber are given in Table 7.5. A plot of R/d against r for all particles mentioned in Table 7.5 is displayed in Figure 7.16, assuming $S_{m,g} = 1.12$ and $K_{g,m} = 0.91$. The results agree very well with the results of Makarewicz and Pszona with only a slight difference at large plate separations for gas particles due to a difference in the choice of kerma and stopping power values.

TABLE 7.1 Factors Involved in the Determination of Average α Particle and ^{9}Be Recoil Energies from ^{12}C (n, α) ^{9}Be Reaction

Options	Reaction X-section mbn	E_α (MeV)	E_B (MeV)
1. $E_1^* = 0$, $E_2^* = 0$	49	2.80	1.69
2. $E_1^* = 0$, $E_2^* = 1.67$MeV	14	1.65	1.17
3. $E_1^* = 0$, $E_2^* = 2.43$MeV	17.5	1.12	0.94
4. $E_1^* = 0$, $E_2^* = 3.03$MeV	14	0.71	0.76
5. $E_1^* = 2.43$MeV, $E_2^* = 0$	17.5	1.12	0.94

TABLE 7.2 Percentages and Average Energies of Particles Produced in Carbon

Particle	Average Energy	Percentage
Carbon Recoil	1.20MeV	66%
α Particle	1.80MeV	23.4%
^{9}Be Recoil	1.27MeV	10.6%

TABLE 7.3 Factors Involved in the Determination of Average α Particle and ^{13}C Recoil Energies from $^{16}O(n,\alpha)\ ^{13}C$ Reaction

Options	Reaction X-section mbn	E_α (MeV)	E_C (MeV)
1. $E_1^* = 0,\ E_2^* = 0$	23	5.34	2.13
2. $E_1^* = 0,\ E_2^* = 3.09$MeV	15	3.02	1.36
3. $E_1^* = 3.09$MeV, $E_2^* = 0$	15	3.02	1.36
4. $E_1^* = 0,\ E_2^* = 3.77$MeV	52	2.51	1.19
5. $E_1^* = 3.77$MeV, $E_2^* = 0$	52	2.51	1.19
6. $E_1^* = 3.09$MeV, $E_2^* = 3.09$MeV	30	0.71	0.59
7. $E_1^* = 3.09$MeV, $E_2^* = 3.77$MeV	67	0.20	0.42
8. $E_1^* = 3.77$MeV, $E_2^* = 3.09$MeV	67	0.20	0.42

TABLE 7.4 Fraction of Total Kerma, f_i and Average Energies of Particles Produced in CO_2

Particle	Average Energy (MeV)	f_i
^{16}O recoil	0.94	0.349
α particle	1.64	0.214
^{13}C recoil	0.90	0.118
^{12}C recoil	1.20	0.200
α particle	1.80	0.071
^{9}Be recoil	1.27	0.032
Others	-	0.016

TABLE 7.5 Values of Linear Attenuation Coefficients $(\mu_{cp})_g$ for particles Produced in Wall and Gas in C/CO_2 Chamber

Particle	Arising in	E_R	E_P	S_P	$\langle S \rangle$	S_H	S_{linear}	$(\mu_{cp})_g$
^{12}C recoil	W	0.6	0.05	860	0.083	2570	4.65	7.76
α particle	W	0.9	-	-	-	1905	3.45	3.85
^{9}Be recoil	W	0.64	0.072	725	0.102	1183	2.14	3.35
^{12}C recoil	G	1.2	0.101	668	0.086	2068	3.75	3.12
α particle	G	1.8	-	-	-	1489	2.70	1.50
^{9}Be recoil	G	1.27	0.142	654	0.104	1088	1.97	1.55
^{16}O recoil	G	0.94	0.059	825	0.103	5438	9.84	10.48
α particle	G	1.63	-	-	-	1562	2.83	1.74
^{13}C recoil	G	0.9	0.07	760	0.084	2298	4.16	4.62

W and G are wall and gas respectively

E_R = energy of particle (MeV)

E_P = energy of proton of same velocity (MeV)

S_P = mass stopping power of proton of same velocity (MeV $g^{-1}cm^2$)

S_H = mass stopping power of recoil or α particle (MeV $g^{-1}cm^2$)

$S_{linear} = S_H/\rho$ where ρ = density of air at 23°C units - MeV cm^{-1}

$(\mu_{cp})_g = \frac{S_{linear}}{E_R}$

TABLE 7.6 $\overline{W}$ Values for Particles Produced in C/CO_2 Chamber

Particle	$\overline{W}$(eV)	Reference	
0.6MeV ^{12}C recoil	42.5	Nguyens et al (1980)	$(\overline{W}_{eff})_w = \overline{W}_2 = 40.5eV$
0.9MeV α particle	34.2	ICRU 31 (1979) for E_α = 5.3MeV	
0.64MeV ^{9}Be recoil	-		
0.94MeV ^{16}O recoil	45.0	Nguyens et al (1980)	$(\overline{W}_{eff})_g = \overline{W}_1 = 41.4eV$
1.63MeV α particle	34.2	ICRU 31 (1979) for E_α = 5.3MeV	
0.9MeV ^{13}C recoil	42.5	Nguyens et al (1980)	
1.2MeV ^{12}C recoil	42.5	Nguyens et al (1980)	
1.27MeV ^{9}Be recoil	-		
1.8MeV α particle	34.2	ICRU 31 (1979) for E_α = 5.3MeV	

TABLE 7.7 Stopping Power Ratios for Particles Produced in Carbon Wall of C/CO_2 Chamber, from Janni (1966) and Powers (1978)

Particle	$(S_{mass})_C$	$(S_{mass})_{CO_2}$	$S_{m,g}$
0.6MeV ^{12}C recoil	2840	2570	1.105
0.9MeV α particle	2063	1855	1.112
0.64MeV ^{9}Be recoil	1389	1183	1.172

S_{mass} units MeV $g^{-1}cm^2$

TABLE 7.8 Kerma Values as Obtained from Computation of Data by Coyne (1980) and Neutron Spectrum of Bonnet (1980)

Element	Kerma Values x 10^{-9} Gy
Hydrogen	38.430
Carbon	0.829
Nitrogen	1.112
Oxygen	0.710

TABLE 7.9 Elemental Composition of Air

Element	Percentage by Weight
O	23.2
N	75.5
Ar	1.3

TABLE 7.10 Factors Involved in the Determination of Average Deuteron and ^{13}C Recoil Energies from ^{14}N (n, d) ^{13}C Reaction

Options	Reaction X-section mbn	E_d (MeV)	E_c (MeV)
$E_1^* = 0$, $E_2^* = 0$	27.4	3.97	0.665
$E_1^* = 3.68$MeV, $E_2^* = 0$	78.7	0.775	0.175

TABLE 7.11 Factors Involved in the Determination of Average α Particle and ^{11}B Recoil Energies from ^{14}N (n, α) ^{11}B Reaction

Options	Reaction X-section mbn	E_α (MeV)	E_B (MeV)
$E_1^* = 0MeV$, $E_2^* = 0MeV$	15.7	5.27	1.96
$E_1^* = 2.214MeV$, $E_2^* = 0MeV$	9.1	3.64	1.37
$E_1^* = 2.214MeV$, $E_2^* = 2.214MeV$	9.1	2.02	0.779
$E_1^* = 4.444MeV$, $E_2^* = 0MeV$	7.4	2.03	0.775
$E_1^* = 4.444MeV$, $E_2^* = 4.444MeV$	7.4	-	-
$E_1^* = 4.444MeV$, $E_2^* = 2.214MeV$	8.2	0.388	0.184
$E_1^* = 5.019MeV$, $E_2^* = 0MeV$	7.4	1.59	0.621

TABLE 7.12 Factors Involved in the Determination of Average Proton and ^{14}C Recoil Energies from ^{14}N (n, p) ^{14}C Reaction

Options	Reaction X-section mbn	E_p (MeV)	E_c (MeV)
$E_1^* = 0$, $E_2^* = 0$	Equally	7.66	0.613
$E_1^* = 6.78$MeV, $E_2^* = 0$	Divided	1.34	0.159

TABLE 7.13 Fraction of Total Kerma, f_i and Average Energies of Particles Produced in Air

Particle	Average Energy (MeV)	f_i
^{16}O recoil	0.94	0.080
α particle	1.64	0.057
^{13}C recoil	0.90	0.027
^{14}N recoil	1.05	0.328
Protons	4.50	0.166
^{14}C recoil	0.40	0.014
Deuteron	1.60	0.028
^{13}C recoil	0.30	0.006
α particle	1.62	0.185
^{11}B recoil	1.08	0.076
Others	-	0.033

TABLE 7.14 Values of Linear Attenuation Coefficients $(\mu_{cp})_g$ for Particles Arising in Both Wall and Gas of C/Air Chamber

Particle	Arising in	E_R	E_P	S_P	$\langle S \rangle$	S_H	S_{linear}	$(\mu_{cp})_g$
^{12}C recoil	W	0.6	0.05	875	0.083	2615	3.11	5.19
α particle	W	0.9	-	-	-	1945	2.31	2.57
^{9}Be recoil	W	0.64	0.072	800	0.102	1306	1.55	2.43
^{16}O recoil	G	0.94	0.059	850	0.069	3765	4.48	4.77
α particle	G	1.64	-	-	-	1552	1.85	1.13
^{13}C recoil	G	0.90	0.070	810	0.084	2449	2.91	3.24
^{14}N recoil	G	1.05	0.076	790	0.076	2942	3.50	3.33
Proton	G	4.5	4.5	74.22	-	74.22	0.088	0.02
^{14}C recoil	G	0.4	0.029	980	0.072	3472	4.13	10.33
α particle	G	2.62	-	-	-	1179	1.40	0.54
^{11}B recoil	G	1.08	0.099	730	0.174	3176	3.78	3.50

W and G are wall and gas respectively

E_R = energy of particle (MeV)

E_P = energy of proton of same velocity (MeV)

S_P = mass stopping power of proton of same velocity (MeV $g^{-1}cm^2$)

S_H = mass stopping power of recoil or α particle (MeV $g^{-1}cm^2$)

$S_{linear} = S_H \rho$ where ρ = density of air at 23°C units - MeV cm^{-1}

$$(\mu_{cp})_g = \frac{S_{linear}}{E_R}$$

TABLE 7.15 Stopping Power Ratios for Particles Produced in Carbon Wall of C/Air Chamber from Janni (1966) and Powers (1978)

Particle	$(S_{mass})_C$	$(S_{mass})_{CO_2}$	$S_{m,g}$
0.6MeV ^{12}C recoil	2840	2730	1.04
0.9MeV α particle	2063	1945	1.06
0.64MeV ^{9}Be recoil	1389	1325	1.05

Units - MeV $g^{-1}cm^2$

TABLE 7.16 Elemental Composition of TE Gas

Element	Percentage by Weight
H	10.2
C	45.6
N	3.5
O	40.7

TABLE 7.17 Fraction of Total Kerma, f_i and Average Energies of Particles Produced in TE Gas

Particle	Average Energy (MeV)	f_i
Proton	4.20	0.847
^{12}C recoil	1.20	0.054
α particle	1.60	0.019
^{9}Be recoil	1.27	0.009
^{14}N recoil	1.05	0.008
^{16}O recoil	0.94	0.031
α particle	1.64	0.019
^{13}C recoil	0.90	0.011
Others	-	0.002

TABLE 7.18 Values of Linear Attenuation Coefficients $(\mu_{cp})_g$ for Particles Produced in Wall and Gas of C/TE Chamber

Particle	Arising in	E_R	E_P	S_P	<S>	S_H	S_{linear}	$(\mu_{cp})_g$
^{12}C recoil	W	0.60	0.05	1433	0.083	4282	4.49	7.49
α particle	W	0.90	-	-	-	2866	3.01	3.34
^{9}Be recoil	W	0.64	0.072	1291	0.102	2107	2.21	3.45
Proton	G	4.20	4.2	101.1		101.1	0.106	0.025
^{12}C recoil	G	1.20	0.101	1143	0.086	3537	3.71	3.09
α particle	G	1.80	-	-	-	2107	2.21	1.23
^{9}Be recoil	G	1.27	0.142	1061	0.104	1764	1.85	1.46
^{14}N recoil	G	1.05	0.076	1283	0.068	4271	4.48	4.27
^{16}O recoil	G	0.94	0.059	1389	0.103	9.42	9.59	10.2
α particle	G	1.64	-	-	-	2250	2.36	1.44
^{13}C recoil	G	0.90	0.070	1309	0.084	3956	4.15	4.61

W and G are wall and gas respectively

E_R = energy of particle (MeV)

E_P = energy of proton of same velocity (MeV)

S_P = mass stopping power of proton of same velocity (MeV $g^{-1}cm^2$)

S_H = mass stopping power of recoil or α particle (MeV $g^{-1}cm^2$)

S_{linear} = S_H where = density of air at 23°C units - MeV cm^{-1}

$(\mu_{cp})_g$ $\frac{S_{linear}}{E_R}$

TABLE 7.19 $\overline{W}$ Values for Particles Produced in C/TE Chamber

Particle	$\overline{W}$(eV)	Reference	
0.6MeV ^{12}C recoil	42.0	Nguyens et al (1980)	
0.9MeV α particle	33.0	ICRU 31 (1979)	$(\overline{W}_{eff})_w = \overline{W}_2 = 39.8eV$
0.64MeV ^{9}Be recoil	-		
1.2MeV ^{12}C recoil	42.0	Nguyens et al (1980)	
1.8MeV α particle	33.0	ICRU 31 (1979)	
1.27MeV ^{9}Be recoil	-		
0.94MeV ^{16}O recoil	45.5	Nguyens et al (1980)	
1.63MeV α particle	33.0	ICRU 31 (1979)	$(\overline{W}_{eff})_g = \overline{W}_1 = 40.9eV$
0.9MeV ^{13}C recoil	42.0	Nguyens et al (1980)	
1.05MeV ^{14}N recoil	40.0	Nguyens et al (1980)	
4.2MeV proton	31.0	ICRU 31 (1979)	

TABLE 7.20 Stopping Power Ratios for Particles Produced in Carbon Wall of C/TE Chamber

Particle	$(S_{mass})_C$	$(S_{mass})_{TE\ gas}$	$S_{m,g}$
0.6MeV ^{12}C recoil	950	1433	0.663
0.9MeV α particle	1850	2866	0.649
0.64MeV ^{9}Be recoil	850	1291	0.658

Units - MeV $g^{-1}cm^2$

FIGURE 7.1 Energy Fluence Spectrum of Particles Produced in Carbon

1. Neutron Energy Fluence Spectrum
2. Energy Fluence Spectrum of ^{12}C (n, α) ^{9}Be Reaction
3. Energy Fluence Spectrum of ^{12}C (n, n'3α) Reaction

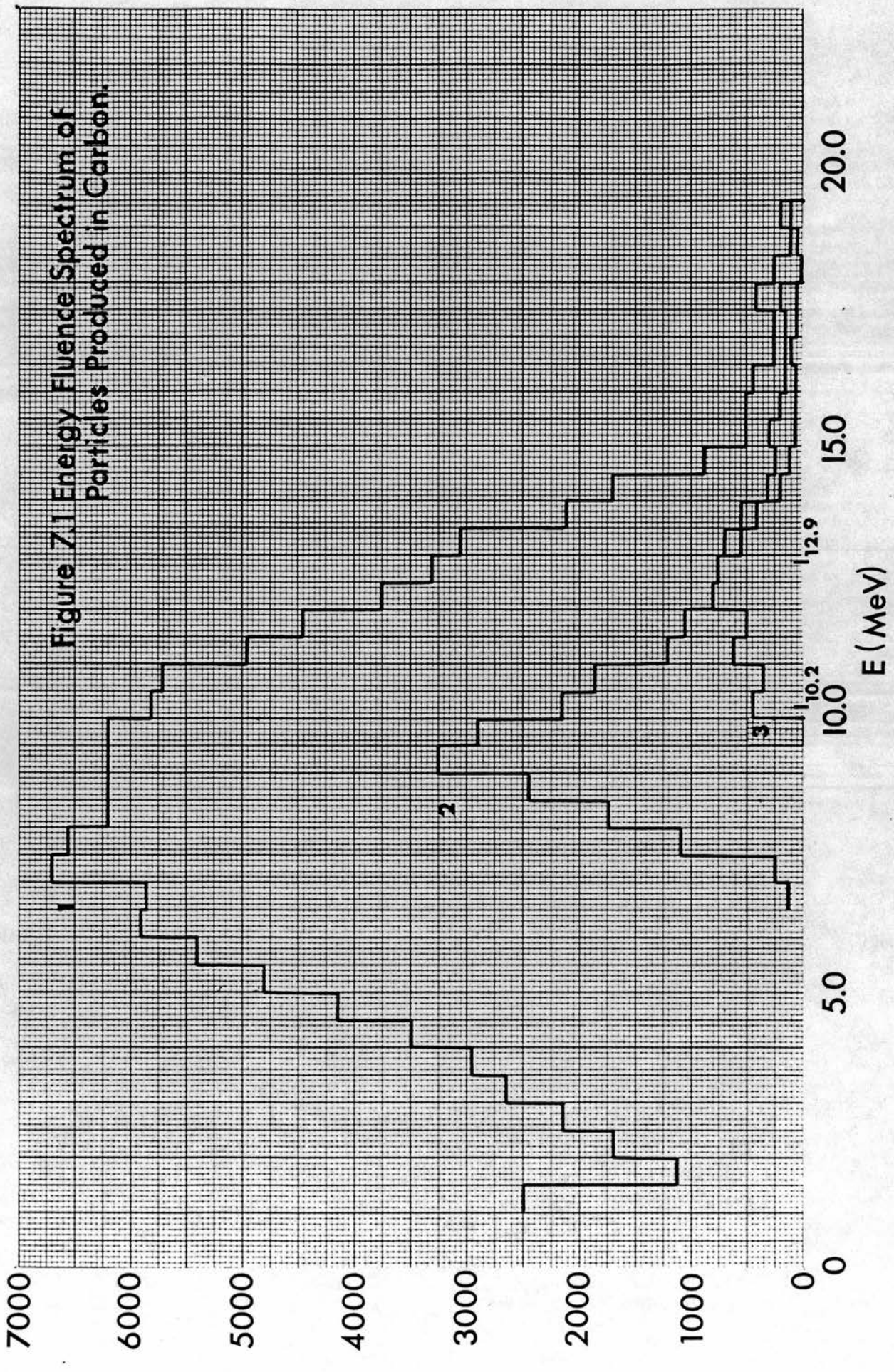
Figure 7.1 Energy Fluence Spectrum of Particles Produced in Carbon.
N.E.N(E)
7000
6000
5000
4000
3000
2000
1000
0
0
5.0
10.0
15.0
20.0
E (MeV)
10.2
12.9
1
2
3

FIGURE 7.2 Energy Fluence Spectrum of Particles Produced in Oxygen

1. Neutron Energy Fluence Spectrum
2. Energy Fluence Spectrum of ^{16}O (n, α) ^{13}C Reaction
3. Energy Fluence Spectrum of ^{16}O (n, n'α) ^{12}C Reaction

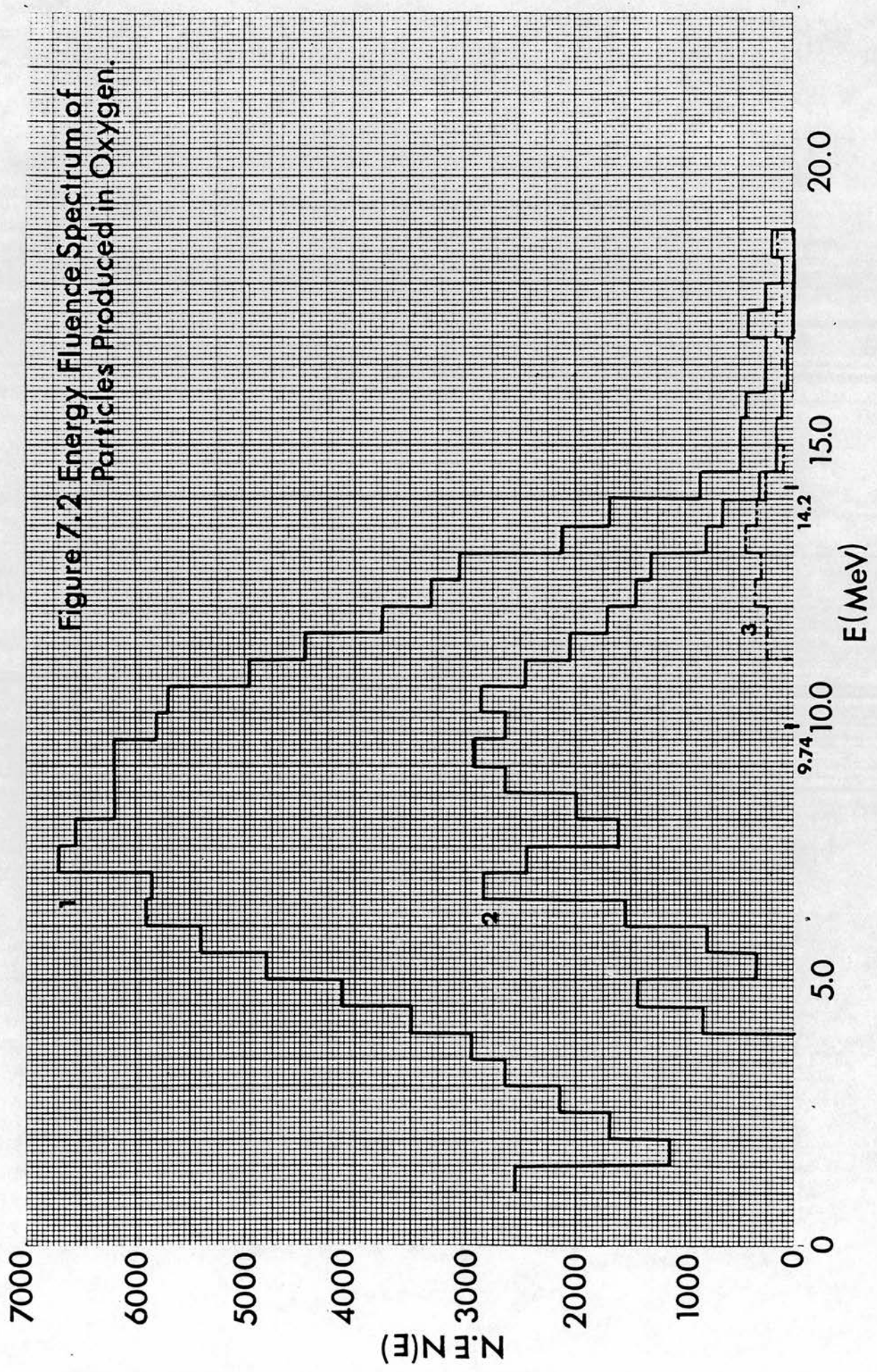

Figure 7.2 Energy Fluence Spectrum of Particles Produced in Oxygen.

FIGURE 7.3 Energy Fluence Spectrum of Particles Produced in Nitrogen

1. Neutron Energy Fluence Spectrum
2. Energy Fluence Spectrum of ^{14}N (n, α) ^{11}B Reaction
3. Energy Fluence Spectrum of ^{14}N (n, p) ^{14}C Reaction
4. Energy Fluence Spectrum of ^{14}N (n, d) ^{13}C Reaction
5. Energy Fluence Spectrum of ^{14}N (n, n'p) ^{13}C Reaction

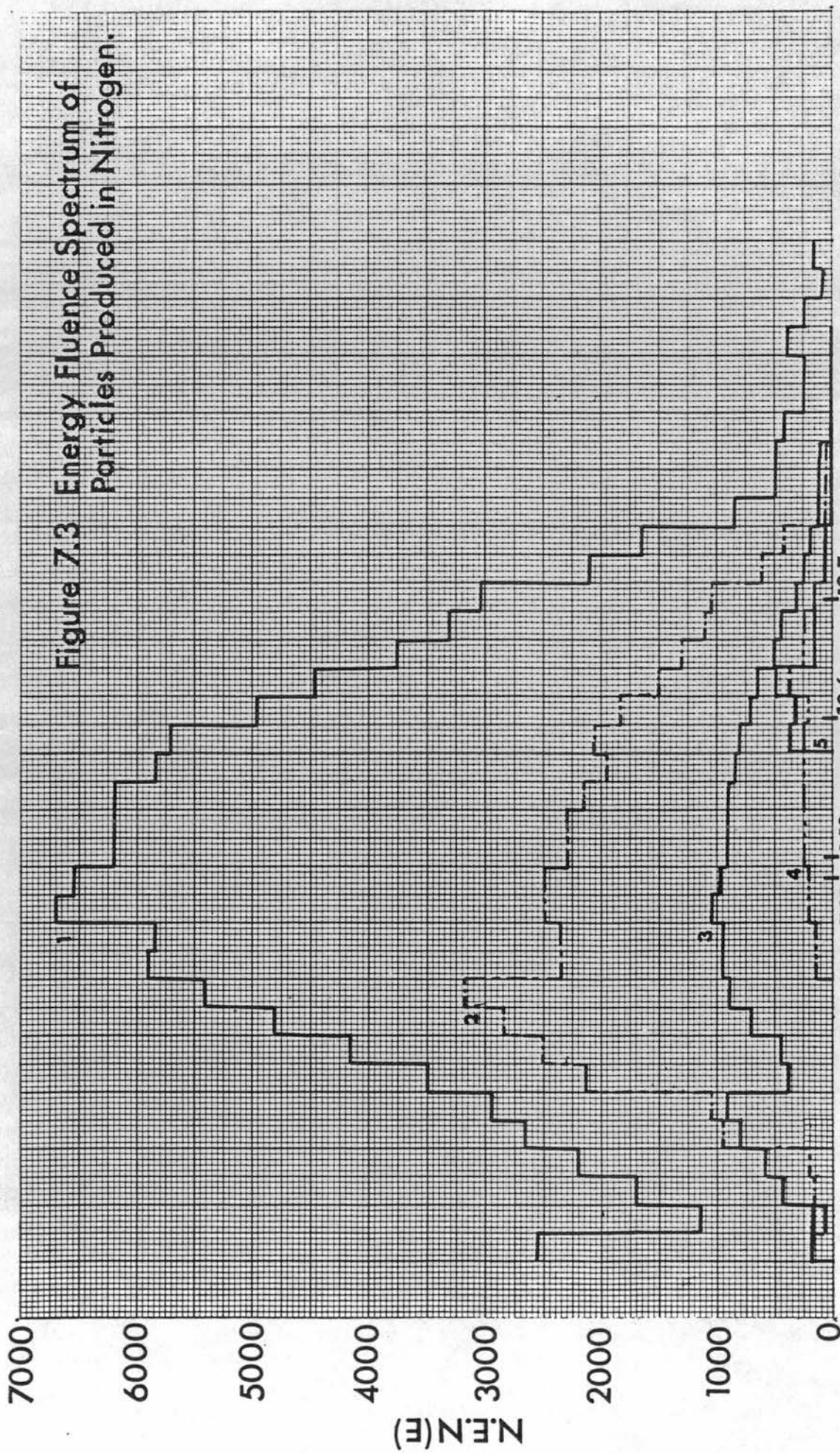

Figure 7.3 Energy Fluence Spectrum of Particles Produced in Nitrogen.

FIGURE 7.4 Individual Contributions to Ionization in C/CO_2 Chamber

1. 0.60MeV ^{12}C Recoils from Wall
2. 0.90MeV α Particles from Wall
3. 0.64MeV ^{9}Be Recoils from Gas
4. 0.94MeV ^{16}O Recoils from Gas
5. 1.63MeV α Particles from Gas
6. 1.20MeV ^{12}C Recoils from Gas
7. 0.90MeV ^{13}C Recoils from Gas
8. 1.80MeV α Particles from Gas
9. 1.27MeV ^{9}Be Recoils from Gas

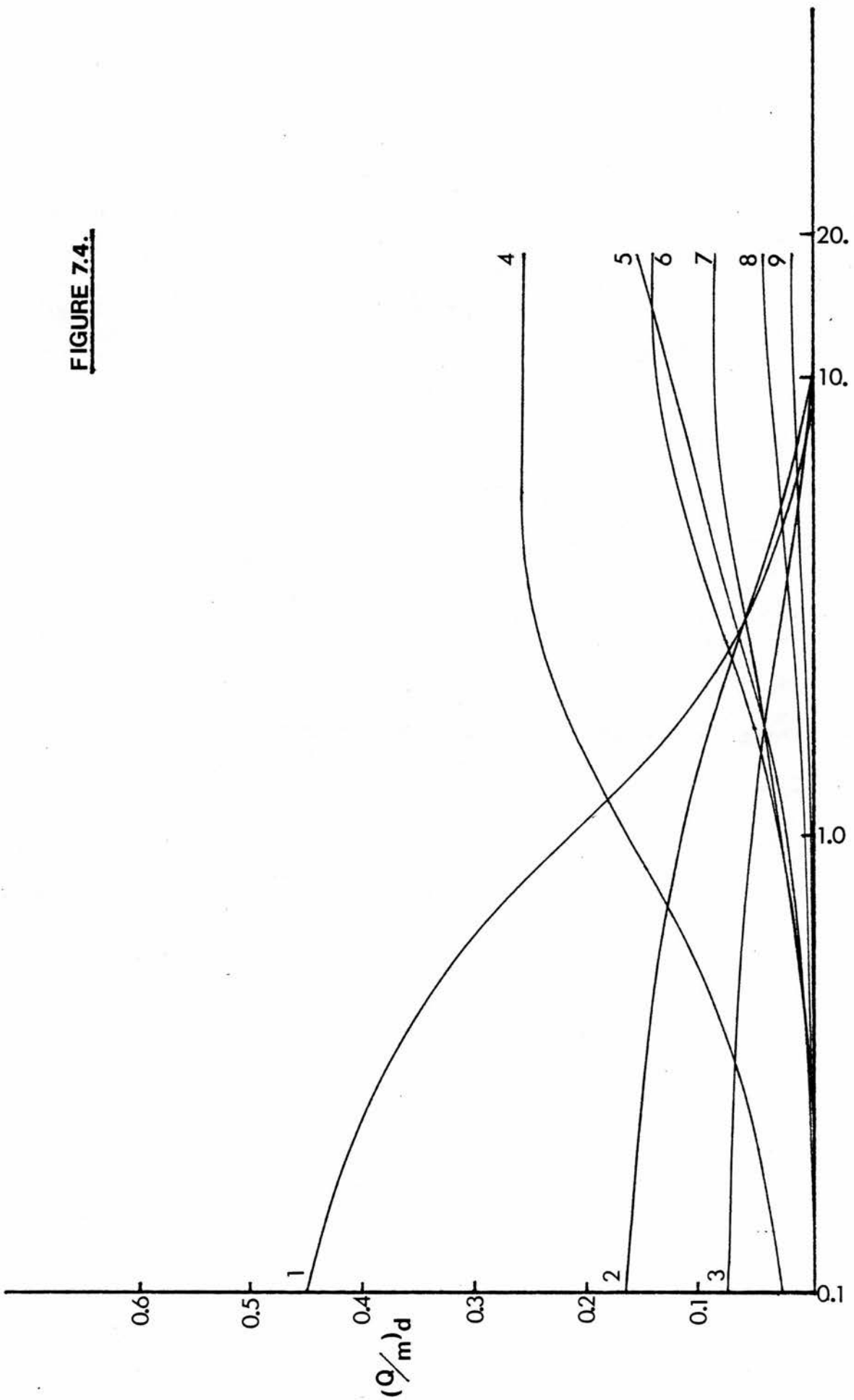

FIGURE 7.4.

FIGURE 7.5 Ionization Contributions Due to Wall and Gas Particles in C/CO_2 Chamber

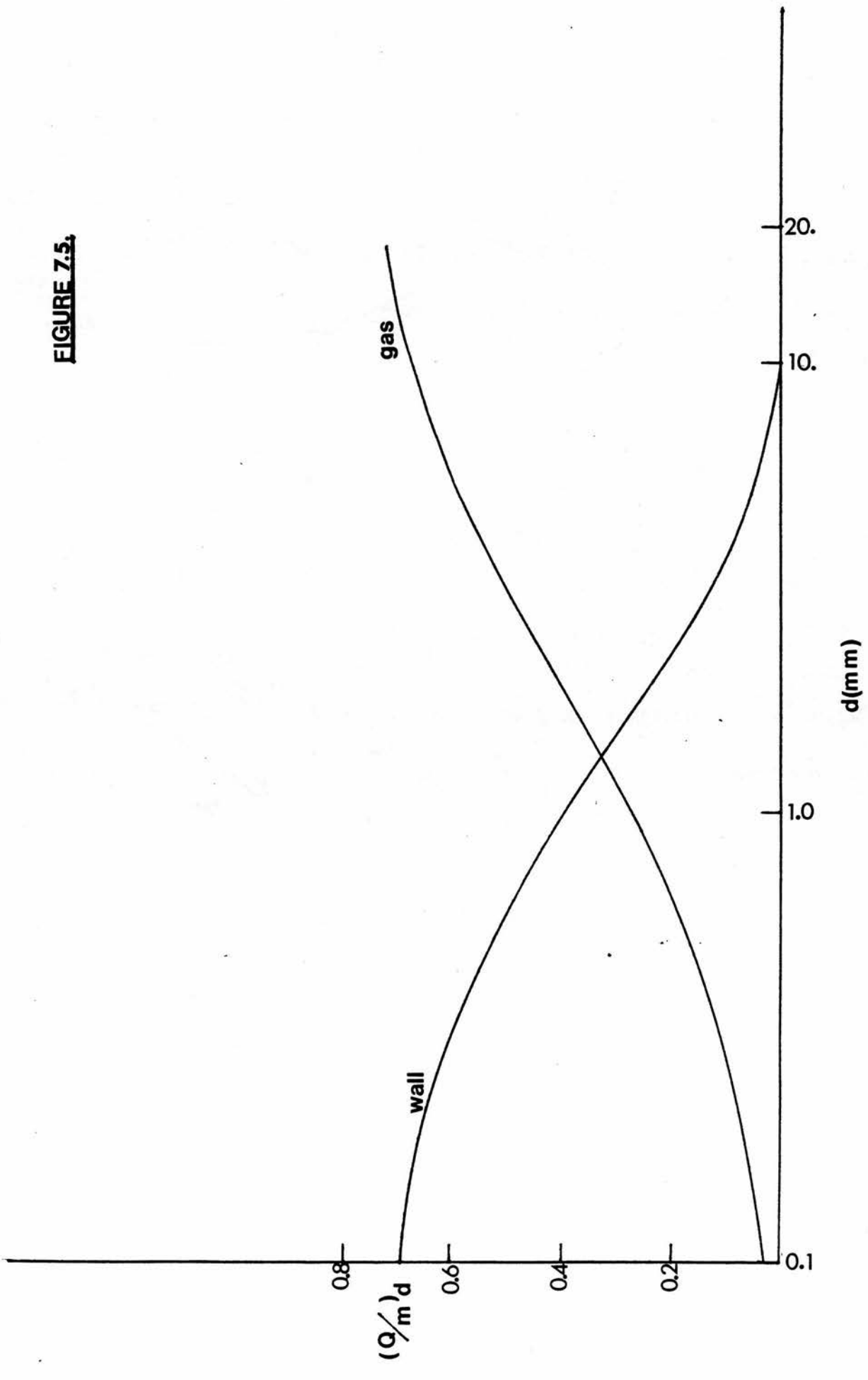

FIGURE 7.5.

FIGURE 7.6 Total Ionization in C/CO_2 Chamber

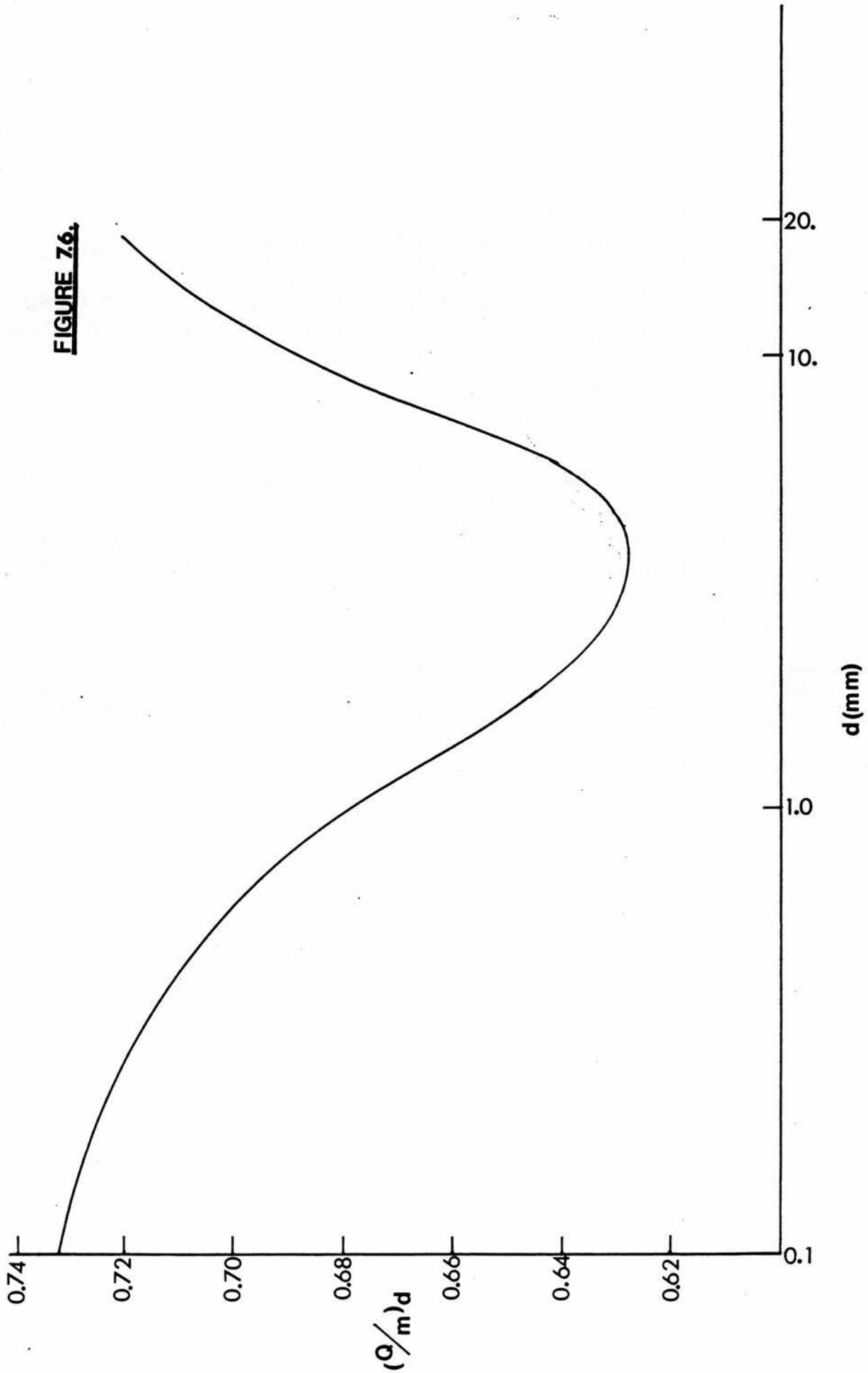

FIGURE 7.6.

FIGURE 7.7 Total Integrated Ionization in C/CO_2 Chamber
Comparison of Theory and Experiment

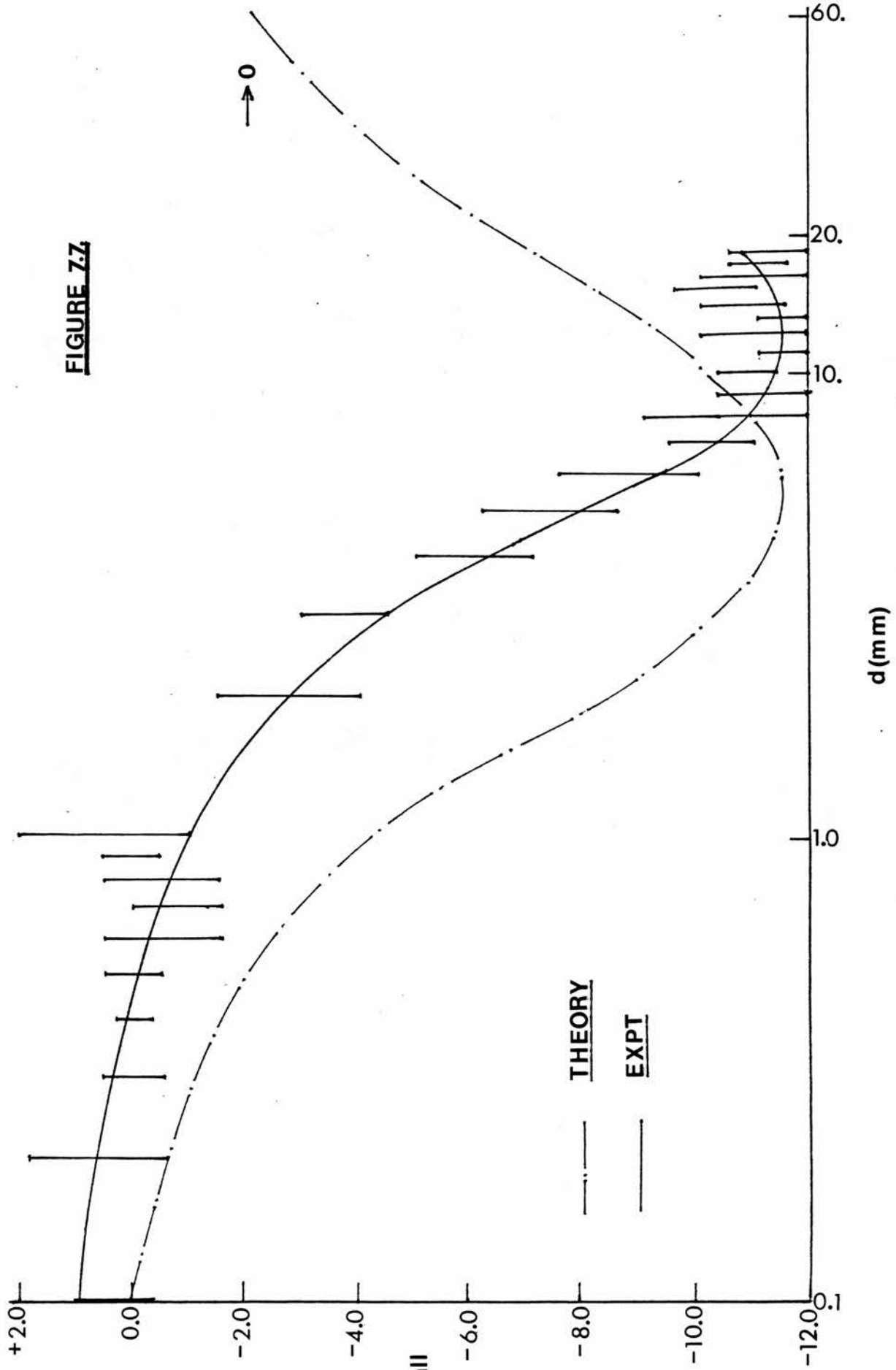
FIGURE 7.7
0
60.
20.
10.
1.0
0.1
d(mm)
+2.0
0.0
-2.0
-4.0
-6.0
-8.0
-10.0
-12.0
% from $(Q/m)_{small}$
THEORY
EXPT

FIGURE 7.8 Individual Contributions to Ionization in C/Air Chamber

1. 0.60MeV ^{12}C Recoils from Wall
2. 0.90MeV α Particles from Wall
3. 0.64MeV ^{9}Be Recoils from Wall
4. 1.05MeV ^{14}N Recoils from Gas
5. 2.62MeV α Particles from Gas
6. 0.94MeV ^{16}O Recoils from Gas
7. 1.08MeV ^{11}B Recoils from Gas
8. 1.64MeV α Particles from Gas
9. 0.90MeV ^{13}C Recoils from Gas
10. 0.40MeV ^{14}C Recoils from Gas

4.50MeV Proton Contribution from Gas is negligible.

FIGURE 7.8.

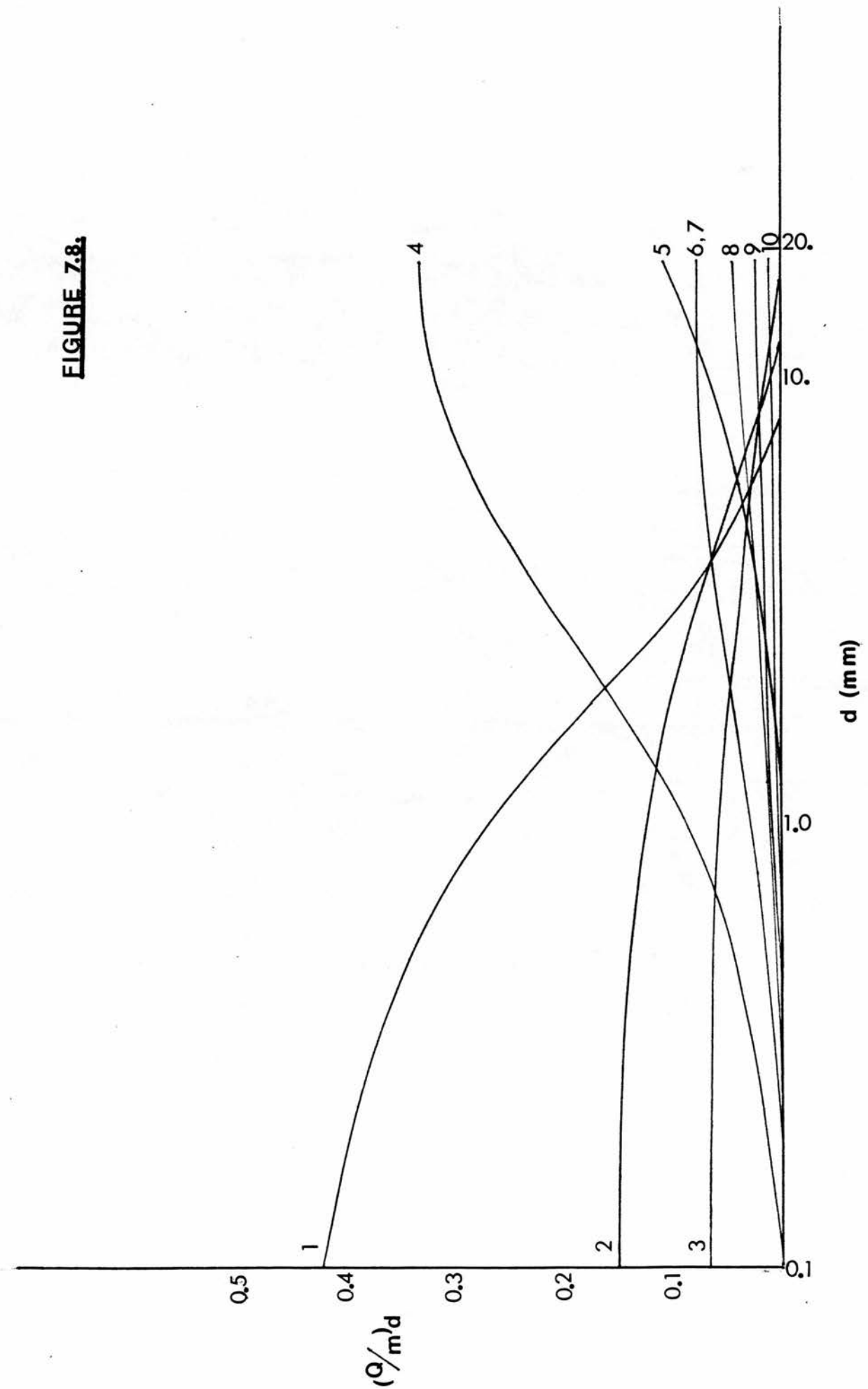

FIGURE 7.9 Ionization Contributions Due to Wall and Gas Particles in C/Air Chamber

FIGURE 7.9

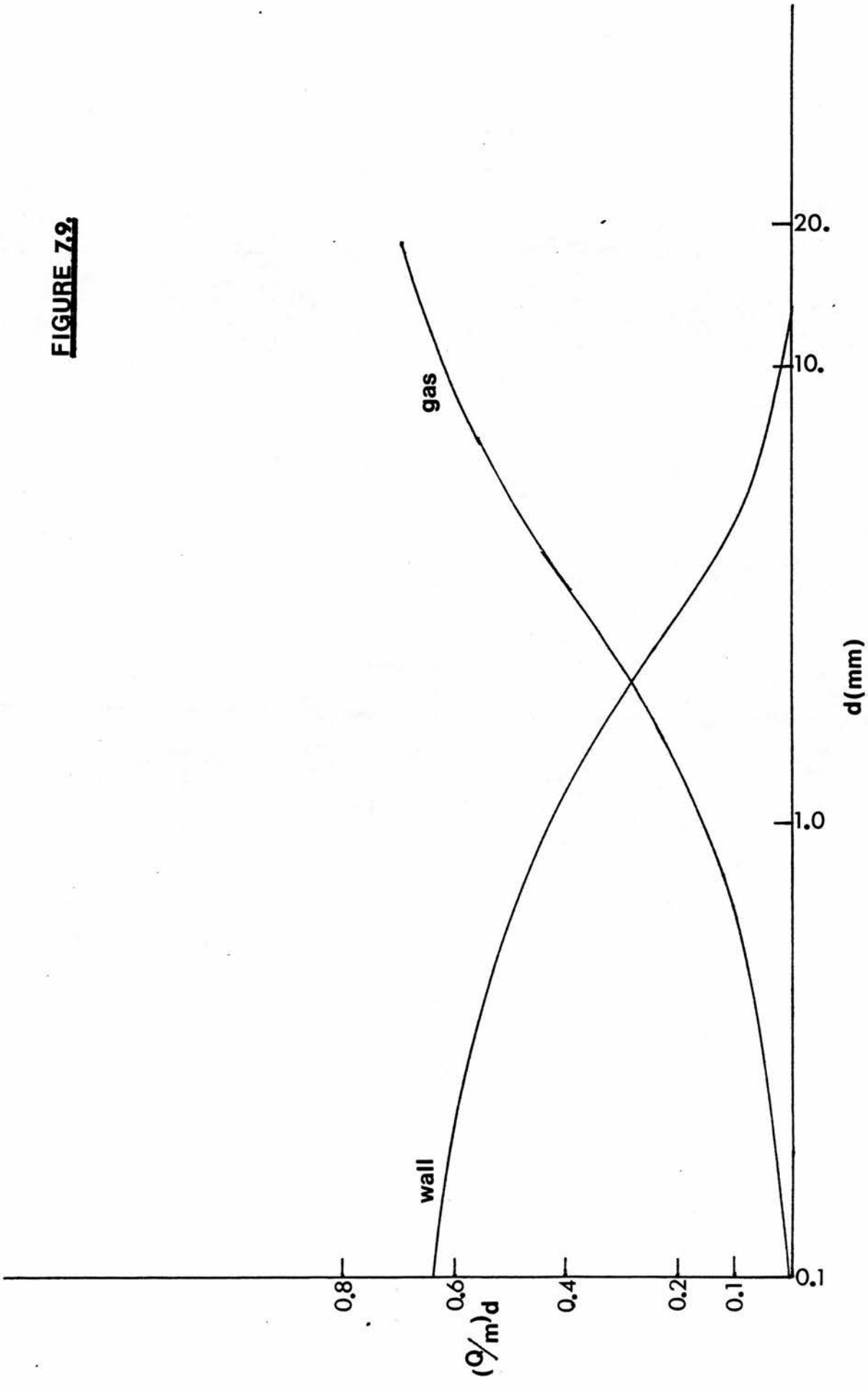

FIGURE 7.10 Total Ionization in C/Air Chamber

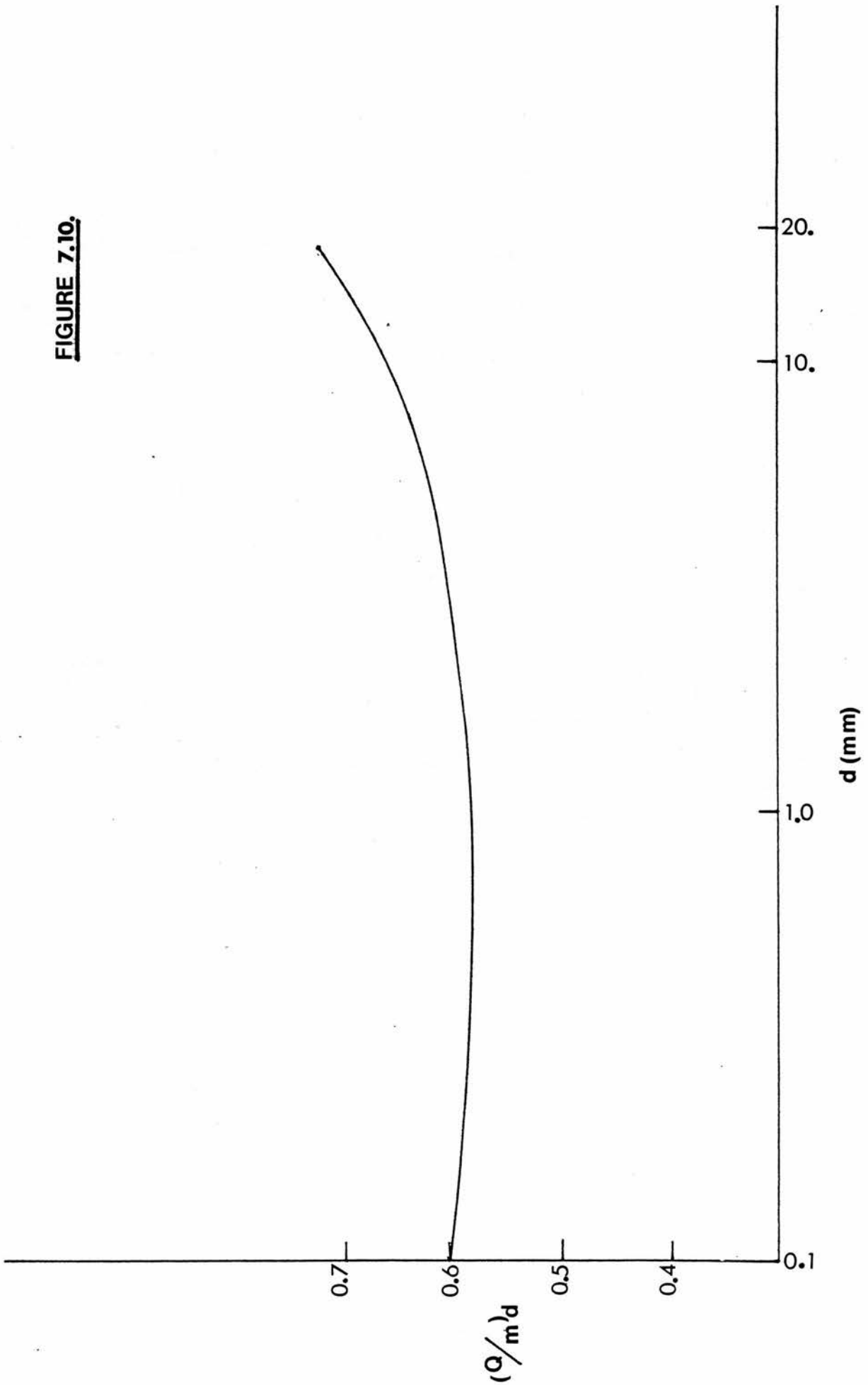

FIGURE 7.10.

FIGURE 7.11 Total Integrated Ionization in C/Air Chamber - Comparison of Theory and Experiment

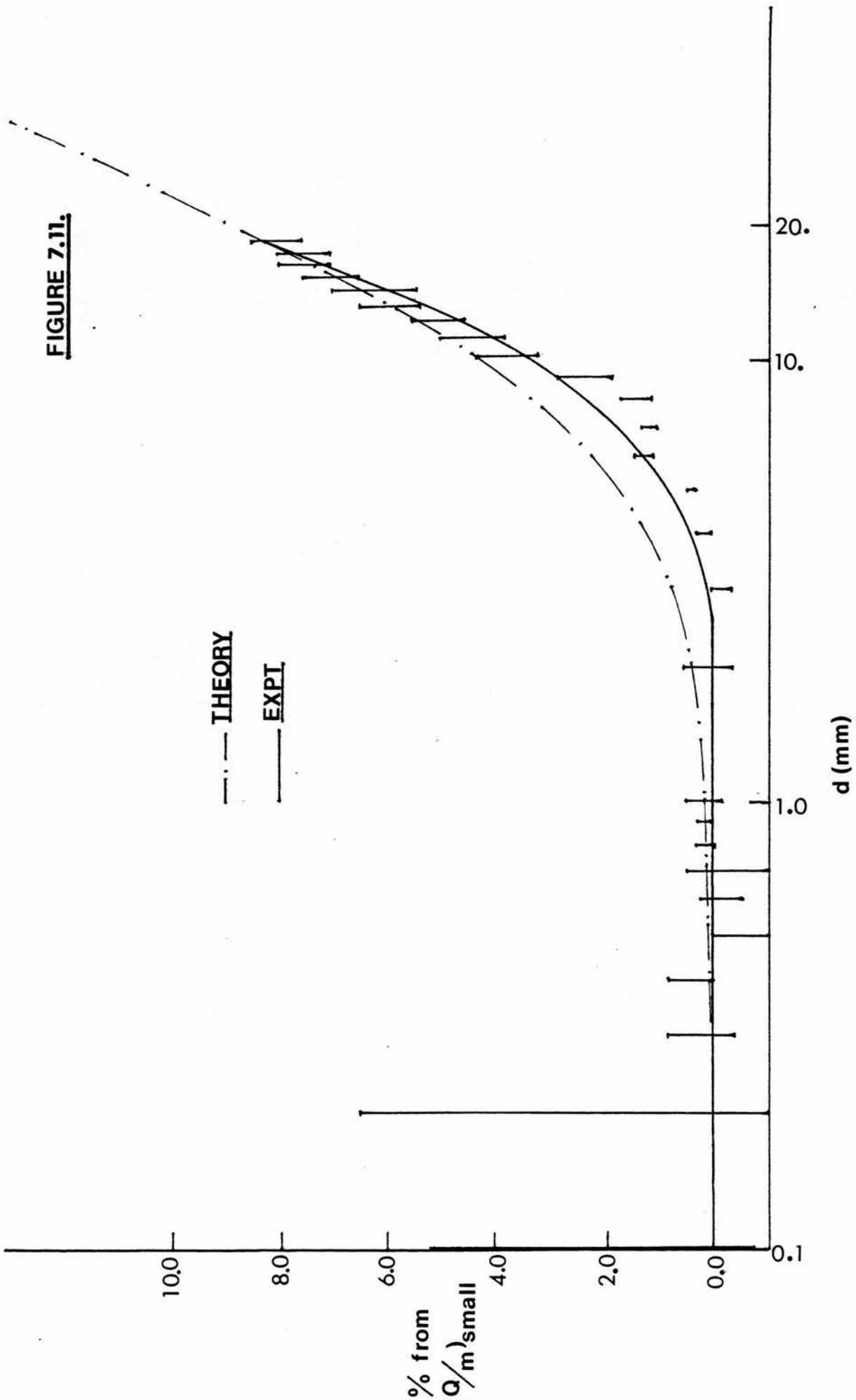
FIGURE 7.11.
THEORY
EXPT
% from $(Q/m)_{small}$
10.0
8.0
6.0
4.0
2.0
0.0
0.1
1.0
10.
20.
d (mm)

FIGURE 7.12 Total Integrated Ionization in C/TE Chamber - Comparison of Theory and Experiment

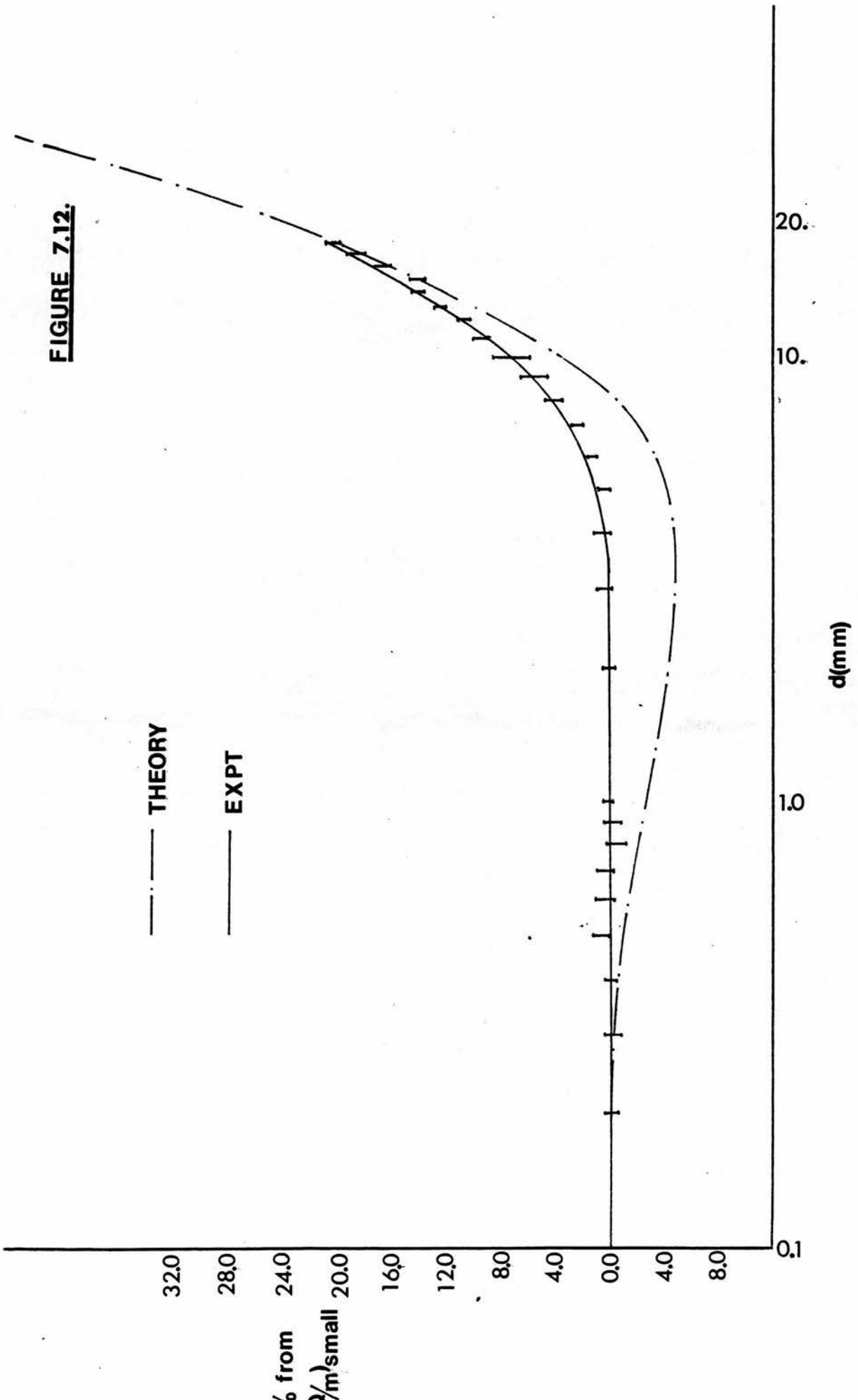
FIGURE 7.12.
THEORY
EXPT
% from $(Q/m)_{small}$
32.0
28.0
24.0
20.0
16.0
12.0
8.0
4.0
0.0
4.0
8.0
0.1
1.0
10.
20.
d(mm)

FIGURE 7.13 Individual Contributions to Ionization in C/TE Chamber

1. 0.60MeV ^{12}C Recoils from Wall
2. 0.90MeV α Particles from Wall
3. 0.64MeV ^{9}Be Recoils from Wall
4. 4.20MeV Protons from Gas
5. 1.20MeV ^{12}C Recoils from Gas
6. 0.94MeV ^{16}O Recoils from Gas
7. 1.80MeV α Particles from Gas
8. 1.63MeV α Particles from Gas
9. 0.90MeV ^{13}C Recoils from Gas
10. 1.05MeV ^{14}N Recoils from Gas
11. 1.27MeV ^{9}Be Recoils from Gas

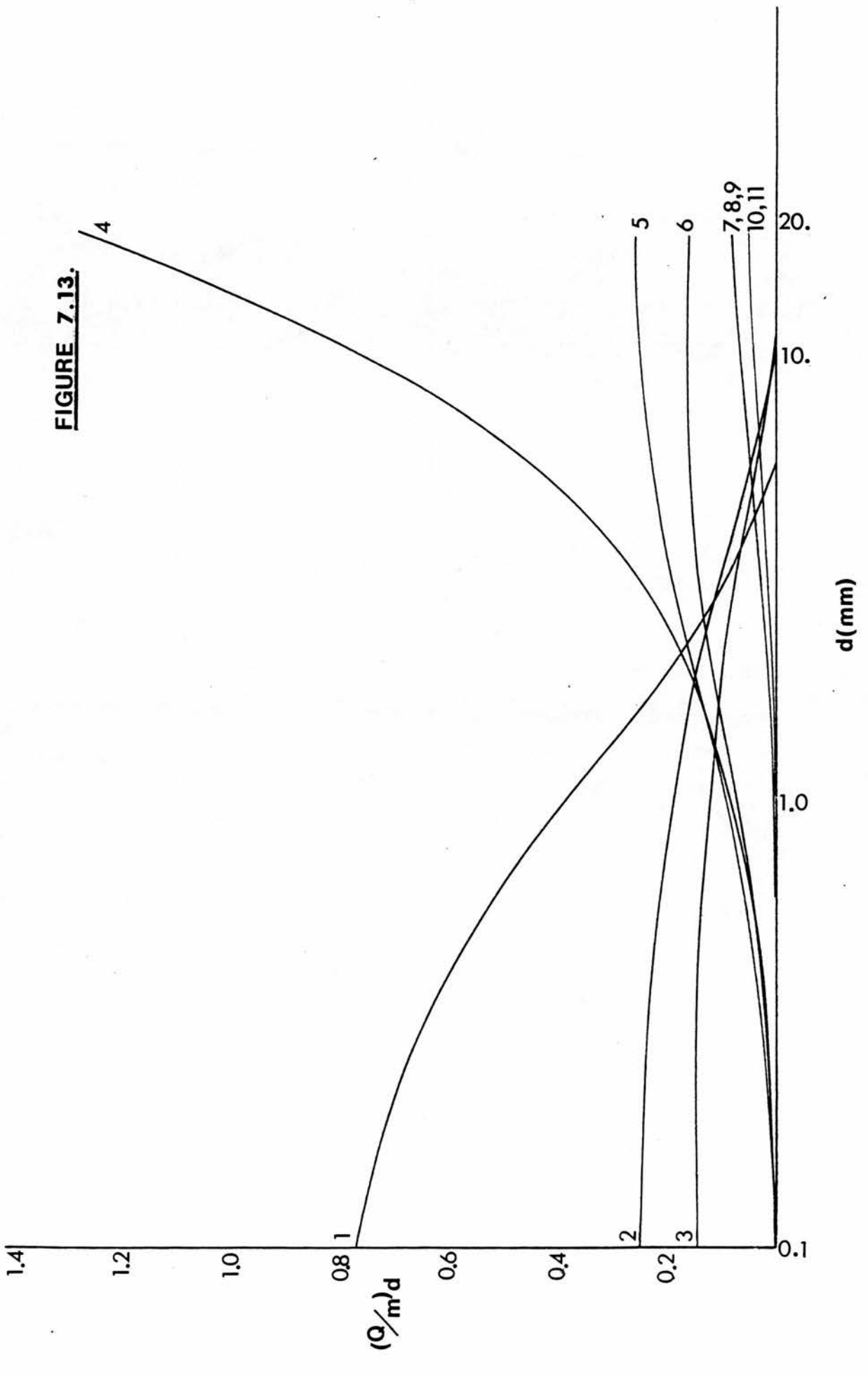

FIGURE 7.13.

FIGURE 7.14 Ionization Contributions Due to Wall and Gas Particles in C/TE Chamber

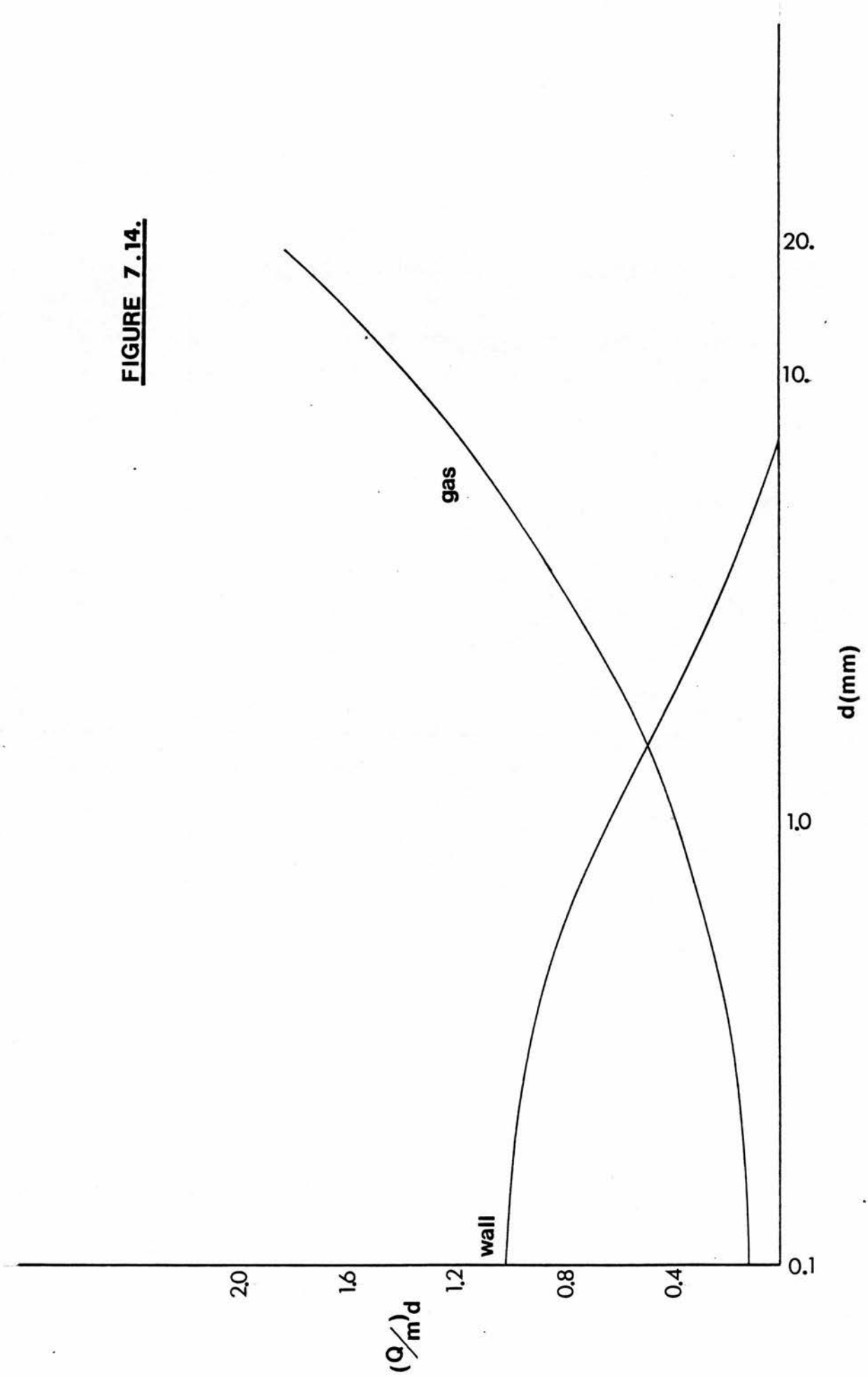

FIGURE 7.14.

FIGURE 7.15 Total Ionization in C/TE Chamber

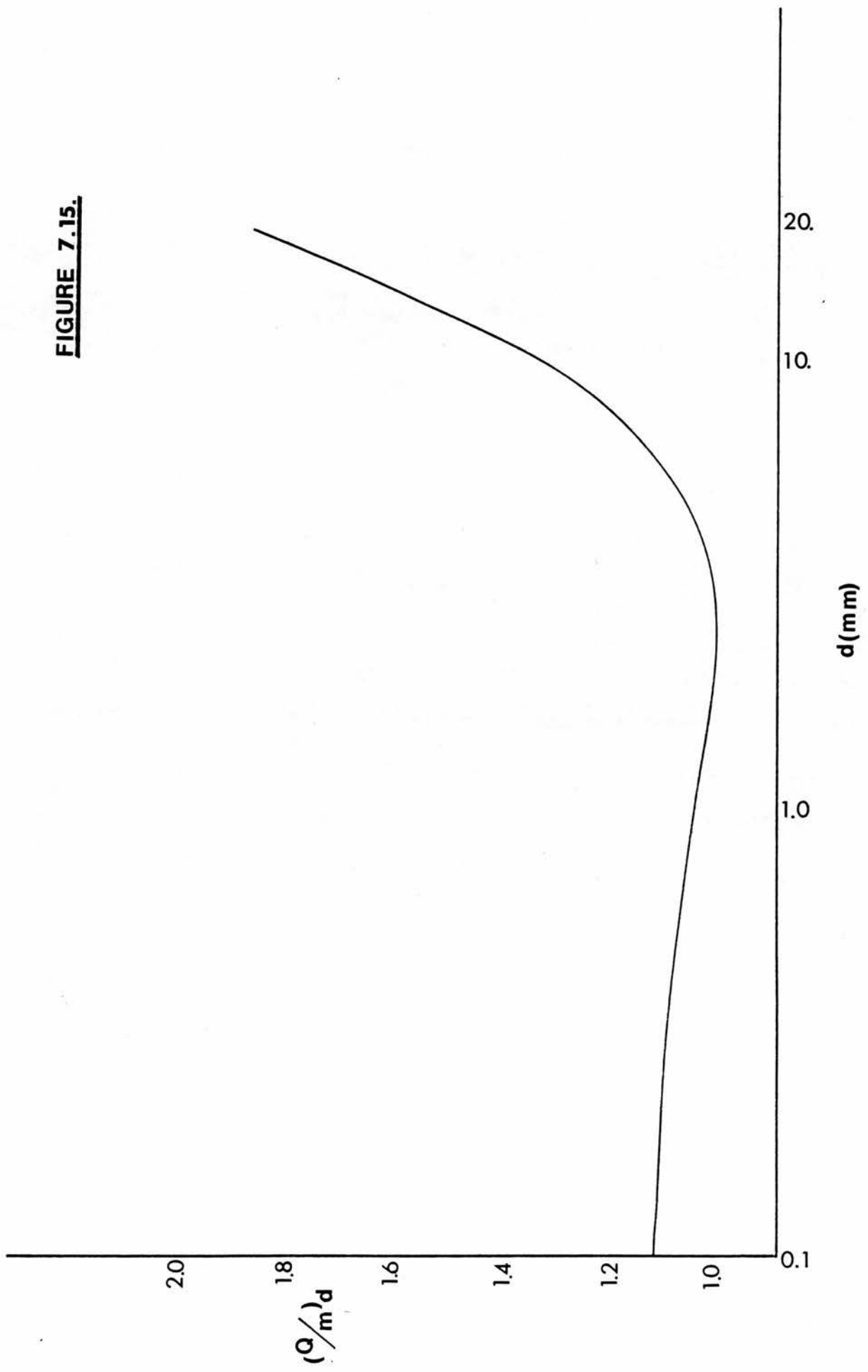

FIGURE 7.15.

FIGURE 7.16 Comparison of Theory to Results of Makarewicz and Pszona (1981)

Results of Makarewicz and Pszona:- Solid Line ——

Results of this thesis as follows:-

Wall Particles:-

- o 0.6MeV ^{12}C Recoils
- ▲ 0.9MeV α Particles
- x 0.64MeV ^{9}Be Recoils

Gas Particles:-

- o 1.2MeV ^{12}C Recoils
- ▲ 1.8MeV α Particles
- x 1.27MeV ^{9}Be Recoils
- \+ 0.94MeV ^{16}O Recoils
- ▽ 1.63MeV α Particles
- □ 0.90MeV ^{13}C Recoils

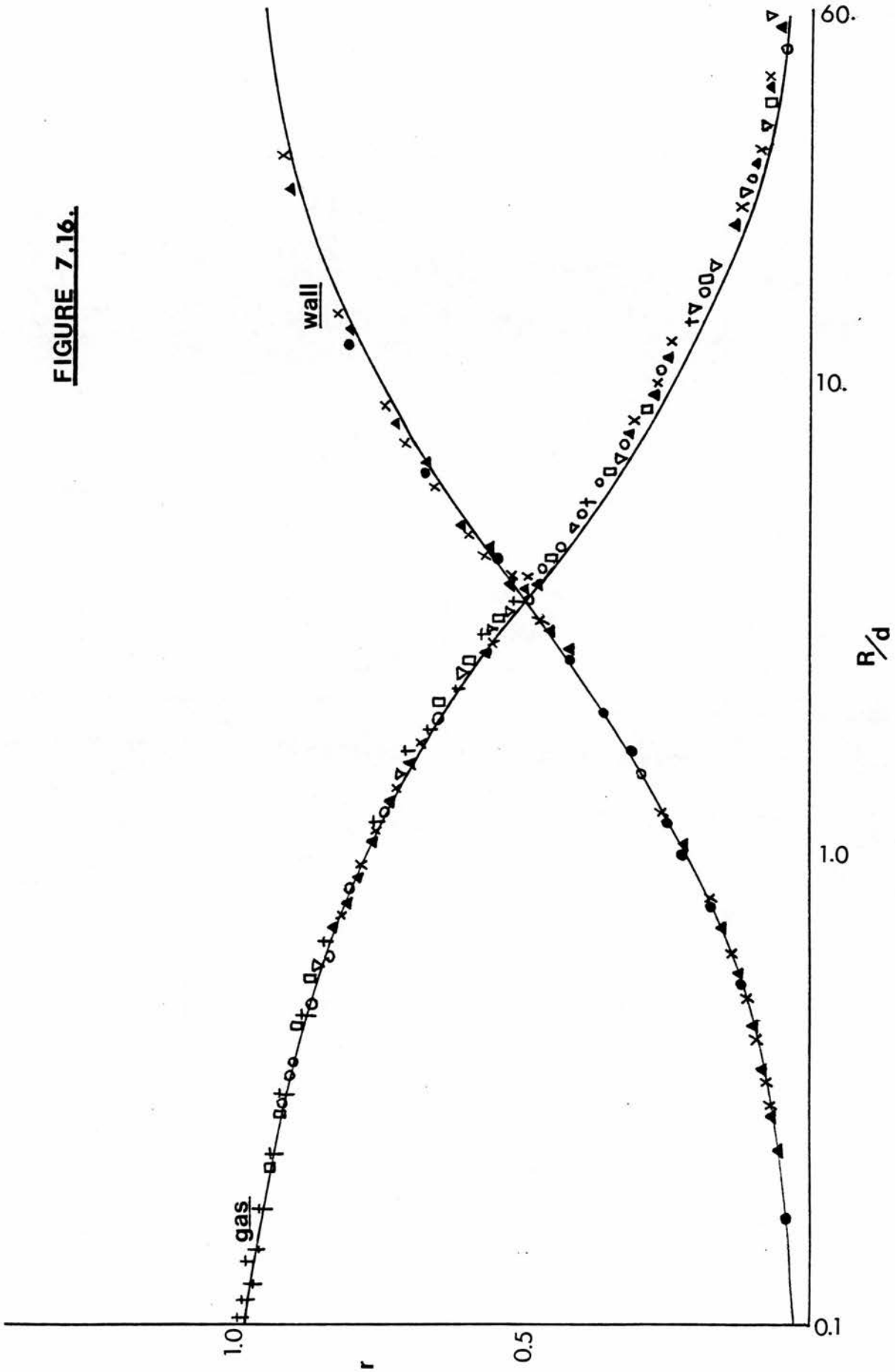

FIGURE 7.16.

CHAPTER 8

METHOD FOR DERIVING THE $\overline{W}$ VALUES FOR PROTONS AND CARBON WALL RECOILS FROM NEUTRON REACTIONS IN VARIOUS GASES FROM KNOWN $\overline{W}$ VALUES

As has been discussed previously, the Bragg-Gray Theory, which relates the absorbed dose, D_m in the material of the wall of the ionization chamber, to the charge collected, Q is

$$D_m = \frac{\overline{W}}{e} (S_{m,g}) \frac{Q}{m} \qquad 8.1$$

where $\overline{W}$ is the average energy required to produce an ion pair, e is the electronic charge, $S_{m,g}$ is the mass stopping power ratio of wall to cavity material, and m is the mass of the gas in the cavity. This theory rests on the basic requirement that the dimensions of the cavity be a very small fraction of the range of the charged particles which cross it. Generally, for the size of the cavities employed in neutron dosimetry, e.g. a plate separation of 5mm, the Bragg-Gray Theory does not hold for reasons described in Chapter 1.

However, if an effective plate separation is obtained by varying the pressure of the gas in the cavity as described in Chapter 5, then the equivalent plate separation can be such that a Bragg-Gray approximation is valid.

Moreover, as is shown by experiment, values of (q_{sat}/d_{eq}) measured at small separations of TE/TE, TE/Air, C/CO_2, C/TE and C/Air chambers, show a constant value of (q_{sat}/d_{eq}) against d_{eq} in the range d = 1mm to d, such that $d \rightarrow 0$.

Therefore, assuming a small enough d_{eq} can be obtained for a Bragg-Gray approximation to be valid, then for the same chamber, and same dose delivered, but for different gases

$$\left(\frac{Q}{m}\ \frac{\overline{W}}{e}\ S_{m,g}\right)_x = \left(\frac{Q}{m}\ \frac{\overline{W}}{e}\ S_{m,g}\right)_y \qquad 8.2$$

where x = first gas, and y = second gas.

Rearranging equation 8.2

$$\frac{\overline{W}_x}{\overline{W}_y} = \frac{\left(\frac{Q}{m}\right)_y\ S_x}{\left(\frac{Q}{m}\right)_x\ S_y}$$

and to express in terms of experiment,

$$\frac{\overline{W}_x}{\overline{W}_y} = \frac{(q_{sat}/d_{eq})_y\ \rho_x\ S_x}{(q_{sat}/d_{eq})_x\ \rho_y\ S_y} \qquad 8.3$$

Therefore, for the same chamber, exposed to the same neutron beam, but filled with different gases, a knowledge of the gas densities, and a knowledge of the predominant particles produced from the wall, their energies and mass stopping powers in each gas, give the $\overline{W}$ ratio for these particles in the gases of interest.

8.1 Experimental Measurements

(q_{sat}/d_{eq}) was obtained at small equivalent plate separations of both TE plastic and carbon chambers by reducing the pressure of the gas in the cavity (as described in Chapter 5) for the gases Methane

(CH_4) and Argon (Ar). This was in addition to values of (q_{sat}/d_{eq}) already obtained for TE gas and air, in both TE plastic and carbon chambers. A value of (q_{sat}/d_{eq}) was also obtained for CO_2 in TE plastic chamber.

Methane, argon and CO_2 gave constant (q_{sat}/d_{eq}) measurements at a variety of equivalent plate separations from 0.3 to 0.9mm, for TE plastic and carbon chambers as applicable, as was the case for TE gas and air. (Values of constant (q_{sat}/d_{eq}) for all the stated gases are shown in Tables 8.1 and 8.6).

Therefore, in all chamber combinations, the constant value of (q_{sat}/d_{eq}) in the range d_{eq} = 0.3 to 0.9mm, was assumed to be the value of (q_{sat}/d_{eq}) as $d_{eq} \rightarrow 0$, and the Bragg-Gray approximation would therefore be valid.

8.1.1 TE Plastic Chamber

The predominant particles produced from the TE plastic wall are assumed to be protons with an average energy of 2.1MeV. (This average energy is obtained by assuming an average neutron energy of 8.4MeV, again based on the neutron energy fluence spectrum of Figure 6.5. Therefore, the mean energy of the protons when first released is 4.2MeV. However, protons emerging from the TE plastic wall will, on average have about half this energy as they will have all energies from 4.2MeV down to zero. Hence the protons emerging from the wall are assumed to have an average energy of 2.1MeV).

The mass stopping powers as obtained from Janni (1966), the (q_{sat}/d_{eq}) measurements as obtained from experiment and the densities at 23°C are shown in Table 8.1 for the 5 gases of interest. S_{mass} for TE gas was obtained by calculation from constituent compounds (i.e. 64.4% CH_4, 32.4% CO_2 and 3.2% N_2 by weight) using the Bragg Additivity Rule.

By inserting the values of Table 8.1 into Equation 8.3, the $\overline{W}$ ratios for each gas combination can be obtained and are shown in Column 5 of Table 8.3. These experimental values of $\overline{W}$ ratios can be compared with the published data of various workers accumulated in ICRU 31, entitled 'Average Energy Required to Produce an Ion Pair'.

For the gases of interest, $\overline{W}$ values for 2.1MeV protons were estimated from this publication and are shown in Table 8.2. A comparison of W ratios as obtained by experiment with $\overline{W}$ ratios from Table 8.2 is shown in Table 8.3.

As can be seen, the gas combinations of CO_2/Air, CO_2/Ar and Air/Ar give very good agreement. The present measurements thus support the $\overline{W}$ values as recommended by ICRU 31 for CO_2, Air and Ar.

The calculations involving CH_4 with Ar, Air and CO_2 give an average difference of 9.67%; the calculations involving TE gas with Ar, Air and CO_2 give an average difference of 5.94%.

This either indicates that one or all of the factors contributing to the experimental $\overline{W}$ value of CH_4 and TE gas (i.e. ρ, S_{mass} or

q_{sat}/d_{eq}) is in error, or that the $\overline{W}$ values obtained from ICRU 31 for CH_4 and TE gas are in error.

In fact the data available from ICRU 31 for protons in CH_4 are limited as is shown in Figure 5.4 of that publication; the estimates of $\overline{W}_{CH_4}$ for protons do not extend beyond 0.5MeV proton energies. Therefore, an experimental estimate of $\overline{W}_{CH_4}$ can be obtained by calculation from the $\overline{W}$ ratios of CO_2/CH_4, Air/CH_4 and Ar/CH_4. The individual estimates are shown in Table 8.4. Therefore a value of $\overline{W}_{CH_4} = 27.4 \pm 1.2$eV is suggested for CH_4 which is nearer the preliminary value suggested by Bichsel and Inokuti (1976) than the results of Figure 5.4 of the ICRU Survey.

The data available from ICRU 31 for protons in TE gas is also limited as shown in Figure 5.1 of that publication; the suggested value of $\overline{W}_{TE\ gas}$ from this figure is 31.0 ± 1.5eV for $20 < E/KeV < 3 \times 10^3$, which incorporates a spread of 10%. Therefore, experimental estimates of $\overline{W}_{TE\ gas}$ are shown in Table 8.5 from the $\overline{W}$ ratios of TE/CO_2, TE/Air and TE/Ar calculations. A value of $\overline{W}_{TE\ gas} = 33.1 \pm 1.5$eV is suggested for TE gas. This range of values of $\overline{W}_{TE\ gas}$ incorporates the value of 31.9eV recommended by Goodman and Coyne (1980) as is used in the absolute calibration of TE/TE parallel-plate chamber (Chapter 9). It must also be noted that the method of obtaining S_{mass} for TE gas using the Bragg Additivity Rule may be unreliable according to Bichsel (1977). In a paper outlining the present state of stopping power data, he states that the Bragg Additivity Rule can only be applied with an uncertainty exceeding 3%.

8.1.2 Carbon Chamber

The carbon wall is more complicated than that of the TE plastic wall in that the predominant particles are assumed to be carbon recoils with an average energy of 0.6MeV (again derived by assuming an average neutron energy of 8.4MeV etc) α particles and ^{9}Be recoils of average energies of 0.9MeV and 0.64MeV respectively (derived by assuming initial particle energies of 1.8MeV and 1.27MeV respectively as calculated in Chapter 7, and assuming that the average energies of the particles emerging from the wall will be half of these values).

Therefore, the $\overline{W}$ values as obtained by experiment, are effective $\overline{W}$ values ($\overline{W}_{eff}$) in various gases, due to the combined effect of carbon recoils, α particles and ^{9}Be recoils.

The relative fraction of energy transferred by carbon recoils, α particles and ^{9}Be recoils emitted from the carbon wall are assumed to be 66%, 23% and 10.6% respectively.

The mass stopping powers as obtained from Janni (1966) for 0.6MeV carbon recoils, 0.9MeV α particles and 0.63MeV ^{9}Be recoils, the (q_{sat}/d_{eq}) measurements as obtained by experiment, and the densities at 23°C are shown in Table 8.6 for the five gases of interest.

The ratios of S_{mass}, q_{sat}/d_{eq} and ρ involved in the calculation of $\overline{W}_{eff}$ ratios are shown in Table 8.8 for all gas combinations. The effective stopping power ratio S_{eff} for each gas combination is

calculated by assuming a weighting of 66% for $S_{carbon\ recoil}$, 23.4% for S_{α}, and 10.6% for S_{Be}.

By inserting these values into Equation 8.3 the $\overline{W}_{eff}$ ratios for each gas combination can be obtained and are shown in Column 8 of Table 8.8. Experimental values of $\overline{W}_{eff}$ ratios can only be compared with the published data of Nguyens et al (1980) for carbon recoils in TE gas, CO_2 and CH_4, and the survey data of ICRU 31 for α particles in TE gas, CO_2, Ar and CH_4 (these $\overline{W}$ values are shown in Table 8.7); no data are available on $\overline{W}$ values for ^9Be recoils. The value of $\overline{W}_{\alpha}$ for CO_2 is for 5.3MeV α particles; the ICRU 31 survey points out that $\overline{W}$ is energy dependent for α particles in this energy region, therefore the $\overline{W}_{\alpha}$ value for CO_2 is likely to be too large to within a maximum difference of 4%. $(\overline{W}_{eff})_{theory}$ values for each gas must be calculated by assuming a weighting of 74% for $\overline{W}$ due to carbon recoils and 26% for $\overline{W}$ due to α particles because of the lack of data on ^9Be recoils. A comparison of $(\overline{W}_{eff})_{expt}$ and $(\overline{W}_{eff})_{theory}$ is shown in Table 8.8 for TE/CO_2, TE/CH_4 and CO_2/CH_4 combinations.

As can be seen, the combinations TE/CO_2 and CO_2/CH_4 show differences of 3.5% and 4.6% respectively. The difference of 8.2% in the case of TE/CH_4 indicates that the differences of 3.5% and 4.6% will lie primarily with the TE gas and CH_4, since the figure of 8.2% is approximately the sum of 3.5% and 4.6%.

These differences are not unexpected under the experimental circumstances. The exclusion of $\overline{W}$ values of ^9Be recoils in a value of $(\overline{W}_{eff})_{theory}$ will contribute to these differences. In addition

the relatively low measurement of (q_{sat}/d_{eq}) may introduce an error of approximately 1% for each gas. Further errors may exist in the estimation of the energy of the α particles emitted from the wall and in the chosen values of $\overline{W}$ for α particles. However, the major source of error is in the determination of stopping power at low recoil energies. As was mentioned in Chapter 6, for proton energies of less than 0.1MeV, approximate mass stopping powers were obtained by continuation of S_{mass} against $(\text{proton energy})^n$ curve to lower energies. An error of approximately 3% is estimated because of these extrapolations; there must also be substantial uncertainties in Janni's data.

Therefore, the present measurements agree with the measurements of Nguyens et al and ICRU 31, to within the limits of experimental error and the errors associated with stopping power data. Bearing this in mind, the $\overline{W}_{eff}$ values for Air and Argon can be obtained from $\overline{W}_{eff}$ values of TE gas, CO_2 and CH_4.

Table 8.9 shows the determinations of $(\overline{W}_{eff})_{air}$ for 0.6MeV ^{12}C recoils, 0.9MeV α particles and 0.64 ^{9}Be recoils from the calculation of the combinations of TE/Air, CO_2/Air and Air/CH_4. A value of $(\overline{W}_{eff})_{air} = 40.0 \pm 2.2$eV is estimated.

Table 8.10 shows the determinations of $(\overline{W}_{eff})_{argon}$ for 0.6MeV ^{12}C ions and 0.9MeV α particles from the calculations of combinations of TE/Ar, CO_2/Ar and Ar/CH_4. A value of $(\overline{W}_{eff})_{argon} = 30.5 \pm 1.1$eV is estimated.

8.1.3 Summary and Conclusion

A method for deriving $\overline{W}$ values for protons and carbon wall recoils from known $\overline{W}$ values, based on the use of Bragg-Gray Theory at very small plate separations, has been presented.

For protons, issuing from the TE plastic wall, the experimental results agree well with the published data of other authors; for recoil particles issuing from the carbon wall, there are few data available for comparison with published data.

In both cases, the method has been established for the determination of the $\overline{W}$ values of protons from TE plastic wall and $\overline{W}_{eff}$ values of recoil particles from carbon wall, in any gas.

TABLE 8.1 TE Plastic Chamber (2.1MeV protons)

Gas	Density at 23°C $gcm^{-3} \times 10^{-3}$	q_{sat}/d_{eq} $10^{-8} Cmm^{-1}$	S_{mass} $MeVg^{-1} cm^2$
TE gas	1.049	0.358	173.09
CO_2	1.811	0.445	130.23
Air	1.190	0.288	130.99
Ar	1.645	0.366	92.11
CH_4	0.660	0.308	196.77

TABLE 8.2 $\overline{W}$ Values Estimated from ICRU 31 for 2.1 MeV Protons

Gas	$\overline{W}$ (eV)	Description of Reference
TE gas	29.5 - 32.5	31.0 $\pm$ 1.5eV from Figure 5.1 30.03 eV from Table 5.11
CO_2	33.0 - 36.0	34.4eV from Table 5.11 34.5 $\pm$ 1.5eV from Figure 5.4
Air	35.2	35.2eV from Table 5.11
Ar	26.0 - 28.0	26.7eV from Table 5.11 26.6 $\pm$ 0.5ev from Table 5.1 27.0 $\pm$ 1.0eV from Figure 5.3
CH_4	29.4 - 31.5	29.4eV from Bichsel and Inokuti (1976) (From ICRU 31) 30.5 $\pm$ 1.0eV from Figure 5.4

TABLE 8.3 Comparison of $\bar{W}$ Ratios Obtained By Experiment With $\bar{W}$ Ratios from ICRU 31 Survey

(1)	(2)	(3)	(4)	(5)	(6)	(7)	(8)
Gas $(\text{Combination})^X_Y$	$(q_{sat}/d_{eq})^X_Y$	$(\rho)^X_Y$	$(S_{mass})^X_Y$	$(\bar{W})^X_Y$ Experiment	$(\bar{W})^X_Y$ ICRU 31 Limits	$(W)^X_Y$ ICRU 31 Average Value	Percentage Difference of (5) and (7)
TE/CO_2	0.804	0.579	1.329	0.957	0.819–0.985	0.902	+ 5.76
TE/Air	1.243	0.882	1.321	0.938	0.923–0.838	0.881	+ 6.04
TE/Ar	0.978	0.638	1.879	1.225	1.250–1.054	1.152	+ 6.01
TE/CH_4	1.162	1.589	0.880	1.203	1.105–0.937	1.021	+15.13
CO_2/Air	1.545	1.522	0.994	0.979	1.023–0.938	0.980	- 0.10
CO_2/Ar	1.216	1.101	1.413	1.280	1.385–1.179	1.282	- 0.16
CO_2/CH_4	1.444	2.744	0.662	1.258	1.224–1.048	1.136	+ 9.67
Air/Ar	0.787	0.723	1.422	1.307	1.257–1.354	1.305	+ 0.12
Air/CH_4	0.935	1.803	0.666	1.284	1.117–1.197	1.157	+ 9.87
Ar/CH_4	1.188	2.493	0.468	0.982	0.952–0.825	0.889	+ 9.47

TABLE 8.4 Estimation of $\overline{W}_{CH_4}$ for 2.1MeV Protons

$(\text{Gas Combination})^X_Y$	Ratio $(\overline{W})^X_Y$ From Table 8.3	$\overline{W}_{CH_4}$ (eV)
CO_2/CH_4	1.258	26.2 - 28.6
Air/CH_4	1.284	27.4
Ar/CH_4	0.982	26.5 - 28.5

TABLE 8.5 Estimation of $\overline{W}_{TE\ Gas}$ for 2.1MeV Protons

$(\text{Gas Combination})^X_Y$	Ratio $(\overline{W})^X_Y$ From Table 8.3	$\overline{W}_{TE\ Gas}$ (eV)
TE/CO_2	0.957	31.6 - 34.5
TE/Air	0.938	33.0
TE/Ar	1.225	31.9 - 34.3

TABLE 8.6 Carbon Chamber (0.6MeV Carbon Recoils, 0.9MeV α Particles and 0.64 ^{9}Be recoils)

Gas	Density at 23°C $gcm^{-3} \times 10^{-3}$	q_{sat}/d_{eq} $Cmm^{-1} \times 10^{-8}$	$(S_{mass})_{MeVg^{-1}cm^{2}}$ $[^{12}C]$	$(S_{mass})_{MeVg^{-1}cm^{2}}$ $[\alpha_2]$	$(S_{mass})_{MeVg^{-1}cm^{2}}$ $[^{9}Be]$
TE gas	1.049	0.0820	1360	800.0	669
CO_2	1.811	0.0880	860	517.7	396
Air	1.190	0.0600	870	526.8	435
Ar	1.645	0.0750	620	333.6	308
CH_4	0.660	0.0705	1630	940.5	803

TABLE 8.7 $\overline{W}_{eff}$ Values Estimated from Nguyens et al (1980) and ICRU 31 (1979)

Gas	$\overline{W}$(eV) (0.6MeV ^{12}C ions) from Nguyens et al	$\overline{W}$(eV) (0.9MeV α Particles) from ICRU 31		$\overline{W}_{eff}$ (eV)
TE gas	40.0	33.0 ± 1.0	Fig 5.5 (E_α = 1.0MeV)	38.2 ± 0.4
CO_2	42.5	34.2	Table 5.11 (E_α = 5.3MeV)	40.4 ± 0.8
CH_4	38.5	30.5 ± 1.0	Fig 5.7 (E_α = 1.0MeV)	36.4 ± 0.4
Ar	-	26.5 ± 0.5	Fig 5.8 (E_α = 1.0MeV)	-

TABLE 8.8 Comparison of $\overline{W}_{eff}$ Ratios Obtained by Experiment with $\overline{W}_{eff}$ Ratios Obtained from Nguyens et al (1980) and ICRU 31 (1979)

(1)	(2)	(3)	(4)	(5)	(6)	(7)	(8)	(9)	(10)
$(\text{Gas (Combination)})^{X}_{Y}$	$(q_{sat}/d_{eq})^{X}_{Y}$	$(\rho)^{X}_{Y}$	$(S_{mass})^{X}_{^{12}C\,Y}$	$(S_{mass})^{X}_{\alpha_Y}$	$(S_{mass})^{X}_{^{9}Be\,Y}$	$(S_{mass})^{X}_{eff_Y}$	$(\overline{W}_{eff})^{X}_{expt_Y}$	$(\overline{W}_{eff})^{X}_{theory_Y}$	Percentage Difference Of (8) & (9)
TE/CO_2	0.932	0.579	1.581	1.545	1.689	1.584	0.984	0.95	+ 3.46
TE/Air	1.367	0.882	1.563	1.520	1.538	1.538	0.992		
TE/Ar	1.093	0.638	2.194	2.398	2.172	2.239	1.307		
TE/CH_4	1.163	1.589	0.834	0.850	0.833	0.837	1.144	1.05	+ 8.22
CO_2/Air	1.467	1.522	0.989	0.983	0.910	0.979	1.016		
CO_2/Ar	1.173	1.101	1.387	1.552	1.286	1.414	1.327		
CO_2/CH_4	1.248	2.744	0.528	0.550	0.493	0.529	1.163	1.11	+ 4.56
Air/Ar	0.800	0.723	1.403	1.579	1.412	1.445	1.306		
Air/CH_4	0.851	1.803	0.533	0.560	0.542	0.540	1.144		
Ar/CH_4	1.064	2.492	0.380	0.355	0.384	0.375	0.878		

TABLE 8.9 Estimation of $(\overline{W}_{eff})_{air}$

$(\text{Gas Combination})_Y^X$	Ratio $(\overline{W}_{eff})_Y^X$ from Table 8.8	$(\overline{W}_{eff})_{air}$ (eV)
TE/Air	0.992	38.5 ± 0.4
CO_2/Air	1.016	39.8 ± 0.8
Air/CH_4	1.144	41.6 ± 0.4

TABLE 8.10 Estimation of $(\overline{W}_{eff})_{argon}$

$(\text{Gas Combination})_Y^X$	Ratio $(\overline{W}_{eff})_Y^X$ from Table 8.8	$(\overline{W}_{eff})_{argon}$ (eV)
TE/Ar	1.307	29.2 ± 0.4
CO_2/Ar	1.327	30.4 ± 0.8
Ar/CH_4	0.878	32.0 ± 0.4

CHAPTER 9

ABSOLUTE CALIBRATION OF TE PLASTIC/TE GAS CHAMBER

9.1 Theory

The final aim of the experimentation in this chapter is to perform an absolute calibration of the TE/TE chamber in a neutron beam and thereafter derive the absorbed dose in tissue as measured by the TE/TE chamber.

In a neutron beam, the determination of the neutron and gamma absorbed dose in the wall of the ionization chamber involves a modification of the Bragg-Gray Theory, as follows:

$$(D_N + D_G)_m = \frac{Q_T}{m} \frac{\bar{W}_N}{e} (S_{m,g}) \frac{1}{(k_A)_T} \qquad (9.1)$$

where subscript T refers to measurements made using a TE/TE chamber in a neutron beam.

Q_T = chamber reading in a neutron beam, corrected for temperature and pressure, saturation, leakage current, polarity and flow-rate.

$(k_A)_T$ = the attenuation and scatter factor, which is obtained as follows.

9.1.1 Measurement of Attenuation and Scatter $(k_A)_T$

The introduction of a measuring device into a radiation field produces attenuation and scatter; because the ionization chamber is

fairly bulky, scatter from the brass, perspex and 'Tufnol' surroundings is likely to be significant and the factor $(k_A)_T$ is estimated as follows.

Using a subsidiary small chamber, (Exradin TE/Air Chamber), charge measurements were taken in isolation and also surrounded by the carbon chamber in the following configurations:-

1. H.T. electrode and support in front of Exradin (Fig. 9.1).
2. Exradin in front of centre and guard electrodes and their support (Fig. 9.2).
3. Exradin between H.T. and centre electrode supports (Fig. 9.3).

The difference in charge measurements of Exradin in isolation compared with measurements in the above configurations, gives the overall scatter factor $(k_A)_T$. A combination of methods 1 and 2 is more likely to be accurate than method 3 alone. This is because the geometry of method 3 is less favourable in that the sensitive tip of the Exradin chamber is less likely to detect scatter from inside the H.T. electrode support.

9.1.2 Determination of the Mass of Gas in the Cavity

One method of obtaining m, the mass of the gas in the cavity, is by performing an absolute calibration of the TE/TE chamber in a photon beam, the details of which will be described during the course of this chapter. This value of m can be checked by calculation from dimensions and gas density.

However, the factors involved in the calibration of the TE/TE chamber in a photon beam are not as well established as the factors involved in the calibration of a C/Air chamber, for example, in a photon beam.

For this reason, the C/Air configuration of chamber was calibrated in a 300kv x-ray beam and the determination of m using this method was checked by calculating m from dimensions and gas density. Also the geometry of the C/Air chamber is favourable as it is of exactly the same dimensions as the TE/TE chamber, and attenuation and scatter factors can also be estimated by using the method of Section 9.1.1.

9.2 Calibration of C/Air Chamber in 300kv X-rays

The absorbed dose to the wall of an ionization chamber is related to the charge collected, Q_c by the Bragg-Gray Theory i.e.

$$(D_m)_c = \frac{Q_c}{m} \frac{\bar{W}_c}{e} (S_{m,g})_c \qquad (9.2)$$

Strictly, for 300kv x-radiation, only a homogenous chamber will satisfy equation 9.2. However, a C/air chamber with plate separation of approximately 2mm, in 300kv x-rays, is likely to be a good Bragg-Gray approximation, since the maximum ranges of the secondary electrons produced in the wall of the ionization chamber are approximately 20cm (ICRU 26).

The absorbed dose to the wall of the ionization chamber can also be obtained by measurement of exposure. An N.P.L. secondary

standard chamber can be used to measure exposure in the absence of the C/air chamber i.e.

$$X_c = MN_c \qquad (9.3)$$

where M = secondary standard reading after correction for temperature and pressure.

N_c = exposure calibration factor for 300kv X-rays.

From exposure, the dose to the wall material of the C/air chamber is obtained by

$$(D_m)_c = X_c (f_m)_c \, (k_A)_c \qquad (9.4)$$

where $$(f_m)_c = \frac{\overline{W}_{air}}{e} \frac{(\mu_{en}/\rho)_{carbon}}{(\mu_{en}/\rho)_{air}}$$

(μ_{en}/ρ) = mass energy absorption coefficient.

$(k_A)_c$ was measured using the method described in Section 9.1.1. The scatter factors for the 3 methods described are shown in Table 9.1; the overall scatter factor $(k_A)_c$ was assumed to be 1.24 as derived from a combination of methods 1 and 2.

By comparing equations 9.2 and 9.4, the dose to the wall of the C/air chamber is

$$(D_m)_c = \frac{Q_c}{m} \frac{\overline{W}_c}{e} (S_{m,g})_c = X_c \, (f_m)_c \, (k_A)_c \qquad (9.5)$$

Therefore, the mass of the gas in the cavity is given by

$$m = \frac{Q_c \; \frac{\overline{W}_c}{e} \; (S_{m,g})_c}{MN_c \; (f_m)_c \; (k_A)_c} \qquad (9.6)$$

Alternatively, the value of m can be obtained by calculation from dimensions as the product of volume and density of gas.

As shown in Table 9.4, m from equation 9.6 and m from dimensions are equal to within 1%. This indicates that the determination of m by photon calibration gives good agreement with the calculation of m from dimensions, and that the method of obtaining $(k_A)_c$ is accurate to within 1%.

9.3 Calibration of TE/TE Chamber in 300kv X-rays

Having established that a photon calibration method compared with a dimension method gives good agreement in the determination of m for a C/air chamber, the same procedure can be adopted to determine m for the TE/TE chamber.

The method involved in deriving m from the photon calibration of the TE/TE chamber is given in detail by Mijnheer and Williams (1980).

In the calibration beam, the dose to the TE plastic wall is

$$(D_m)_c = \frac{Q_c}{m} \; \frac{\overline{W}_c}{e} \; (S_{m,g})_c$$

The dose to tissue is therefore,

$$(D_t)_c = \frac{Q_c}{m} \; \frac{\overline{W}_c}{e} \; (S_{m,g})_c \; (\mu_{en}/\rho)^t_m \qquad (9.7)$$

The dose to tissue is also obtained from a secondary standard reading as described previously in equation 9.3 i.e.

$$(D_t)_c = X_c \frac{\bar{W}_{air}}{e} (\mu_{en}/\rho)^t_{air} (k_A)_c \qquad (9.8)$$

$$= X_c (f_t)_c (k_A)_c$$

Measurements of $(k_A)_c$ for TE chamber in 300kv X-rays are given in Table 9.2.

Equating equations 9.7 and 9.8

$$m = \frac{Q_c}{X_c} \frac{\bar{W}_c}{e} \frac{(S_{m,g})_c (\mu_{en}/\ )^t_m}{(f_t)_c (k_A)_c} \qquad (9.9)$$

The quantity $\frac{X_c (f_t)_c (k_A)_c}{Q_c}$ can be defined as α_c, the absorbed dose calibration factor.

Therefore $$m = \frac{1}{\alpha_c} \frac{\bar{W}_c}{e} (S_{m,g}) (\mu_{en}/\rho)^t_m \qquad (9.10)$$

Alternatively, the value of m can be obtained by calculation from dimensions as the product of volume and density of gas.

As shown in Table 9.5, m from equation 9.10 and m from dimensions are equal to within 1%. This again indicates that the method of obtaining $(k_A)_c$ is accurate to within 1%.

9.4 Determination of the Absorbed Dose in the Neutron Beam Using TE/TE Chamber

Having established a value of m from a photon calibration and from dimensions, and established the attenuation and scatter factor $(k_A)_T$ as shown in Table 9.3, the neutron and gamma absorbed dose in the wall of the ionization chamber can be obtained from Equation 9.1 i.e.

$$(D_N + D_G)_m = \frac{Q_T}{m} \frac{\bar{W}_N}{e} (S_{m,g}) \frac{1}{(k_A)_T} \qquad (9.11)$$

This equation is an approximation which assumes that $\frac{D_G}{D_G + D_N}$ is small, i.e. the absorbed dose due to neutrons is very much greater than the absorbed dose due to gamma rays (Williams and Greening 1980). For the neutron beam used, D_G generally accounts for less than 4% of the total absorbed dose within the main beam for measurements made in air (Williams et al 1979). This equation also assumes that the quantity $\frac{h_T - k_T}{k_T}$ is small, where k_T and h_T are defined as the sensitivities of the chamber to neutrons and to gamma rays respectively, relative to its sensitivity to the radiation used for calibration. It is usual to assume that h_T is unity and that generally k_T lies in the range 0.95 - 1.00.

To relate the absorbed dose in the wall of the ionization chamber to the absorbed dose in tissue, $(D_N + D_G)_m$ must be multiplied by the kerma ratio of tissue to TE plastic i.e.

$$(D_N + D_G)_t = \frac{Q_T}{m} \frac{\bar{W}_N}{e} (S_{m,g})_N \frac{1}{(k_A)_T} \left(\frac{K_t}{K_m}\right)_N \qquad (9.12)$$

where subscript t refers to tissue.

The value of absorbed dose $\left[(D_N + D_G)_t\right]_1$ of 0.1002 Gy obtained by this method is shown in Table 9.6 along with all factors contributing to this value. The subscript 1 refers to the value of absorbed dose in the neutron beam obtained by the TE/TE chamber.

9.5 Comparison of Absorbed Dose Determination Using TE/TE Parallel Plate Chamber to Absorbed Dose Determination Using Polythene/Air Chamber

Having obtained a value of absorbed dose in the neutron beam by measurement with the TE/TE parallel plate chamber, this value of absorbed dose can be compared with the absorbed dose in a neutron beam as measured by the polythene/air chamber, which has been used as a reference chamber for all charge measurements.

The polythene/air chamber, undergoes a routine calibration by comparing charge readings with those of an Exradin TE/TE chamber. The Exradin TE/TE chamber, in turn has been calibrated in a 4MV photon beam by a similar method as was described in Section 9.2 for the C/Air chamber in 300kv x-rays, (Williams and Greening 1980), the difference being that no direct measurement of $(k_A)_c$ was made.

Therefore a single charge reading of the polythene/air chamber in a neutron beam corresponds to a certain absorbed dose value, after correction has been made for temperature and pressure (Williams 1980). This value of absorbed dose $\left[(D_N + D_G)_t\right]_2$ is shown in Table 9.6. The subscript 2 refers to the value of absorbed dose in the neutron beam obtained by the polythene/air chamber.

Comparing $\left[(D_N + D_G)_t\right]_1$ as measured by TE/TE parallel plate chamber and $\left[(D_N + D_G)_t\right]_2$ as measured by the polythene/air chamber, both methods give the same value to within 1%.

TABLE 9.1 Carbon Chamber - Estimation of $(k_A)_c$ in 300kv X-rays

Configuration of Exradin	Charge Measurement (10^{-9}C)	Estimation of $(k_A)_c$
In isolation	4.33	
As in Figure 1	4.72	1.24
As in Figure 2	4.99	
As in Figure 3	5.28	1.22

TABLE 9.2 TE Plastic Chamber - Estimation of $(k_A)_T$ in neutron beam

Configuration of Exradin	Charge Measurement (10^{-9}C)	Estimation of $(k_A)_T$
In isolation	1.88	
As in Figure 1	2.00	1.12
As in Figure 2	1.99	
As in Figure 3	2.09	1.11

TABLE 9.3 TE Plastic Chamber - Estimation of $(k_A)_c$ in 300kv X-rays

Configuration of Exradin	Charge Measurement (10^{-9}C)	Estimation of $(k_A)_c$
In isolation	4.12	
As in Figure 1	4.49	1.24
As in Figure 2	4.75	
As in Figure 3	5.10	1.24

TABLE 9.4 Factors Involved in the Absolute Calibration of C/Air Chamber in 300kv X-rays

Method	Factors Involved	Source of Reference	m (kg)
Calibration Method	$Q_c = 25.4 \times 10^{-9} C$		
	$\frac{W_c}{e} = 33.73\ JC^{-1}$	Attix et al (1968)	
	$S_{m,g} = 1.015$	Attix et al (1968)	
	$M = 32.6$		
	$(\mu_{en}/\rho)_{carbon} = 1.347 \times 10^{-2} m^2\ kg^{-1}$ $(\mu_{en}/\rho)_{air} = 1.355 \times 10^{-2} m^2\ kg^{-1}$	Hubbell (1977) for 150 keV x-rays	
	$(f_m)_c = 33.53\ Gy\ C^{-1}\ kg$		
	$N_c = 2.724 \times 10^{-4} C\ kg^{-1}$	Williams and Greening (1980)	2.40×10^{-6}
Dimension Method	Volume = $2.001 cm^3$ Density = $1.19 mgcm^{-3}$ at 23°C		2.38×10^{-6}

TABLE 9.5 Factors Involved in the Absolute Calibration of TE/TE Chamber in 300kv X-rays

Method	Factors Involved	Source of Reference	m (kg)
	$Q_c = 1.92 \times 10^{-8} C$		
	$M = 30.59$		
	$N_c = 2.724 \times 10^{-4} C\ kg^{-1}$	Williams and Greening (1980)	
	$\frac{\bar{W}_{air}}{e} = 33.73\ JC^{-1}$	Attix et al (1968)	
	$\frac{\bar{W}_c}{e} = 29.25\ JC^{-1}$	Goodman and Coyne (1980)	
	$(\mu_{en}/\rho)_{air} = 1.355 \times 10^{-2} m^2\ kg^{-1}$ $(\mu_{en}/\rho)_t = 1.49 \times 10^{-2} m^2\ kg^{-1}$ $(\mu_{en}/\rho)_{A-150} = 1.481 \times 10^{-2} m^2\ kg^{-1}$	Hubbell (1977) for 150keV x-rays	
	$(S_{m,g}) = 1.00$		1.474×10^{-6}
Dimension Method	Volume $= 1.412 cm^3$ Density $= 1.049 mgcm^{-3}$ at 23°C		1.481×10^{-6}

TABLE 9.6 Comparison of Absorbed Dose as Measured by TE/TE Chamber with Absorbed Dose as Measured by Polythene/Air Chamber

Method	Factors Involved	Source of Reference	Absorbed Dose
TE/TE Chamber	$Q_T = 5.05 \times 10^{-9} C$ $\frac{\bar{W}_N}{e} = 31.9\ JC^{-1}$ $S_{m,g} = 1.0$ $\frac{K_m}{K_T\ N} = 0.971$ $m = 1.478 \times 10^{-6} kg$	Goodman and Coyne (1980) Data from Coyne (1980) Spectrum from Bonnet (1979)	$\left[(D_N + D_G)_t\right]_1 = 0.1002$ Gy
Polythene/ Air Chamber	$Q_T = 1.407 \times 10^{-9} C$		$\left[(D_N + D_G)_t\right]_2 = 0.1008$ Gy

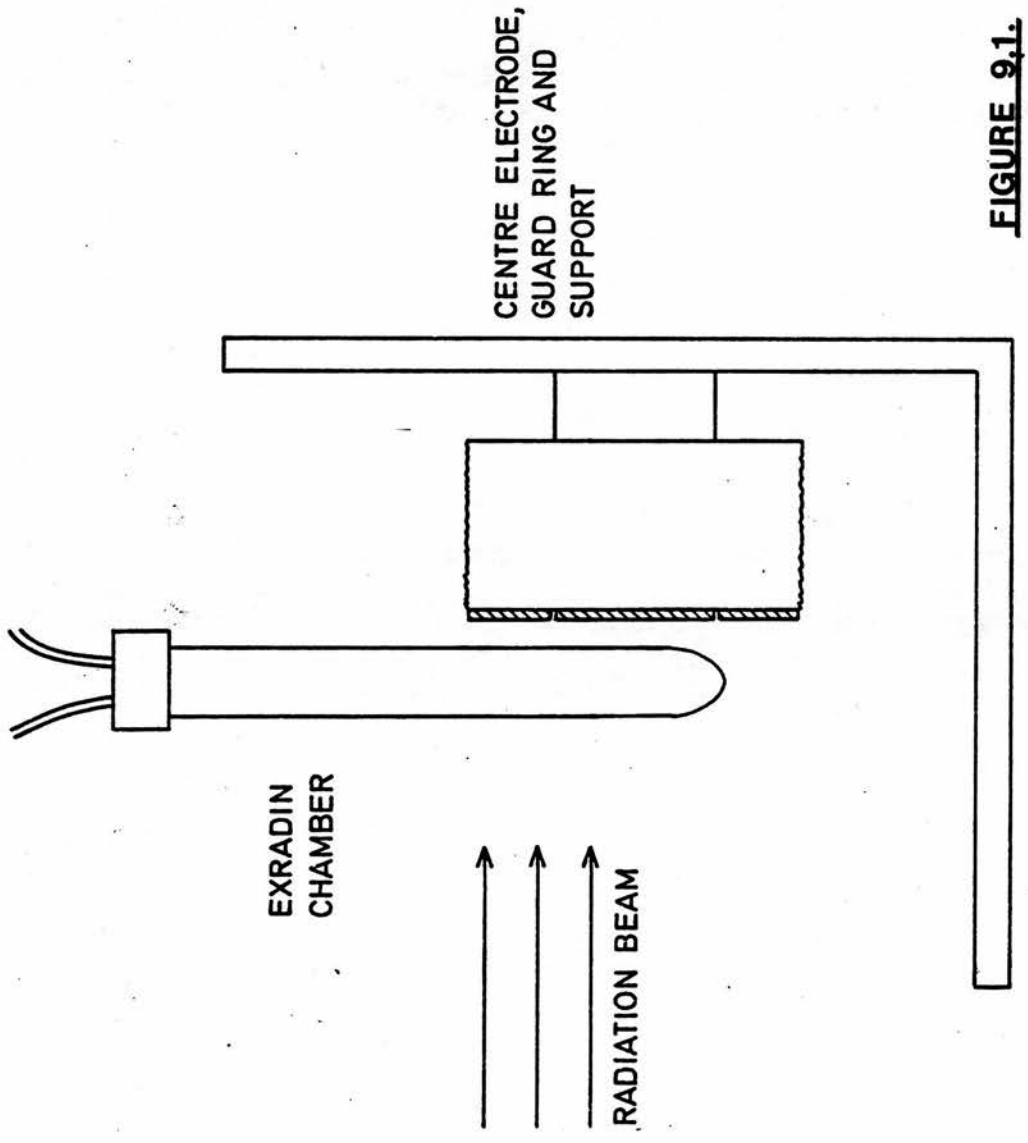
CENTRE ELECTRODE,
GUARD RING AND
SUPPORT
EXRADIN
CHAMBER
RADIATION BEAM

FIGURE 9.1.

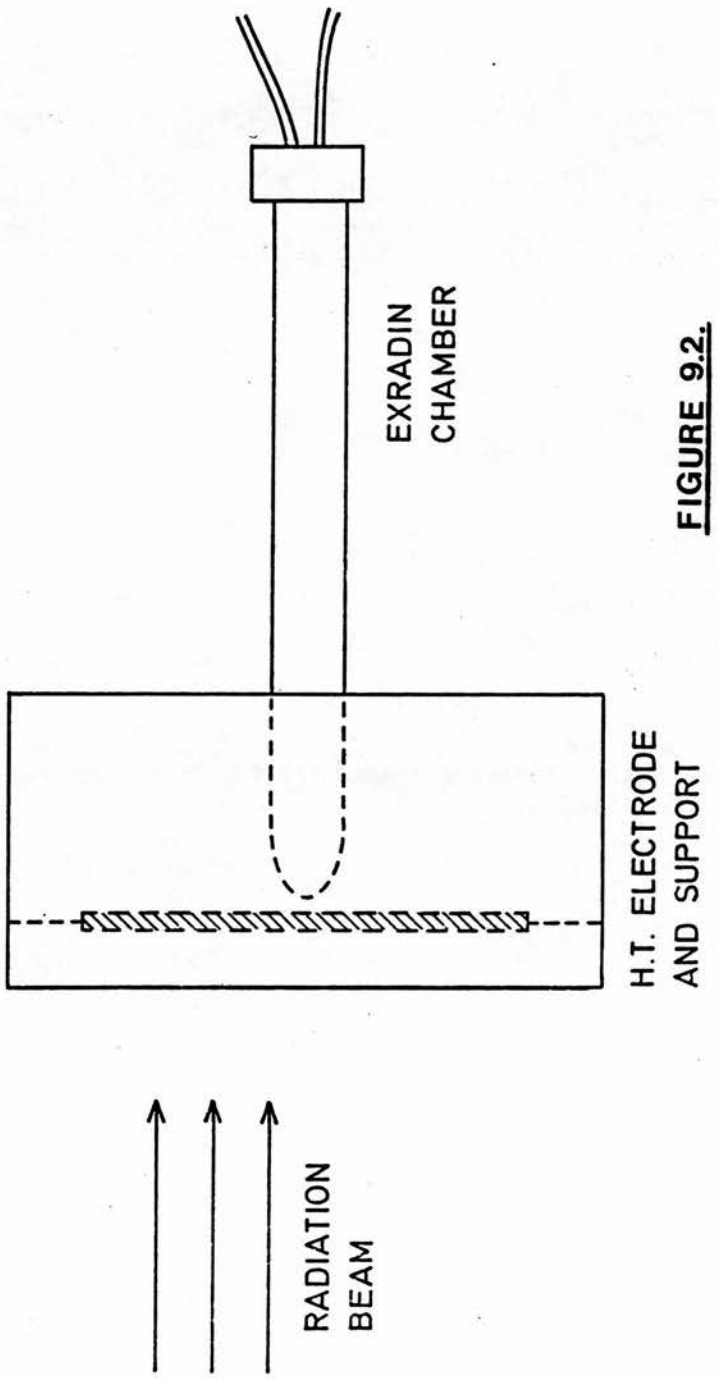

FIGURE 9.2.

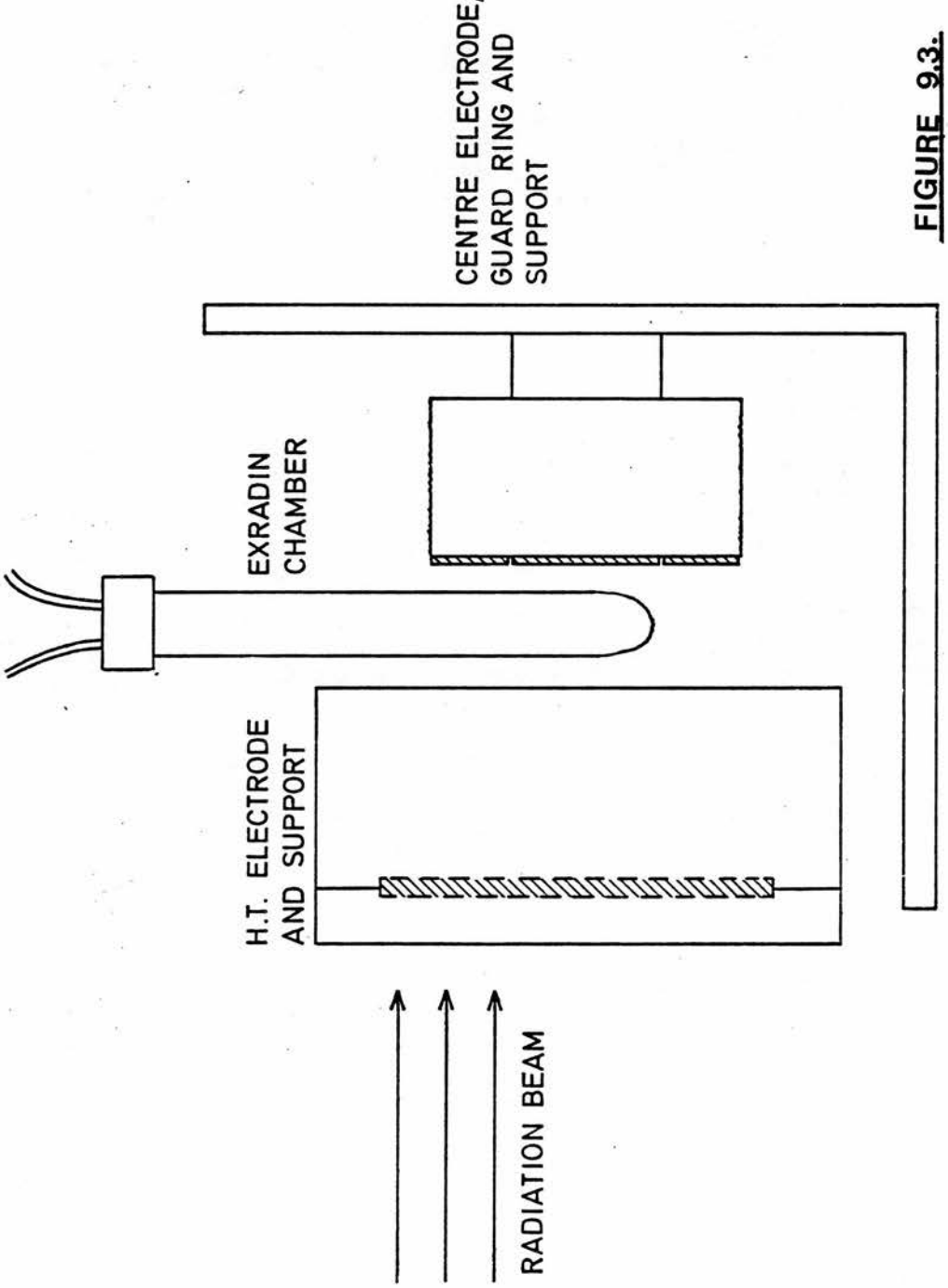
CENTRE ELECTRODE, GUARD RING AND SUPPORT
EXRADIN CHAMBER
H.T. ELECTRODE AND SUPPORT
RADIATION BEAM

FIGURE 9.3.

CHAPTER 10

RATIOS OF SENSITIVITY OF VARIOUS CHAMBERS: COMPARISON WITH OTHER AUTHORS

The sensitivities of various chambers are frequently required, particularly in the determination of the individual neutron and gamma dose in a mixed radiation field.

For this reason, the responses of the chamber combinations used in the experiments of Chapter 6 are compared with the responses of chambers of other authors, where available.

The ratio of responses, $\frac{A_1}{B_1}$, of chambers used in this thesis are shown in Table 10.1. These are compared with the ratio of responses $\frac{A_2}{B_2}$ of other parallel-plate and also thimble type chambers as used by Kühn (1979), Attix et al (1980), Hiroaka et al (1971) and Kuchnir et al (1979) as detailed in Table 10.1.

10.1 Comparison of Parallel-Plate Chambers

10.1.1 TE/TE - TE/Air

The ratio of sensitivities, $\frac{A_1}{B_1}$, of a combination of TE/TE and TE/Air chambers, at 6, 4 and 2mm plate separations, shows good agreement with the ratio of sensitivities $\frac{A_2}{B_2}$ at both 3.3 and 15MeV of a similar parallel-plate chamber as described by Kühn (1979). The fact that the ratio of sensitivities in all cases is approximately the same value implies that the sensitivities of both TE/TE and TE/Air chamber do not vary with plate separation or energy.

The plate separation constancy is confirmed by Chapter 6 which shows that the sensitivities of both chambers do not vary in the range 0.1 - 10mm.

10.1.2 C/CO_2 - C/Air

The ratio of sensitivities $\frac{A_1}{B_1}$ represent neutrons with an average energy of 8.4MeV (Chapter 7). Comparison with Kühn's results for neutron energy of 15.0MeV shows a generally higher ratio of $\frac{A_2}{B_2}$; comparison with neutron energy of 3.3MeV shows a generally lower ratio of $\frac{A_2}{B_2}$.

A combination of experimental results and those of Kühn indicates a definite linear relationship between the ratio of sensitivities of C/CO_2 - C/Air chambers with increasing energy, at the plate separations of 8, 6 and 4mm.

10.1.3 Thimble Type Chambers

Comparison is also given in Table 10.1 of ratio of sensitivities of the parallel-plate chamber with certain thimble type chambers. The plate separations of the thimble type chambers are calculated as the distance ~~of radius~~ between the tip of the centre electrode and the spherical guard ring. As is shown in all cases, a realistic comparison between the parallel-plate chambers and thimble type chambers of the same material cannot be made, which is not unexpected.

TABLE 10.1 Ratio of Responses of the Parallel-Plate Chamber, and Comparison with other Authors

Chamber Combination A, B	Parallel-Plate Chamber		Comparison				
	Plate Sep. d.	Relative Sensitivity $\frac{A_1}{B_1}$	Chamber Type	Sep/Volume	Neutron Energy (MeV)	Relative Sensitivity $\frac{A_2}{B_2}$	Author
TE/TE-TE/Air	6mm	1.25	Parallel-Plate	6mm	15.0	1.24	" Kuhn (1979)
TE/TE-TE/Air	4mm	1.25	"	4mm	15.0	1.23	" Kuhn (1979)
TE/TE-TE/Air	2mm	1.25	"	2mm	15.0	1.23	" Kuhn (1979)
TE/TE-TE/Air	6mm	1.25	"	6mm	3.3	1.29	" Kuhn (1979)
TE/TE-TE/Air	4mm	1.25	"	4mm	3.3	1.24	" Kuhn (1979)
TE/TE-TE/Air	2mm	1.25	"	2mm	3.3	1.25	" Kuhn (1979)
C/CO_2-C/Air	8mm	1.27	"	8mm	15.0	1.61	" Kuhn (1979)
C/CO_2-C/Air	6mm	1.27	"	6mm	15.0	1.52	" Kuhn (1979)
C/CO_2-C/Air	4mm	1.35	"	4mm	15.0	1.58	" Kuhn (1979)
C/CO_2-C/Air	8mm	1.27	"	8mm	3.3	1.13	" Kuhn (1979)
C/CO_2-C/Air	6mm	1.27	"	6mm	3.3	1.12	" Kuhn (1979)
C/CO_2-C/Air	4mm	1.35	"	4mm	3.3	1.16	" Kuhn (1979)
TE/TE-TE/CO_2	6mm	0.80	Thimble Type	1cm^3	14.8	1.34	Attix et al (1980)
C/TE-C/CO_2	6mm	1.06	"	1cm^3	14.8	1.36	"
TE/TE-C/CO_2	10mm	4.55	"	4.2cm^3	7.0	6.21	Hiraoka et al (1971)
C/Air-C/CO_2	8mm	0.79	"	2cm^3	8.0	1.31	Kuchnir et al (1979)

CHAPTER 11

DISCUSSION AND CONCLUSION

A variable plate separation, variable gas pressure, detachable plate ionization chamber has been constructed and tested. Some considerable problems were encountered during construction e.g. machining of graphite screws, sealing of vacuum tight tank etc. (Chapter 2). The problems encountered during the testing of each chamber configuration have been described in Chapter 3.

The ionization chamber has functioned as expected, (confirmed by Kuhn, Chapter 10). From a design point of view, it has proved to be advantageous in the following ways. The detachable plates enable the ionization chamber to be used in a routine fashion to obtain $\overline{W}$ information on any machinable solid or any gas. The variable pressure facility enables a Bragg-Gray approximation in the measurement of $\overline{W}$ values in any gas, for protons and carbon wall recoils. Indeed, if the $\overline{W}$ value is known for recoils from a particular wall material in a particular gas, then the $\overline{W}$ values of the same recoils in any gas can be estimated. Because of its bulk, the scattering coefficient, k_A, of the ionization chamber can be estimated using a smaller chamber. In this respect, the design of the ionization chamber is advantageous over thimble type chambers which would require the construction of a much smaller chamber, hence is impractical to construct a smaller chamber. The design of the chamber has enabled the C/Air chamber to be used as a confirmation of the photon calibration method of obtaining m, the mass of gas in the cavity, before an absolute calibration of the TE/TE chamber was performed.

The charge per unit plate separation (q_{sat}/d) has been determined for TE/Air, TE/TE, C/Air, C/CO_2 and C/TE chambers in the range d = 0.1 - 18mm (Chapters 4, 5 and 6). It has been shown that q_{sat}/d for both TE/TE and TE/Air chambers is constant in this range. In routine dosimetry, a TE/TE chamber is generally used for comparison of dose for day-to-day measurements. The fact that both TE/TE and TE/Air chambers exhibit a constancy of q_{sat}/d with increasing d indicates that a TE/Air chamber could be used routinely, with a simple correction made as an initial calibration. This would avoid the problems associated with gas flow, porosity of gas carrying tubes (Williams 1980), setting up of gas transporting apparatus etc., and would be less expensive.

Comparison of q_{sat}/d measurements of C/CO_2 and C/TE chambers in an air atmosphere, with measurements in a CO_2 and TE gas atmosphere respectively, has shown that air contamination does occur as a result of the porosity of graphite. If other chamber materials are to be used, diffusion and gas flow measurements must be made to ensure no gas contamination by air. The issue can be avoided entirely by using the chamber inside the vacuum tight tank. q_{sat}/d for C/CO_2, C/Air and C/TE chambers is not constant in the range d = 0.1 - 18mm, but is in agreement with appropriate kerma, stopping power, density and range data (Chapter 6).

The fact that the value of (q_{sat}/d) for all chamber combinations is the same for extrapolation of saturation curve and for corrected fixed voltage measurements, indicates that there is no charge soakage in the ionization chamber plates leading to inaccurate consecutive charge measurements.

The relative charged particle contribution in C/CO_2, C/Air and C/TE ionization chambers has been estimated (Chapter 7). Agreement of theory and experiment is generally good except in the case of the C/TE chamber where protons and heavy recoils are treated simultaneously. This lack of agreement is due primarily to the properties of the protons e.g. energy, range, etc. vastly differing from those of the heavy recoils. This means that a small change in one parameter of the protons results in a large change in the overall relative charged particle contribution due to protons.

It is apparent that there is a lack of data concerning heavy recoils, particularly C, O and N ions, and no data concerning the less abundant recoils of Be and B. In particular, the method for deriving the stopping power of these recoils from that of protons (Chapter 7) is an empirical method which takes no account of the charge of the various recoils, In addition, the extrapolation of the proton stopping powers to low energies introduces further errors (Chapter 6).

The lack of accurate stopping power data for heavy recoils and α particles has repercussions on both relative charged particle contribution measurements and $\bar{W}$ value measurements, and indeed in most aspects of neutron dosimetry.

APPENDIX 1

HIGH VOLTAGE PROTECTION CIRCUIT FOR COMPARATOR

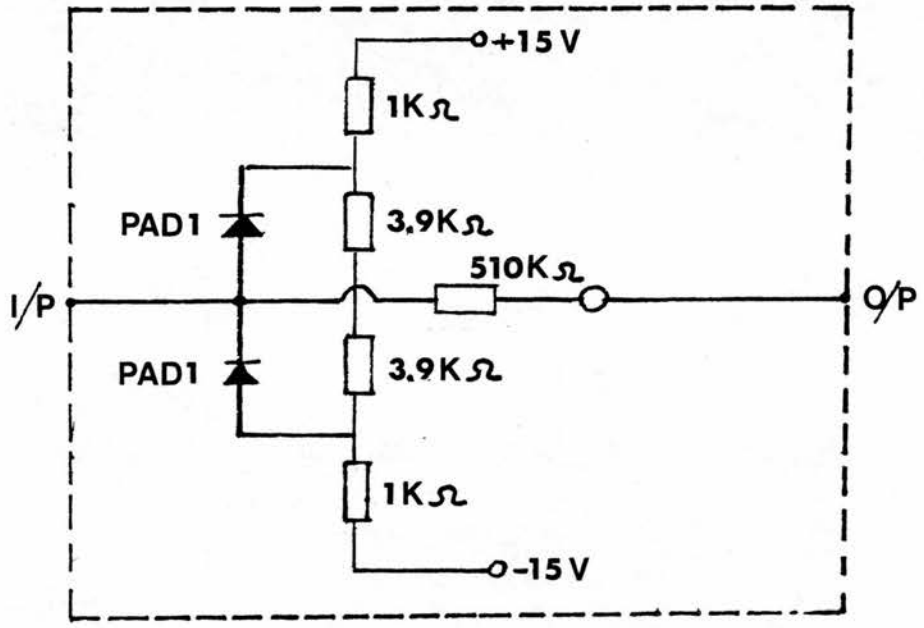

The diodes are specially selected low leakage (1pA maximum) so that when they are reverse biased as in normal operation, they take no current from the input signal.

When the input signal is > 12V (+ve), diode D_1 is turned on and limits positive excursion.

When the input signal is > 12V (-ve), diode D_2 is turned on and limits negative excursion.

APPENDIX 2

GENERALISED EQUATIONS FOR PARTICLE ENERGIES AND SPECTRA RESULTING FROM NEUTRON INTERACTIONS

The general problem is that a neutron of mass, m, and energy E_n, reacts with a nucleus of mass A. The result of the interaction is the production of two particles with masses M_1 and M_2 with excitation energies of E_1^* and E_2^*. The energy, Q, released in the reaction is given by the differences in rest mass between the initial and final products i.e.

$$Q = \left[(A + n) - (M_1 + M_2)\right] \times 931.141 \text{ MeV} \qquad 2.1$$

(masses in a.m.u.)

$Q = -E_T$ (the threshold energy for the reaction)

In most reactions, Q will be negative.

The angles made by the products M_1 and M_2 with the initial direction of the neutron in the centre of mass system are θ_1 and θ_2, where $\theta_2 = \frac{\pi}{2} + \theta_1$.

Applying considerations of conservation of energy and momentum in centre of mass space

$$M_1 v_1 = M_2 v_2$$

$$M_1 v_1^2 + M_2 v_2^2 = \left[\frac{A}{m + A} E_n\right] + Q - E_1^* - E_2^*$$

Hence

$$v_1^2 = \frac{2M_2}{M_1 (M_1 + M_2)} \left(\frac{A}{m + A} E_n + (Q - E_1^* - E_2^*) \right)$$

The velocity, u_1, of the particle in the laboratory system is given by

$$u_1^2 = v_1^2 + v_2^2 + 2v_1 v_2 \cos \theta_1$$

$$= \frac{2M_2}{M_1 (M_1 + M_2)} \left(\frac{A}{m + A} E_n + (Q - E_1^* - E_2^2) \right) + \frac{2m E_n}{(A + m)^2}$$

$$+2 \left[\frac{2M_2}{M_1 (M_1 + M_2)} \left(\frac{A}{m + A} E_n + (Q - E_1^* - E_2^*) \right) \right]^{\frac{1}{2}} \left[\frac{2m E_n}{(A + m)^2} \right]^{\frac{1}{2}} \cos \theta_1$$

2.2

The energy E_1 of the particle in the laboratory system is

$$E_1 = \left(1 - \frac{M_1}{M_1 + M_2}\right) \left(\frac{A}{m + A} E_n + (Q - E_1^* - E_2^*) \right) + \frac{m M_1}{(A + m)^2} E_n$$

$$+2 \left[\left(1 - \frac{M_1}{M_1 + M_2}\right) \left(\frac{A}{m + A} E_n + (Q - E_1^* - E_2^*) \right) \right]^{\frac{1}{2}} \left[\frac{m M_1}{(A + m)^2} E_n \right]^{\frac{1}{2}} \cos \theta_1$$

2.3

It may be assumed that the third term in Equation B.3 is very much smaller than the first and second terms, therefore, for ease of calculation, the approximation is made that

$$E_1 = \left(1 - \frac{M_1}{M_1 + M_2}\right)\left(\frac{A}{m + A}\right) E_n = (Q - E_1^* - E_2^*)) + \frac{m M_1}{(A + m)^2} E_n$$

REFERENCES

AJZENBERG-SELOVE, F. (1970)

Energy levels of light nuclei A = 13 - 15.

Nuclear Physics, A152, 1

ATTIX, F.H., PEARSON, D.W., DE LUCA, P.M. JR, GOETSCH, S.J. (1980)

Comparison of the Bragg-Gray Theory corollaries to fast neutron cavity ionization measurements at 14.8MeV.

Health Physics, Vol. 38, p.p. 623-633

AUXIER, J.A., JONES, T.D., HUBBELL, H.H. (1969)

Review of depth dose calculation and experimentation.

Proc. Symposium on Neutrons in Radiobiology, Oak Ridge,

U.S. Atomic Energy Commission, Oak Ridge. CONF-691106

p. 73

BEWLEY, D.K. (1963)

Physical aspects of the fast neutron beam.

British Journal of Radiology 36 81-88

BICHSEL, H. (1977)

Stopping power data for neutron and pion dosimetry with ionization chambers.

Report for the Committee on Stopping Power of the ICRU,

Internal Report # 77.5

BICHSEL, H., RUBACH, A. (1978)

Uncertainty of the determination of absolute neutron dose with ionization chambers.

Proc. 3rd Symposium on Neutron Dosimetry in Biology and Medicine, p. 549. Edit. G. Burger, H.G. Ebert, CEC EUR 5848

BOAG, J.W. (1964)

Distortion of electric field in an ionization chamber due to a difference in potential between guard ring and collector.

Physics in Medicine and Biology, Vol. 9, No. 1, 25

BOAG, J.W. (1966)

Ionization chambers.

Radiation Dosimetry. Vol. 2

BOAG, J.W. (1963)

Space charge distortion of the electric field in a parallel-plate ionization chamber.

Physics in Medicine and Biology, Vol. 8, No. 4, 461-467

BONNETT, D.E. (1979)

Personal Communication

BOTTRILL, D., JEFFRIES, D. (1979)

Personal Communication

BURLIN, T.E. (1961)

An experimental examination of theories relating the absorption of x-ray energy in a medium to the ionization produced in a cavity.

Physics in Medicine and Biology, 6, p. 33

CASWELL, R.S., COYNE, J.J. (1972)

Interaction of neutrons and secondary charged particles with tissue: secondary particle spectra.

Radiation Research, 52, 448-470

CATTERALL, M. (1974)

The treatment of advanced cancer by fast neutrons from the Medical Research Council's Cyclotron at Hammersmith Hospital, London.

European Journal of Cancer, Vol. 10, pp 343-347

CATTERALL, M., BEWLEY, D.K., SUTHERLAND, I. (1977)

Second report on results of a randomized clinical trial of fast neutrons compared with x or gamma rays in treatment of advanced tumours of the head and neck.

British Medical Journal, 1, 1642

CATTERALL, M., SUTHERLAND, I., BEWLEY, D.K. (1975)

First results of a randomized clinical trial of fast neutrons compared with x or gamma rays in treatment of advanced tumours of the head and neck.

British Medical Journal, 21st June

CHURCHILL-DAVIDSON, I., SANGER, C., THOMLINSON, R.H. (1957)
Oxygenation in Radiotherapy, II Clinical application.
British Journal of Radiology, 30, 406

COYNE, J.J. (1980)
Kerma values by particle type.
Ion Chambers for Neutron Dosimetry, Edit. J.J. Broerse
(Brussels, CEC)

DENNIS, J.A. (1973)
Computed ionization and kerma values in neutron irradiated gases.
Physics in Medicine and Biology, Vol. 18, No. 3, 379-395

DENNIS, J.A. (1979)
Stopping power in the interpretation of ionization chamber measurements.
CENDOS, September

EDWARDS, A.A. (1978)
The derivation of tissue doses from measurements with a tissue-equivalent ionization chamber.
Proc. 3rd Symposium on Neutron Dosimetry in Biology and Medicine, p. 535, Edit. G. Burger, H.G. Ebert, CEC EUR 5848

FOWLER, J.F. (1956)
X-ray induced conductivity in insulating materials.
Proceedings of the Royal Society, A, Vol. 236, p. 464-480

FOWLER, J.F., FARMER, F.T. (1954)

Conductivity induced in insulating materials by x-rays.

Nature, Vol. 173, p. 317

FOWLER, J.F., FARMER, F.T. (1955)

Conductivity induced in unplasticized perspex by x-rays.

Nature, Vol. 175, p. 516

GOODMAN, L.J., COYNE, J.J. (1980)

$\overline{W}_N$ and neutron kerma for methane based TE gas.

Radiation Research, 82, 13-26

GRAY, L.H., CONGER, A.D., EBERT, M., HORNSEY, S., SCOTT, O.C.A. (1953)

The concentration of oxygen dissolved in tissues at the time of irradiation as a factor in radiotherapy.

British Journal of Radiology, 26, 638

GREENING, J.R. (1964)

Saturation characteristics of parallel-plate ionization chambers.

Physics in Medicine and Biology, Vol. 9, No. 2, 143-154

HIRAOKA, T., KAWASHIMA, K., INADA, T., MATSUZAWA, H. (1971)

Paired ionization chambers for measurement of neutrons and gamma rays.

Strahlentherapie 141, 1, p.p. 64-68

HUBBELL, J.H. (1977)

Photon mass attenuation and mass energy absorption coefficients for H, C, N, O, Ar and seven mixtures from 0.1KeV to 20MeV.

Radiation Research, 70, 58

INTERNATIONAL COMMISSION ON RADIATION UNITS AND MEASUREMENTS REPORT NO. 26 (WASHINGTON D.C. 1977)

Neutron dosimetry for biology and medicine.

INTERNATIONAL COMMISSION ON RADIATION UNITS AND MEASUREMENTS REPORT NO. 31 (WASHINGTON D.C. 1979)

Average energy required to produce an ion pair.

JANNI, J.F. (1966)

Calculations of energy loss, range, pathlength, straggling, multiple scattering and the probability of inelastic nuclear collisions for 0.1 to 1000MeV protons.

Air Force Weapons Laboratory Rep. AFWL-TR-65-150, National Tech. Info. Service AD-643-837

KUCHNIR, F.T., VYBORNY, C.J., SKAGGS, L.S. (1975)

A precise method for measuring the neutron response of a neutron insensitive dosimeter.

Biomedical Dosimetry, IAEA-SM-193/51, p. 107 (IAEA Vienna)

KÜHN, H. (1975)

Characteristics of different ionization chambers for fast neutron dosimetry.

Proc. 2nd Symposium on Neutron Dosimetry in Biology and Medicine, EUR 5273, Edit. G. Burger, H.G. Ebert, Vol. 1, p.p. 241-261 (Commission of the European Communities Luxembourg)

LOVE, W.H., WHITE-SMITH, W.B. (1935)

Field distortion in the standard ionization chamber.

British Journal of Radiology, Vol 9, No. 97

MAKAREWICZ, M., PSZONA, S. (1981)

Specification of cavity size effect in the ionization chamber used for neutron dosimetry.

Proc. 4th Symposium on Neutron Dosimetry, EUR 7448, Edit. G. Burger, H.G. Ebert, Vol. 2, p.p. 307-314 (Commission of the European Communities Luxembourg)

MIJNHEER, B.J., WILLIAMS, J.R. (1981)

Determination of absorbed dose and kerma in a neutron field from measurements with a tissue-equivalent ionization chamber.

Physics in Medicine and Biology, Vol. 26, No. 1, 57-69

NGUYENS, V.D., CHEMTOB, M., CHARY, J., POSNY, F., PARMENTIER, N. (1980)

Recent experimental results on $\overline{W}$ values for heavy particles.

Physics In Medicine and Biology, 25, 3

PEARSON, D.W., ATTIX, F.H., DE LUCA, P.M. JR, GOETSCH, S.J., TORTI, R.P. (1980)

Ionization error due to porosity of graphite ionization chambers.

Physics in Medicine and Biology, 25, 333-338

POWERS, D. (1978)

Stopping cross sections and ranges of α particles in matter energy 1KeV - 20MeV.

Prepared for the ICRU Stopping Power Committee

SCOTT, PATRICIA B., GREENING, J.R. (1963)

The determination of saturation currents in free-air ionization chambers by extrapolation methods.

Physics in Medicine and Biology, Vol. 8, No. 1, p. 51

SHELINE, G.E., PHILLIPS, T.L., FIELD, STANLEY B., BRENNAN, J.T., RAVENTOS, A. (1971)

Effects of fast neutrons on human skin.

American Journal of Roentgenology, 111, 31-41

SMATHERS, JAMES B., OTTE, VICTOR A., SMITH, ALFRED R., ALMOND, PETER R. ETC. (1977)

Composition of A-150 tissue-equivalent plastic.

Medical Physics, Vol. 4, No. 1

STONE, R.S. (1948)

Neutron therapy and specific ionization: Janeway memorial lecture (1948)

American Journal of Roentgenology, Vol. 59, No. 6

STONE, R.S. LARKEN, J.C. (1942)

The treatment of cancer with fast neutrons.

Radiology, 39, 608-620

STONE, ROBERT S., LAWRENCE, JOHN H., AEBERSOLD, PAUL C. (1940)

A preliminary report on the use of fast neutrons in the treatment of malignant disease.

25th Meeting of Radiobiological Society of N. America, Atlanta

WILLIAMS, J.R. (1980)

Problems in neutron dosimetry associated with the incorrect composition of tissue-equivalent gas.

Physics in Medicine and Biology, Vol. 25, No. 3, 501-508

WILLIAMS, J.R., BONNETT, D.E., PARNELL, C.J. (1979)

The fixed horizontal neutron therapy beam at Edinburgh dosimetry and radiation protection.

British Journal of Radiology, 52, 197-208

WILLIAMS, J.R., GREENING, J.R. (1980)

The photon calibration of a TE chamber for neutron dosimetry.

Physics in Medicine and Biology, 25

ZANSTRA, H., TRANSLATED BY SYKES, J.B. (1935)

A short method for determining the saturation current according to Jaffé's theory of column ionization.

Physica, Vol. 2, p.p. 817-824

ZIEGLER, J.F. (1977)

Helium stopping powers and ranges in all elements.

Pergamon Press